

Physics at the LHC

-From Standard Model measurements to Searches for New Physics-

Karl Jakobs

Physikalisches Institut, University of Freiburg, Germany

Abstract

The successful operation of the *Large Hadron Collider* (LHC) during the past two years allowed to explore particle interaction in a new energy regime. Measurements of important Standard Model processes like the production of high- p_T jets, W and Z bosons and top and b -quarks were performed by the LHC experiments. In addition, the high collision energy allowed to search for new particles in so far unexplored mass regions. Important constraints on the existence of new particles predicted in many models of physics beyond the Standard Model could be established. With integrated luminosities reaching values around 5 fb^{-1} in 2011, the experiments reached as well sensitivity to probe the existence of the Standard Model Higgs boson over a large mass range. In the present report the major physics results obtained by the two general-purpose experiments ATLAS and CMS are summarized.

1 Introduction

In March 2010 the Large Hadron Collider started its operation at the highest centre-of-mass energy ever reached and delivered first proton-proton collisions at 7 TeV. The years 2010 and 2011 showed a very successful operation of both the collider and the associated experiments. During the start-up year 2010 data corresponding to an integrated luminosity of about 48 pb^{-1} could be delivered. This successful operation was followed by an even more successful year 2011 where the collider delivered data corresponding to an integrated luminosity of 5.5 fb^{-1} and exceeded the original design goal of 1 fb^{-1} by far. In April 2011 the world record on the instantaneous luminosity was reached with a luminosity of $4.7 \cdot 10^{32} \text{ cm}^{-2}\text{sec}^{-1}$. Meanwhile luminosities beyond $3 \cdot 10^{33} \text{ cm}^{-2}\text{sec}^{-1}$ have been reached.

However, not only the accelerator but also the experiments showed an extremely successful operation. They were able to record the delivered luminosity with efficiencies of the order of 94%. All detector subsystems worked well with a high number of functioning channels, typically exceeding 99%.

The data were used to test the Standard Model [1,4] of particle physics in the new energy regime. At the LHC as a hadron collider the production of particles via the strong interaction is dominating. Therefore, the test of Quantum Chromodynamics (QCD) [4], the theory of strong interactions, was in the focus during the early phase. Tests of QCD can be performed at small distances or for processes with large momentum transfer. Among them the production of jets with large transverse momenta (p_T) has the largest cross section. The investigation of the production of W and Z bosons, their associated production with jets and the production of top quarks constitute other important tests of QCD in the new energy regime.

Due to the high centre-of-mass energy of 7 TeV the LHC has a large discovery potential for new particles with masses beyond the limits set by the Tevatron experiments, even already in the initial phase of operation. Due to the dominating strong production, this holds in particular for particles that carry colour charge, like e.g. the supersymmetric partners of quarks and gluons. Due to the excellent luminosity performance of the LHC in 2011 the sensitivity for many models of new physics were pushed far beyond the mass range explored so far.

In this review the physics motivation for the LHC is briefly recalled in Section 2. The phenomenology of proton-proton collisions and the calculation of cross sections is briefly reviewed in Section 3. The

measurement of important Standard Model processes at the LHC is discussed in Section 4. The status of the search for the Standard Model Higgs boson is summarized in Section 5. It should be noted that in this paper the status of the Higgs boson search as of March 2012 is presented. Given the large increase in the integrated luminosity during the second half of 2011, these results supersede by far those presented at the school in September 2011. In the remaining sections of the paper the searches for physics beyond the Standard Model are discussed. The search for supersymmetric particles is described in Section 6, the search for other scenarios is summarized in Section 7.

2 The Physics Questions at the LHC

The Standard Model is a very successful description of the interactions of particles at the smallest scales (10^{-18}m) and highest energies accessible to current experiments. It is a quantum field theory which describes the interactions of spin- $1/2$ pointlike fermions whose interactions are mediated by spin-1 gauge bosons. The bosons are a consequence of local gauge invariance of the underlying Lagrangian under the symmetry group $SU(3)\times SU(2)\times U(1)$ [1].

The $SU(2) \times U(1)$ symmetry group, which describes the electroweak interactions, is spontaneously broken by the existence of a postulated scalar field, the so-called Higgs field, with a non-zero vacuum expectation value [7–12]. This leads to the emergence of massive vector bosons, the W and Z bosons, which mediate the weak interaction, while the photon of electromagnetism remains massless. One physical degree of freedom remains in the Higgs sector which should manifest as a neutral scalar boson H which is so far unobserved. The description of the strong interaction (Quantum Chromodynamics or QCD) is based on the gauge group $SU(3)$ [4]. Eight massless gluons mediate this interaction.

All experimental particle physics measurements performed up to date are in excellent agreement with the predictions of the Standard Model. The only noticeable exception is the evidence for non-zero neutrino masses observed in neutrino-oscillation experiments [13]. There remain, however, many key questions open and it is generally believed that the Standard Model can only be a low energy effective theory of a more fundamental underlying theory. One of the strongest arguments for an extension of the Standard Model is the existence of Dark Matter [14] in the universe. There is no explanation for such a type of matter in the Standard Model.

The key questions can be classified to be linked to mass, unification and flavour:

- Mass: What is the origin of mass?
How is the electroweak symmetry broken? Is the solution, as implemented in the Standard Model, realized in Nature, and linked to this, does the Higgs boson exist?
- Unification: What is the underlying fundamental theory?
Can the three interactions which are relevant for particle physics be unified at larger energy and are there new symmetries found towards unification? Are there new particles, e.g. supersymmetric particles, at higher energy scales? And finally, it must also be answered how gravity can eventually be incorporated.
- Flavour: Why are there three generations of matter particles? What is the origin of CP violation in the weak interaction? What is the origin of neutrino masses and mixings?

The high energy and luminosity of the LHC offers a large range of physics opportunities. The primary role of the LHC is to explore the TeV-energy range where answers to at least some of the aforementioned questions are expected to be found. In the focus is certainly the search for the Higgs boson. The LHC experiments have the potential to explore the full relevant mass range and either to discover the Standard Model Higgs boson or to exclude its existence.

Another focus area constitutes the search for supersymmetric particles which can be carried out at the LHC up to the masses of a few TeV. If such particles are discovered, their link to the dark matter in the universe must be investigated. This can only be done in conjunction with experiments on direct dark matter detection [15].

However, it is important to stress that the remit of the LHC is not only to look for the *expected* or theoretically favoured models, but to carry out a thorough investigation of as many final states as possible. It is important to search for any deviation from the Standard Model predictions. This implies that the Standard Model predictions must be reliably tested in the new energy domain. In particular during the early phase of experimentation at the LHC, detailed measurements of Standard Model processes must be carried out. Some of these processes can as well be used for the understanding of the detector response and its calibration.

Finally, with increasing precision of the Standard Model measurements, it is also important to test the consistency of the model via quantum corrections. Important contributions from the LHC in this area will be precise measurements of the W mass and of the top-quark mass, which can be used to constrain the Higgs boson mass. A direct confrontation of this prediction to a direct Higgs boson mass measurement may constitute the ultimate test of the Standard Model at the LHC.

3 Phenomenology of proton-proton collisions

Scattering processes at high-energy hadron colliders can be classified as either hard or soft. Quantum Chromodynamics is the underlying theory for all such processes, but the approach and level of understanding is very different for the two cases. For hard processes, e.g. high- p_T jet production or W and Z production, the rates and event properties can be predicted with good precision using perturbation theory. For soft processes, e.g. the total cross section, the underlying event etc., the rates and properties are dominated by non-perturbative QCD effects, which are less well understood. An understanding of the rates and characteristics of predictions for hard processes, both signals and backgrounds, using perturbative QCD (pQCD) is crucial for tests of the theory and for searches for new physics.

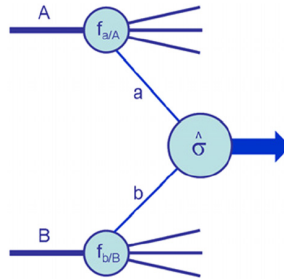


Fig. 1: Diagrammatic structure of a generic hard-scattering process (from Ref. [16]).

The calculation of a hard-scattering process for two hadrons A and B can be illustrated as displayed in Fig. 1. Two partons of the incoming hadrons undergo a hard scattering process characterized by the cross section $\hat{\sigma}$. The structure of the incoming hadrons is described by the parton density functions (PDFs) $f_{a/A}(x_a, \mu_F^2)$ (see Section 3.1), i.e. the probability to find a parton a in hadron A with a momentum fraction x_a at the energy scale μ_F^2 . To obtain the hadron-hadron cross section, a summation over all possible parton-parton scattering processes and an integration over the momentum fractions has to be performed [16]:

$$\sigma_{AB} = \sum_{a,b} \int dx_a \cdot dx_b f_{a/A}(x_a, \mu_F^2) f_{b/B}(x_b, \mu_F^2) \hat{\sigma}_{ab}(x_a, x_b, \alpha_s(\mu_R^2)). \quad (1)$$

The calculations of the hard scattering process $\hat{\sigma}_{ab}$ are performed in perturbative QCD and the results depend on the strong coupling constant α_s and its renormalization scale μ_R . The scale μ_F that appears in the parton density functions is the so-called factorization scale, which can be thought of as the scale that separates long- and short-distance physics [16]. Large logarithms related to gluons emitted collinear with incoming quarks can be absorbed in the definition of the parton densities, giving rise to logarithmic scaling violations which can be described via the DGLAP¹ evolution equations [17]. The perturbative calculation can be written as

$$\hat{\sigma}_{ab}^{[n]} = \hat{\sigma}_{ab}^{[0]} + \sum_{j=k+1}^{k+n} c_j \cdot \alpha_s^j, \quad (2)$$

where $\hat{\sigma}_{ab}^{[0]}$ denotes the leading order (LO) cross section and n denotes the perturbative order of the calculation. The index k denotes the order of α_s appearing in the leading order calculation, which might as well be 0, like for the Drell-Yan production of W and Z bosons, as discussed below. The cross sections at higher orders, which are usually denoted as next-to-leading order (NLO) and next-to-next-to-leading order (NNLO) etc., are often parametrized in terms of total K factors, defined at each perturbative order $[n]$ as the ratio of the cross section computed to that order normalized to the Born level cross section:

$$\sigma^{[n]} = \sigma^{[0]} \cdot K_{\text{tot}}^{[n]}. \quad (3)$$

As discussed above, the scale μ is an arbitrary parameter, which in general is, however, chosen to be of the order of the energy characterizing the parton-parton interaction, like, for example, the mass of the vector bosons or the transverse momenta of outgoing jets. The more orders are included in the perturbative expansion, the weaker the dependence on μ . As an example, the production of W and Z bosons is discussed in Section 3.3.

Those partons which do not take part in the hard scattering process will produce what is generally called the ‘underlying event’. Finally, it should be stressed that Eq. 2 does not describe the bulk of the events which occur at a hadron collider. It can only be used to describe the most interesting classes of events which involve a hard interaction. Most events result from elastic and soft inelastic interactions generally called ‘minimum bias’ events. In the following a few specific examples of hard scattering processes are discussed.

3.1 Parton Distribution Functions

The parton distribution functions (PDFs) $f(x, Q^2)$ for a hadron provide the probability density of finding a parton with momentum fraction x at momentum transfer Q^2 which defines the energy scale of the process. The Q^2 dependence is induced by the usage of perturbation theory and the resulting higher order corrections. It is described by the DGLAP evolution equations [17]. However, the functional form of the PDFs is not predicted by perturbative QCD and has to be measured experimentally.

Various classes of experiments are sensitive to the proton PDFs, such as deep inelastic scattering at fixed target experiments with electron, muon or neutrino beams, and electron-proton scattering at the HERA collider. Also experiments at pure hadronic colliders such as the Tevatron ($p\bar{p}$) and the LHC (pp) can yield valuable information.

In order to determine the parton distributions from the measurements, a parametrization is assumed to be valid at some starting value $Q^2 = Q_0^2$. The DGLAP evolution functions are used to evolve the PDFs to a different Q^2 where predictions of the measured quantities (e.g. structure functions) are obtained. The predictions are then fitted to the measured datasets, thus constraining the parameters (typically 10 to 20) of the parametrisation [18]. Various collaborations performed fits to the available datasets and provided PDF sets for the proton, for instance the groups ABKM [19], CTEQ [20], CT10 [21], HERAPDF [22,23], JR [24], MSTW [25] and NNPDF [26, 27]. The NNPDF collaboration has already included the first

¹Dokshitzer-Gribov-Lipatov-Altarelli-Parisi

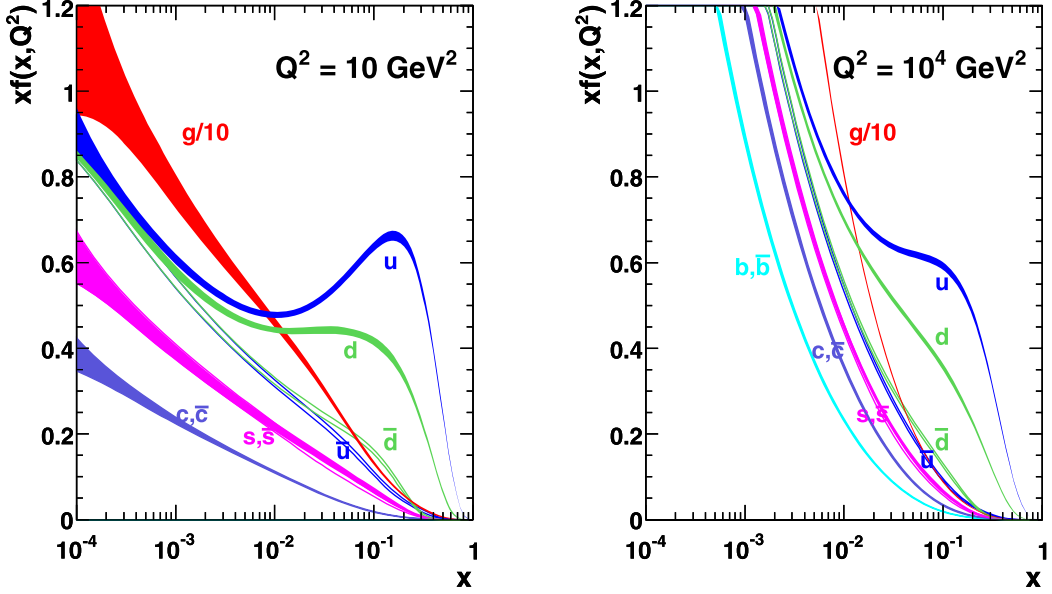


Fig. 2: Parton distribution functions of the proton as determined for the MSTW08 PDF set for (left) $Q^2 = 10 \text{ GeV}^2$ and (right) $Q^2 = 10^4 \text{ GeV}^2$. The bands reflect the uncertainties at the 68% confidence level (from Ref. [25]).

lepton charge asymmetry measurements in the W boson production by the ATLAS [28] and CMS [29] experiments in their fit [30]. The PDFs determined by MSTW are shown in Fig. 2 at two different Q^2 scales. For example, it can be observed that gluons dominate the low x region and the contributions from sea quarks become more dominant at higher Q^2 .

3.2 Jet Production via QCD scattering processes

Two-jet events result when an incoming parton from one hadron scatters off an incoming parton from the other hadron to produce two high transverse momentum partons which are observed as jets. The parton processes that contribute at leading order are shown in Fig. 3. The matrix elements have been calculated at leading order [31] and next-to-leading order [32, 33]. At the LHC, terms involving gluons in the initial state are dominant at low p_T . Unlike in lowest order, where a direct correspondence between a jet cross

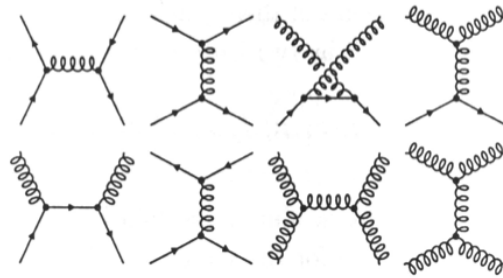


Fig. 3: Leading order diagrams for the production of high- p_T jets.

section and the parton cross section can be made, a prescription is needed to derive jet cross sections in next-to-leading order. When such prescriptions are applied, the next-to-leading order cross sections show substantially smaller sensitivities to variations of the renormalization scale than at lowest order.

3.3 W and Z Production

In leading order the production of the vector bosons W and Z is described by the Drell-Yan process, where a quark and an antiquark from the incoming hadrons annihilate. This process has been calculated up to next-to-next-to-leading order in the strong coupling constant α_S [34–37]. Some of the relevant Feynman diagrams are given in Fig. 4. When going from LO to NLO the cross sections increase by

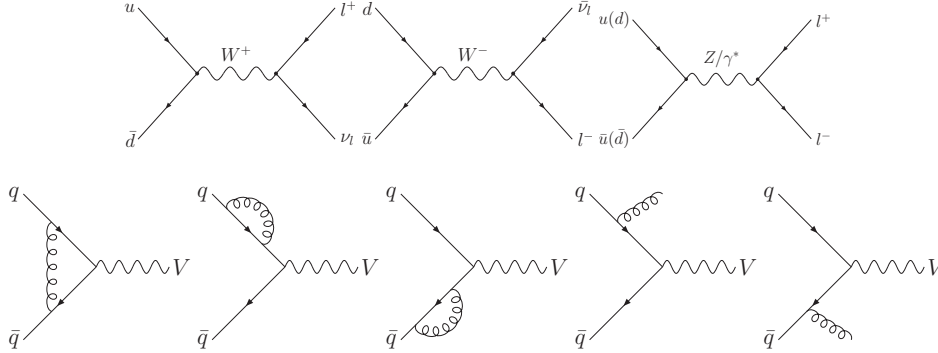


Fig. 4: Leading order (top) and some next-to-leading order diagrams (bottom) for the production of W and Z bosons.

about 20% and the factorization and renormalization scale uncertainties decrease. This is nicely shown in Fig. 5. Including NNLO contributions slightly decreases the cross-sections but the result is consistent

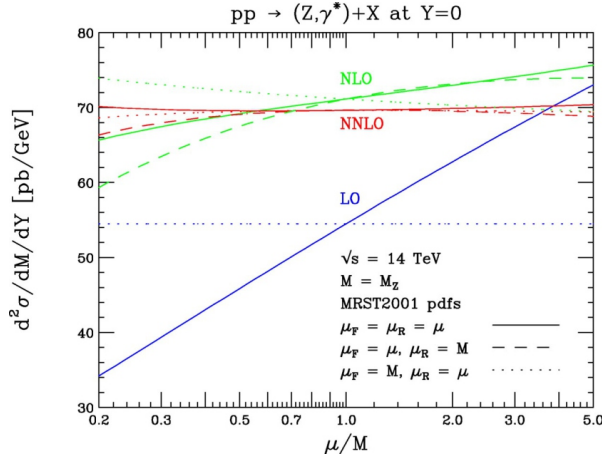


Fig. 5: Dependence of the production cross section of on-shell Z bosons at rapidity $y = 0$ on the choice of the renormalization and factorization scales. For each order in perturbation theory (LO, NLO, NNLO), three curves are shown. The solid curve represents the results obtained under a common variation of $\mu_R = \mu_F = \mu$ over the range $M/5 < \mu < 5M$. The dashed (dotted) curves represent the results obtained under variations of the factorization (renormalization) scale alone, holding the other scale fixed (from Ref. [37]).

with the NLO prediction within the NLO scale uncertainty, indicating that the perturbative expansion converges. The impact of higher order corrections on the predicted rapidity² distributions of the W and Z bosons is shown in Fig. 6 for proton-proton collisions with a centre-of-mass energy of $\sqrt{s} = 14$ TeV. This figure also illustrates that larger cross sections for W^+ production than for W^- production are

²The rapidity y of a particle is related to its energy E and the projection of its momentum on the beam axis p_z by $y = \frac{1}{2} \ln[(E + p_z)/(E - p_z)]$. The pseudorapidity η is defined as $\eta = -\ln \tan \frac{\theta}{2}$, where θ is the polar angle.

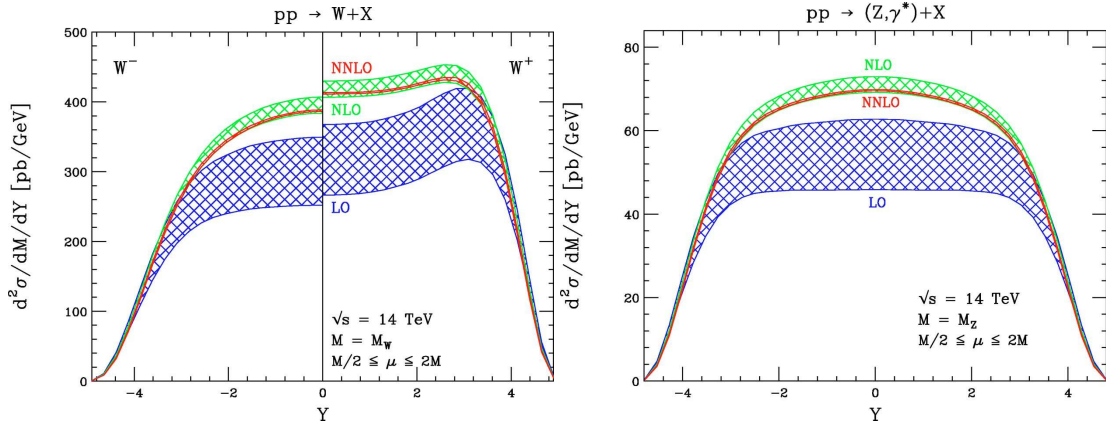


Fig. 6: Theory predictions at LO, NLO and NNLO of the rapidity distributions for W (left) and Z (right) boson production in proton-proton collisions at $\sqrt{s} = 14$ TeV. The bands indicate the factorization and renormalization scale uncertainties, obtained by scale variations in the range $M_{W/Z}/2 \leq \mu \leq 2M_{W/Z}$ (from Ref. [37]).

expected at the LHC. This asymmetry results from the dominance of u over d valence quarks in the incoming protons (see also Fig. 2).

Electroweak radiative corrections for the W and Z boson production have been computed up to next-to-leading order [38, 39]. These corrections change the production cross sections and affect kinematic properties like the lepton transverse momenta, lepton rapidities and the transverse and invariant masses of the lepton pairs. In particular for precision measurements like that of the W boson mass, it is therefore important to take electroweak radiative corrections into account.

3.4 Cross Sections at the LHC

An overview of cross sections of some benchmark processes at proton-proton and proton-antiproton colliders as a function of the centre-of-mass energy is shown in Fig 7. The total inelastic proton-proton cross section is dominant and reaches a huge value of about 70 mb at the LHC. Processes which can proceed via the strong interaction have a much larger cross section than electroweak processes. The dominant electroweak process, the production of W and Z bosons is found to be about six and seven orders of magnitude smaller than the total inelastic proton-proton cross section. However, this process constitutes the most copious source of prompt high- p_T leptons, which are important for many physics measurements and searches for new physics at the LHC. The production processes of the Standard Model Higgs boson and of other non-coloured heavy new particles have small cross sections and therefore require a correspondingly high integrated luminosity for their detection. The Higgs boson production cross section is found to be ten to eleven orders of magnitude smaller than the inelastic pp cross section. The exact values depend strongly on the mass of the Higgs boson, as further discussed in Section 5.1.

4 Measurement of Standard Model processes

4.1 The production of high- p_T jets

A measurement of the production of high- p_T jets constitutes an important test of QCD in the new energy regime of the LHC. Events with two high transverse momentum jets (dijets) arise from parton-parton scattering where the outgoing scattered partons manifest themselves as hadronic jets. The measurements of the inclusive jet production cross section or the dijet production cross section are therefore also sensitive to the structure of the proton and may lead to further constraints on the PDFs. In addition, the precise measurement of jet production is important for searches of physics beyond the Standard Model. New

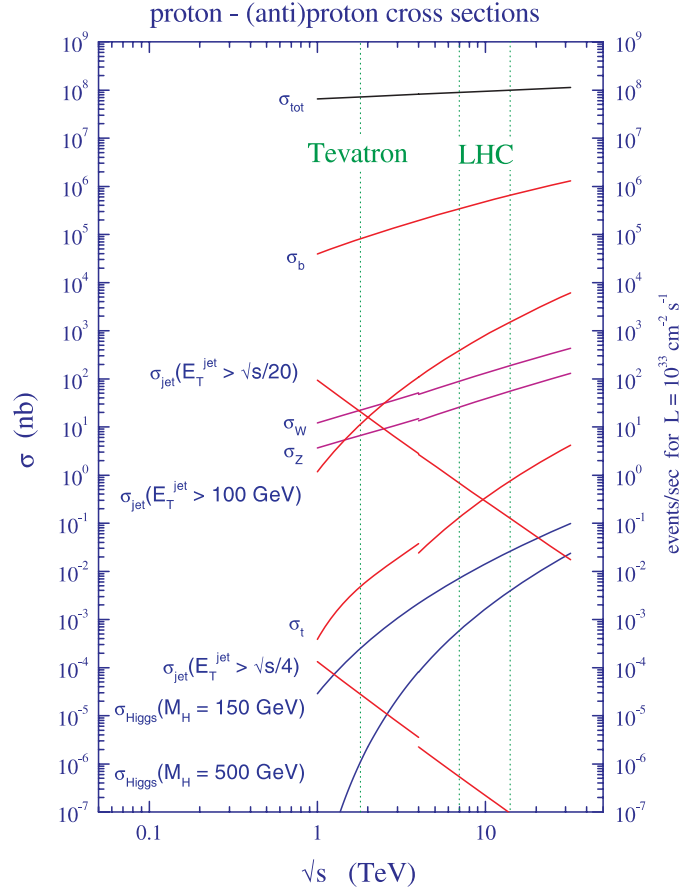


Fig. 7: Standard Model cross sections at the Tevatron and LHC colliders as function of the centre-of-mass energy \sqrt{s} . In case of the LHC both the energy during data taking in 2010/2011 ($\sqrt{s} = 7$ TeV) and the nominal energy ($\sqrt{s} = 14$ TeV) are marked (adapted from Ref. [16]).

physics may lead to significant deviations from the expected QCD behaviour. For example, a substructure of quarks may manifest itself in deviations of the measured inclusive jet-production cross section from the expected behaviour at high transverse momenta. The measurement of the dijet cross section as a function of the dijet mass m_{jj} allows for a sensitive search for physics beyond the Standard Model, such as dijet resonances or contact interactions of composite quarks.

The production of multijets provides as well an important background in the search for physics beyond the Standard Model. In many cases, leptons and missing transverse energy are used as final states signatures. Although they do not appear at first place in QCD jet production, they might originate from decays of heavy quarks, from mis-measurements of jet energies or from mis-identification of jets as leptons. Although the probability for this to happen is small, the contributions to the background can be sizeable, give the huge jet production cross sections.

4.1.1 Jet reconstruction and calibration

For the reconstruction of jets both the ATLAS and CMS experiments use the infrared- and collinear-safe *anti- k_T* jet clustering algorithm [40] with distance parameters $0.4 \leq R \leq 0.7$. The inputs are either topological calorimeter cluster energies [41,42] in the ATLAS experiment or particle flow objects [43,44] in the CMS experiment. For the theoretical comparison the input can also be four-vectors from stable particles in generator-level simulations. In all cases residual jet-level corrections are needed to account

for energy losses not detectable on cluster or particle flow level. These jet-level calibrations are Monte Carlo based correction functions in pseudorapidity $|\eta|$ and p_T . The jet energy scale and the attached uncertainties are validated with in-situ methods using the balance of transverse momenta in dijet and γ -jet events. The systematic jet energy scale uncertainties are found to be typically in the range of $\pm(3 - 6)\%$ over a large range of η and p_T . The larger values are reached at large $|\eta|$ as well as at very low and very high p_T .

4.1.2 Jet cross section measurements

The inclusive jet production cross section has been measured by both the ATLAS [45] and CMS [46] experiments as a function of the jet transverse momentum (p_T) and jet rapidity (y). In addition, double differential cross sections in the maximum jet rapidity y_{\max} and dijet mass m_{jj} for dijet events are measured [45, 47]. The data are corrected for migration and resolution effects due to the steeply falling spectra in p_T and mass. The NLO perturbative parton-level QCD predictions are corrected for hadronisation and the underlying event activity. Figure 8 (left) shows the inclusive jet cross-section measurement for jets with size $R = 0.4$ as a function of jet transverse momentum from the ATLAS collaboration [45], based on the total data set collected in 2010 corresponding to an integrated luminosity of 37 pb^{-1} . The experimental systematic uncertainties are dominated by the jet energy scale uncertainty. There is an additional overall uncertainty of $\pm 3.4\%$ due to the luminosity measurement. The theoretical uncertainties result mainly from the choice of the renormalization and factorization scales, parton distribution functions, $\alpha_s(m_Z)$ and the modelling of non-perturbative effects.

The cross section measurement as a function of the dijet invariant mass from the CMS collaboration [47] is shown in Fig. 8 (right). Like for the inclusive jet cross section measurements, the experimental uncertainties are in the range 10-20% and are dominated by uncertainties on the jet energy scale and resolution.

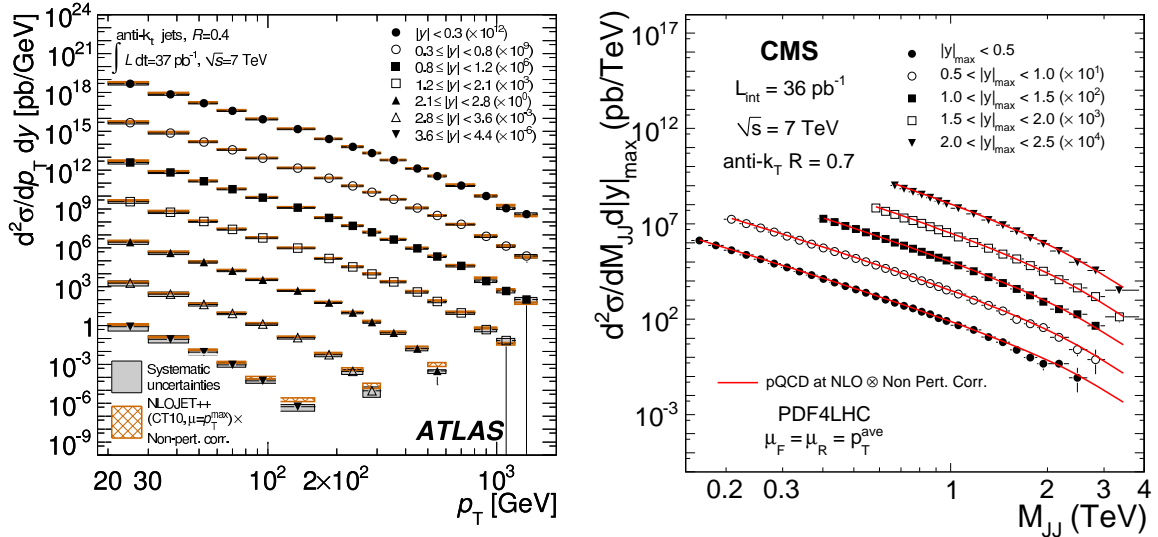


Fig. 8: (Left): Inclusive jet double-differential cross section as a function of jet p_T in different regions of $|y|$ from the ATLAS collaboration. (Right): Measured double-differential dijet cross sections (points) as a function of the dijet invariant mass m_{jj} in bins of the variable y_{\max} from the CMS collaboration. The data are compared in both cases to NLO pQCD calculations to which non-perturbative corrections have been applied. The error bars indicate the statistical uncertainty on the measurement. The dark-shaded band indicates the quadratic sum of the experimental systematic uncertainties, excluding the uncertainties from the luminosity. The theory uncertainty is shown as the light, hatched band (from Refs. [45, 47]).

Different NLO pQCD predictions, using different PDF sets, are compared to the data and the corresponding ratios of data to the NLO predictions. Figure 9 shows an example from the ATLAS collaboration [45]. Within the experimental and theoretical uncertainties the data are well described by the predictions, although they are found to be systematically higher than the data. The deviations become larger at large $|y|$ and p_T . However, it is impressive to see that the QCD calculations are able to describe the data over many orders of magnitude and up to the highest values of p_T and mass ever observed.

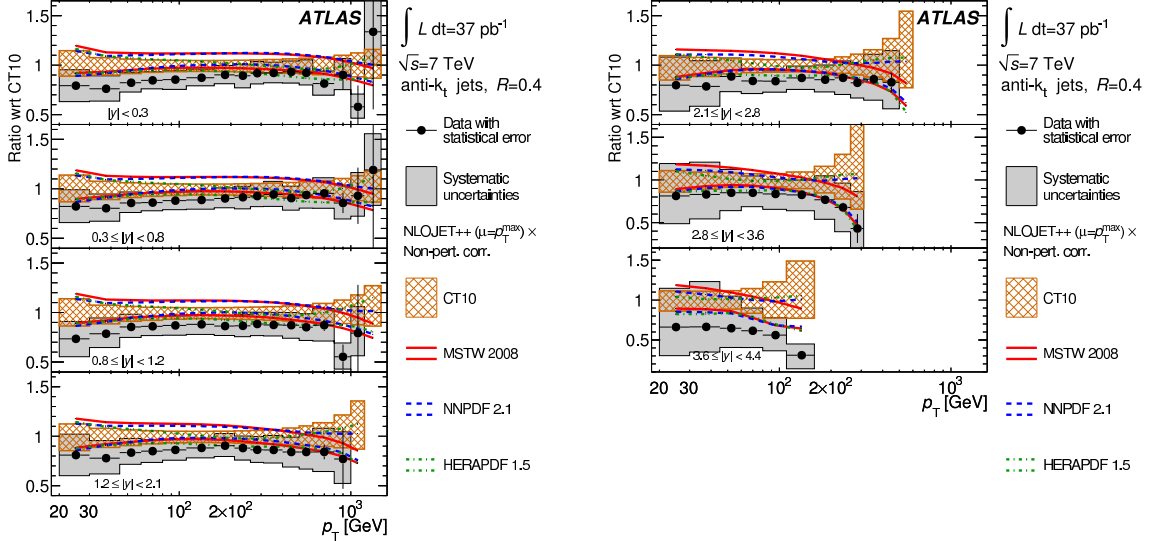


Fig. 9: Ratios of inclusive jet double-differential cross sections to the theoretical predictions. The ratios are shown as a function of jet p_T in different regions of $|y|$. The theoretical error bands obtained by using NLOJET++ with different PDF sets (CT10, MSTW 2008, NNPDF 2.1, HERAPDF 1.5) are shown (from Ref. [45]).

The ATLAS and CMS collaborations have performed many further studies on jet production, including the measurement of dijet angular distributions [48] and dijet angular decorrelations [45, 49]. At Born level, dijets are produced with equal transverse momenta p_T and back-to-back in the azimuthal angle ($\Delta\phi_{\text{dijet}} = |\phi_{\text{jet1}} - \phi_{\text{jet2}}|$). Gluon emission will decorrelate the two highest p_T jets and cause smaller angular separations. The measurement of the angular distribution between the highest p_T jets is therefore also a sensitive test of perturbative QCD with the advantage that the measurement is not strongly affected by the dominant systematic uncertainty on the jet energy scale. The predictions from NLO pQCD are found to be in reasonable agreement with the measured distributions [45, 49].

In addition, the production of multijets was studied [50, 51]. In a data sample corresponding to an integrated luminosity of 2.4 pb^{-1} the ATLAS collaboration has identified 115 events with more than six jets. One such event is shown in Fig. 10. The transverse energy deposition in the calorimeter is shown as a function of η and ϕ . For this event the six jets are well separated spatially. Leading-order Monte Carlo simulations have been compared to the measured multi-jet inclusive and differential cross sections. For events containing two or more jets with $p_T > 60 \text{ GeV}$, of which at least one has $p_T > 80 \text{ GeV}$, a reasonable agreement is found between data and leading-order Monte Carlo simulations with parton-shower tunes that describe adequately the ATLAS $\sqrt{s} = 7 \text{ TeV}$ underlying event data. The agreement is found after the predictions of the Monte Carlo simulations are normalized to the measured inclusive two-jet cross section.

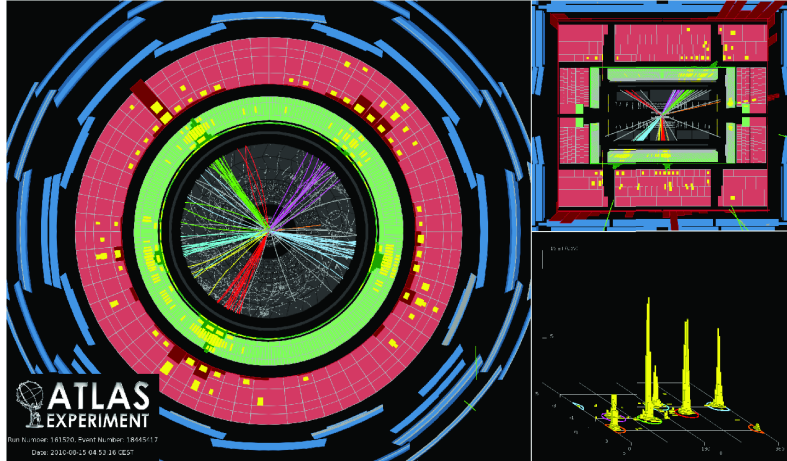


Fig. 10: Event display of a six-jet event passing the ATLAS multijet selection requirements. The towers in the bottom right figure represent transverse energy deposited in the calorimeter projected on a grid of η and ϕ . Jets with transverse momenta ranging from 84 to 203 GeV are measured in this event (from Ref. [50]).

4.2 The production of W and Z bosons

W and Z bosons are expected to be produced abundantly at the LHC. The large dataset and the high LHC energy allow for detailed measurements of their production properties in a previously unexplored kinematic domain. These conditions, together with the proton-proton nature of the collisions, provide new constraints on the parton distribution functions and allow for precise tests of perturbative QCD. Besides the measurements of the W and Z boson production cross sections, the measurement of their ratio R and of the asymmetry between the W^+ and W^- cross sections (see Section 3.3) constitute important tests of the Standard Model. This ratio R can be measured with a higher relative precision because both experimental and theoretical uncertainties partially cancel. With larger data sets this ratio can be used to provide constraints on the W -boson width Γ_W [52].

4.2.1 Inclusive cross-section measurements

Measurement of the W^+ , W^- and Z/γ^* boson inclusive production cross sections are performed using the leptonic decay modes $W \rightarrow \ell\nu$ and $Z \rightarrow \ell\ell$. Already in 2010, the two collaborations published first measurements in the electron and muon decay modes [53,54]. They were updated with the full data sample taken in 2010 corresponding to an integrated luminosity of 36 pb^{-1} [55,56]. In this data sample the ATLAS experiment has observed a total of about 270.000 $W \rightarrow \ell\nu$ decays and a total of about 24.000 $Z/\gamma^* \rightarrow \ell\ell$ decays. The measurements in the electron and muon channels were found to give consistent results and were combined to obtain a single joint measurement taking into account the statistical and systematic uncertainties and their correlations. The results are displayed in Fig. 11 together with previous measurements of the total W and Z production cross sections by the UA1 [57] and UA2 [58] experiments at $\sqrt{s} = 0.63 \text{ TeV}$ at the CERN Sp \bar{p} S and by the CDF [52] and D $\bar{\phi}$ [59] experiments at $\sqrt{s} = 1.8 \text{ TeV}$ and $\sqrt{s} = 1.96 \text{ TeV}$ at the Fermilab Tevatron collider and by the PHENIX [60] experiment in proton-proton collisions at $\sqrt{s} = 0.5 \text{ TeV}$ at the RHIC collider. These measurements are compared to the NNLO theoretical predictions for proton-proton and proton-antiproton collisions. All measurements are in good agreement with the theoretical predictions and the energy dependence of the total W and Z production cross sections is well described. The precision of the integrated W and Z/γ^* cross sections in the fiducial regions is $\sim \pm 1.2\%$ with an additional uncertainty of $\pm 3.4\%$ resulting from the knowledge of the luminosity. It should be noted that the experimental uncertainties are already dominated by systematic uncertainties. The total integrated cross sections are obtained from an extrapolation of the measurement

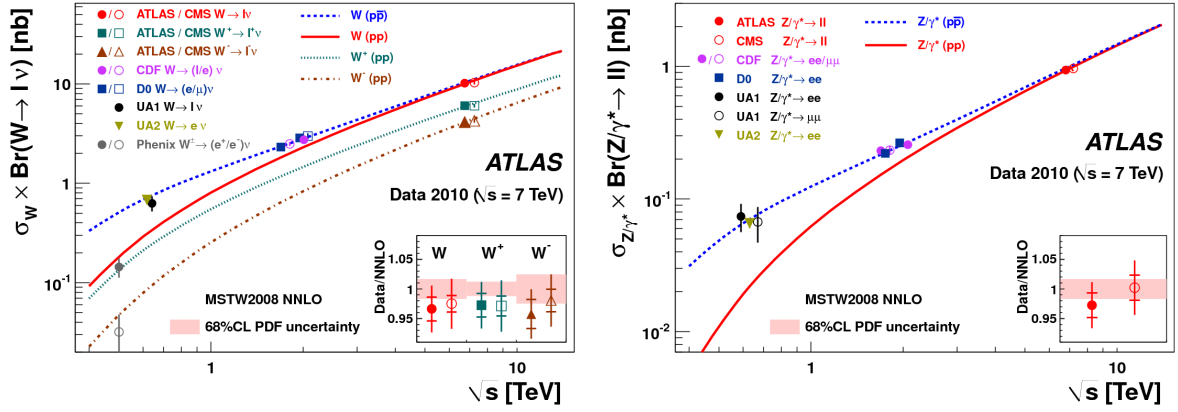


Fig. 11: The measured values of $\sigma_W \cdot \text{BR}(W \rightarrow \ell\nu)$ for W^+ , W^- and for their sum (left) and of $\sigma_{Z/\gamma^*} \times \text{BR}(Z/\gamma^* \rightarrow \ell\ell)$ (right) compared to the theoretical predictions based on NNLO QCD calculations. Results are shown for the combined measurements of electron and muon final states. The predictions are shown for both proton-proton (W^+ , W^- and their sum) and proton-antiproton colliders (W) as a function of \sqrt{s} . In addition, previous measurements at proton-antiproton and proton-proton colliders are shown. The data points at the various energies are staggered to improved readability. The data points are shown with their total uncertainty. The theoretical uncertainties are not shown in this figure (from Ref. [56]).

in the fiducial regions to the full acceptance. Due to uncertainties on the acceptance corrections, the uncertainties on the total cross sections are about twice as large.

A summary of the ratios of the measured total W^+ , W^- , W and Z/γ^* cross sections by the CMS collaboration to the theoretical NNLO calculations is shown in Fig. 12 (left). Within the experimental and theoretical uncertainties there is excellent agreement. This figure also includes a comparison of the measured ratios $R_{W/Z} = \sigma_W \cdot \text{BR}(W \rightarrow \ell\nu)/\sigma_Z \cdot \text{BR}(Z \rightarrow \ell\ell)$ and $R_{+/-} = \sigma_{W^+} \cdot \text{BR}(W^+ \rightarrow \ell^+\nu)/\sigma_{W^-} \cdot \text{BR}(W^- \rightarrow \ell^-\nu)$. Due to the cancellation of uncertainties, most notably the luminosity uncertainty, the precision of these ratio measurements is more precise. Also the measured ratios are well described by the theoretical NNLO calculations.

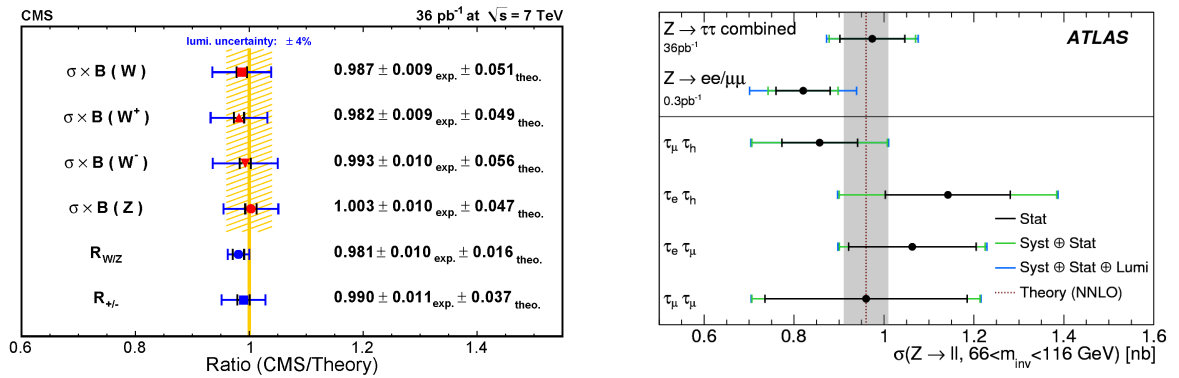


Fig. 12: (Left): Ratio of CMS measurement of W and Z cross sections to theory expectations. The experimental uncertainty is the sum in quadrature of the statistical and the systematic uncertainties not including the uncertainty on the extrapolation to the full acceptance due to parton density functions (taken from Ref. [55]). (Right): Measurements of the $Z \rightarrow \tau\tau$ cross sections from the ATLAS experiment in various τ decay modes and comparison to theoretical predictions and to the measurements in the electron and muon channels (taken from Ref. [61]).

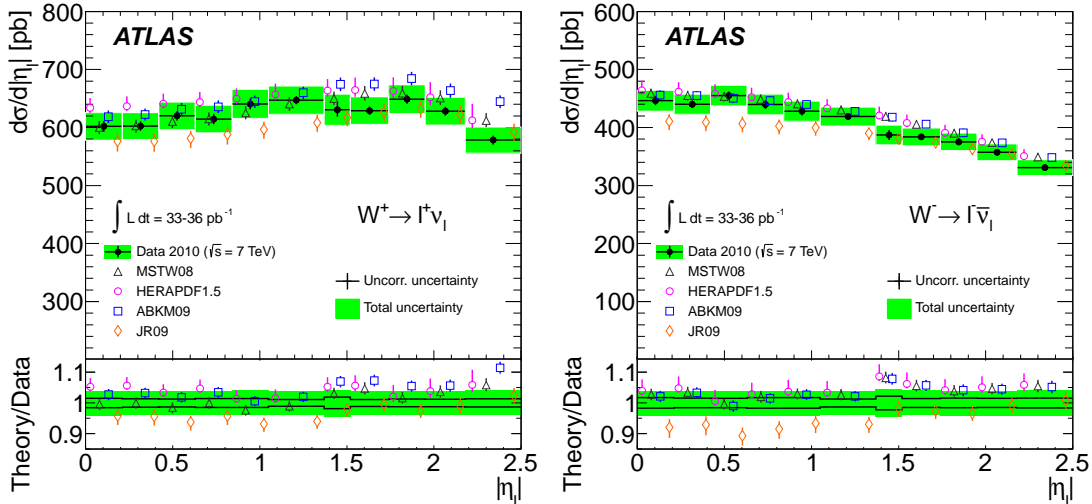


Fig. 13: Differential cross-section measurement $d\sigma/d|\eta_\ell|$ for W^+ (left) and W^- (right) for $W \rightarrow \ell\nu$ from the ATLAS collaboration compared to the NNLO theory predictions using various PDF sets. The kinematic requirements are $p_T(\ell) > 20$ GeV, $p_T(\nu) > 25$ GeV and $m_T > 40$ GeV. The ratio of theoretical predictions to data is also shown. Theoretical points are displaced for clarity within each bin (from Ref. [56]).

Meanwhile the cross sections have also been measured in the $W \rightarrow \tau\nu$ [62] and $Z \rightarrow \tau\tau$ [61, 63] decay modes, where hadronically decaying τ leptons are identified and reconstructed. The results obtained by the ATLAS collaboration in various τ decay modes are displayed in Fig. 12 (right). They are found to be in good agreement with theoretical predictions and with the results obtained in the $Z \rightarrow e^+e^-$ and $Z \rightarrow \mu\mu$ final states.

4.2.2 Differential cross section measurements

With the complete data set collected in 2010 more differential cross-section measurements became possible. Both the ATLAS and CMS collaborations have performed measurements as a function of lepton pseudorapidity η_ℓ , for the W^\pm cross sections, and of the boson rapidity, y_Z , for the Z/γ^* cross section [55, 56]. For the Z/γ^* case, all values refer to dilepton mass windows from 66 - 116 GeV and 60 - 110 GeV for the ATLAS and CMS analyses, respectively. The cross sections are measured in well-defined kinematic regions within the detector acceptance, defined by the pseudorapidity of the charged lepton and the transverse momentum of the neutrino. The differential W^+ and W^- cross sections as measured by the ATLAS collaboration are shown in Fig. 13. The measurements for the electron and muon final states were found to be in good agreement with each other and were combined. These data are compared with the theoretical NNLO predictions using various NNLO PDF sets (JR09, ABKM09, HERAPDF1.5 and MSTW08). The differential Z/γ^* cross section as a function of the boson rapidity as measured by the ATLAS and CMS collaborations are shown in Fig. 14. Although the gross features of these differential W and Z cross-section measurements are well described by the theoretical calculations, the (pseudo)rapidity dependence shows some disagreement which carries important information on the underlying parton density functions. It is expected that these differential measurements will reduce the uncertainties on the parton density functions. Very recently, these data have been used together with the ep scattering data from HERA to extract the ratio or the strange-to-down sea quark density at Bjorken x values around 0.01. The ratio is found to be consistent with 1 and supports the hypothesis that the density of the light sea quarks is flavour independent [64]. The general agreement between theory and experiment is remarkable and provides evidence for the universality of the PDFs and the reliability of perturbative QCD calculations in the kinematic regime of the LHC.

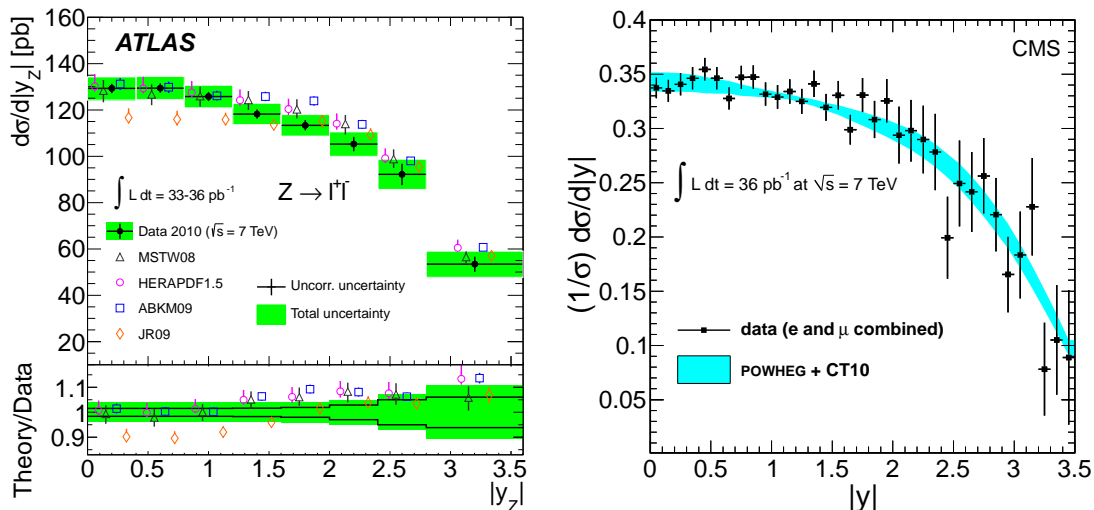


Fig. 14: Differential cross-section measurements $d\sigma/d|y_Z|$ for $Z \rightarrow \ell\ell$ from the ATLAS (left) and CMS (right) collaborations compared to NNLO theory predictions using various PDF sets. The kinematic requirements are $66 < m(\ell\ell) < 116$ GeV and $p_T(\ell) > 20$ GeV. The ratio of theoretical predictions to data is also shown for the ATLAS measurements. Theoretical points are displaced for clarity within each bin (from Refs. [55, 56]).

4.2.3 Measurements of the associated W and Z + jet production

The study of the associated production of vector bosons with high- p_T jets constitutes another important test of the perturbative QCD. In addition, these final states are a significant background to studies of other Standard Model processes, such as $t\bar{t}$ or diboson production, as well as for searches for the Higgs boson and for physics beyond the Standard Model.

The ATLAS and CMS collaborations have presented detailed measurements of these processes based on the complete dataset from 2010, corresponding to an integrated luminosity of 36 pb^{-1} [65–68]. Cross sections have been determined for the associated W and Z +jet production as a function of inclusive jet multiplicity, N_{jet} , for up to five jets. At each multiplicity, the cross sections have also been presented as a function of jet transverse momenta of all jets. The results, corrected for all detector effects and for all backgrounds such as diboson and top quark pair production, are compared with particle-level predictions from perturbative QCD. As an example, the W +jets cross-section measurements as a function of jet multiplicity are shown in Fig. 15 (left) and as a function of the p_T of the first jet in the event in Fig. 15 (right). Leading-order multiparton event generators like *ALPGEN* [69] or *SHERPA* [70], normalized to the NNLO total cross section for inclusive W -boson production, describe the data reasonably well for all measured inclusive jet multiplicities. Next-to-leading-order calculations from *MCFM* [71], studied for $N_{\text{jet}} \leq 2$, and *BlackHat-Sherpa* [72], studied for $N_{\text{jet}} \leq 4$, are found to be mostly in good agreement with the data. This also holds for the measurement of the transverse momentum distributions of the W and Z boson, which are correlated to the jet activity in the W and Z events.

4.3 Production of top quarks

4.3.1 Measurement of production cross sections

The top quark is the heaviest known elementary particle with a mass of about 173 GeV. Due to its high mass it is believed to play a special role in the electroweak symmetry breaking and possibly in models of new physics beyond the Standard Model. In that context it is remarkable that its Yukawa coupling λ_t is close to one. We still know little about the properties of the top quark, like spin, charge, lifetime, decay properties (rare decays) or the gauge and Yukawa couplings. Another important parameter is the mass

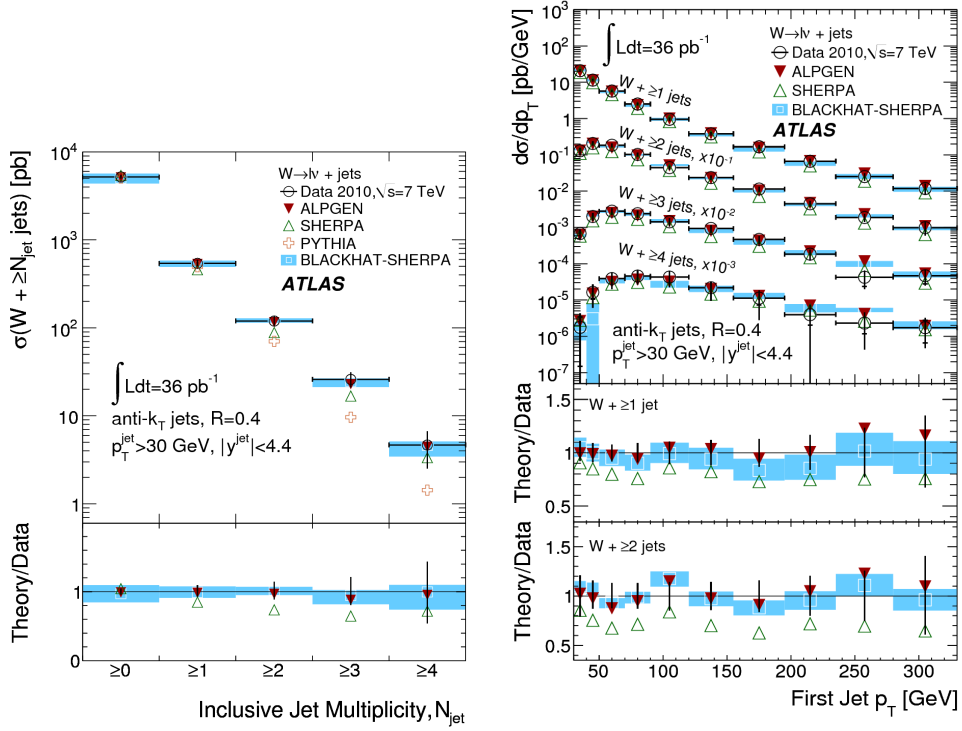


Fig. 15: The measured W +jets cross sections as a function of jet multiplicity (left) and as a function of the p_T of the first jet in the event (right). The p_T of the first jet is shown separately for events with ≥ 1 jet to ≥ 4 jets. Shown are predictions from ALPGEN, SHERPA and BlackHat-SHERPA, and the ratio of theoretical predictions to data (from Ref. [68]).

of the top quark, which has, however, been relatively precisely measured at the Tevatron collider to be $m_{\text{top}} = 173.2 \pm 0.90 \text{ GeV}$, i.e. with a precision of 0.5%. A further improvement here is important for a precise test of electroweak radiative corrections.

Due to the high mass, the top quarks decays mainly via $t \rightarrow Wb$ before it hadronizes. The production of $t\bar{t}$ pairs at the LHC proceeds mainly via gluon initiated processes and is expected to be a factor of 20 larger at the LHC with $\sqrt{s} = 7 \text{ TeV}$ than at the Tevatron. The decays studied are characterized by the number of charged leptons in the final state. A large fraction of the branching ratio is devoted to lepton-hadron decays, where one of the W s decays leptonically and the other one into a pair of jets, i.e. $t\bar{t} \rightarrow Wb Wb \rightarrow \ell\nu b q\bar{q}$. The final state in this case consists of a lepton, missing transverse momentum (carried away by the neutrino) and four jets out of which two are originating from b-quarks. The complementary dilepton decay mode is also important for top-quark physics at hadron colliders. The fully hadronic channel is more difficult to trigger on and shows a worse signal-to-background ratio, but despite this has also been measured at the LHC.

Both the ATLAS and CMS collaborations measured the production cross section for the pair production of top quarks in all above-mentioned final states [73–77]. The results are displayed in Fig. 16. The most precise measurement comes from the single lepton channel, which shows already a precision of the order of $\pm 7\%$. In this channel the cross sections are measured with and without the requirement of a b-tagged jet. The results obtained in the dilepton channel are consistent with these results. The measurements are found to be in good agreement with the approximate NNLO calculations [78, 79], although the experimental values are found to be about 1σ higher in each experiment. The experimental measurement is already limited by the experimental systematic uncertainties (jet energy scale, b-tagging,

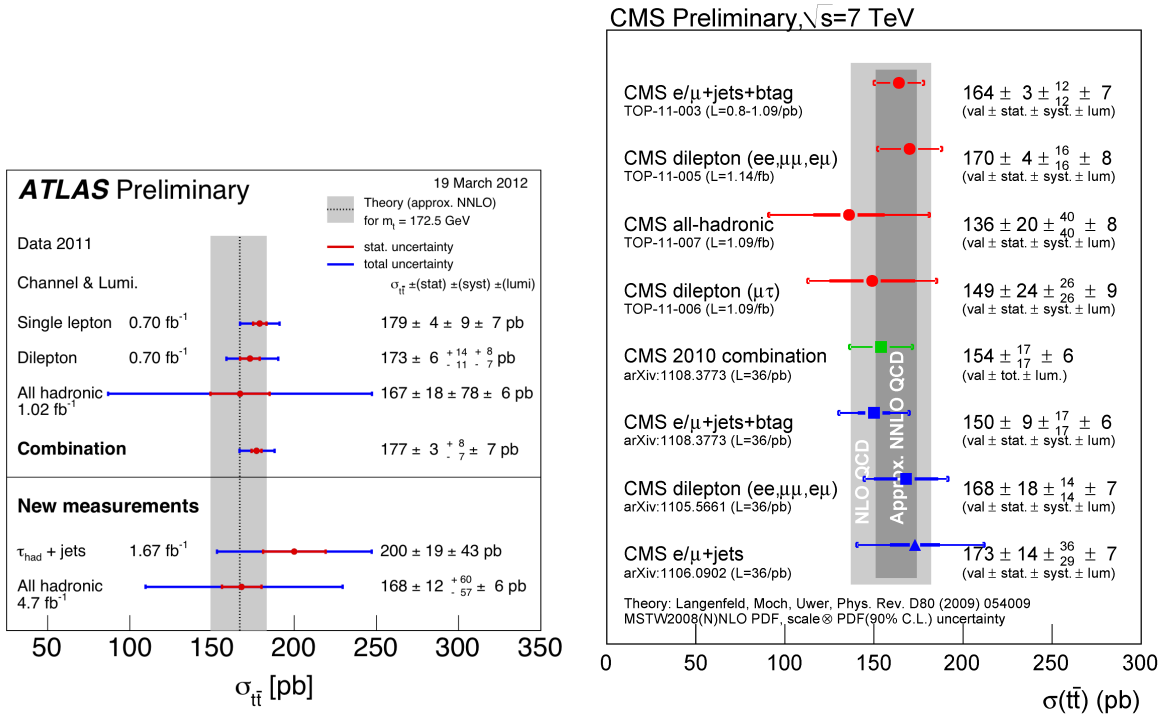


Fig. 16: The measured value of $\sigma_{t\bar{t}}$ in the various decay modes and the combination of these measurements from the ATLAS (left) and CMS (right) experiments. The approximate NNLO prediction with its uncertainty is also shown (from Refs. [74, 77]).

...) and by the uncertainty on the luminosity.

Single top quarks can be produced at the LHC via electroweak processes. The t -channel production of single top-quarks has been measured by both the ATLAS [80] ($L = 0.7 \text{ fb}^{-1}$) and CMS [81] ($L = 1.5 \text{ fb}^{-1}$) collaborations. The results are found to be consistent with the Standard Model expectations. The measured cross section value from the CMS collaboration is shown in Fig. 17 in comparison to the theoretical expectation and the measurements at the Tevatron.

4.3.2 Measurement of the top-quark mass

Among the various top-quark properties, the ATLAS and CMS collaborations have already presented first measurements on the top-quark mass m_t in several final states [82–85]. The most precise result was presented recently as a preliminary result by the CMS collaboration [84]. The top-quark mass has been measured using a sample of $t\bar{t}$ candidate events with one muon and at least four jets in the final state. The full 2011 data set corresponding to an integrated luminosity of 4.7 fb^{-1} was used. In this sample 2391 candidate events were selected and using a likelihood method the top-quark mass was measured from fits to kinematic distributions, simultaneously with the jet energy scale (JES). The result of $m_t = 172.6 \pm 0.6 \text{ (stat + JES)} \pm 1.2 \text{ (syst)} \text{ GeV}$ is consistent with the Tevatron result (see Fig. 17 (right)). It is impressive that such a precision, in particular on the systematic uncertainty, can be claimed after only two years of operation of the LHC. The dominant contribution to this systematic uncertainty results from uncertainties on the b -jet energy scale and from modelling uncertainties estimated via changes of the factorization scale [84]. However, it remains to be seen whether the small overall uncertainty can be confirmed by the ATLAS experiment. The results of the present measurements at the LHC are summarized in Fig. 17 together with the Tevatron results.

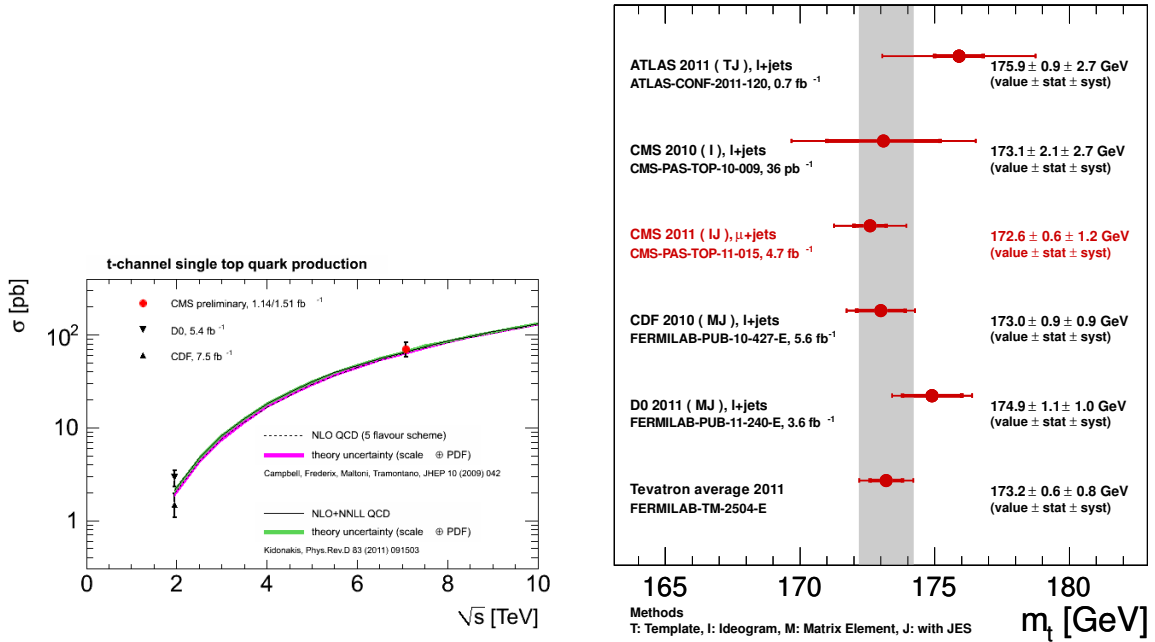


Fig. 17: (Left): Measured cross section for single-top quark production via the t -channel process in the CMS experiment in comparison to the theoretical expectation and the measurements at the Tevatron (from Ref. [81]). (Right): Compilation of the top-quark mass measurements from the ATLAS, CDF, CMS and DØ experiments (from Ref. [84]).

4.4 The production of diboson pairs

The production of pairs of bosons ($W\gamma$, WW , WZ , ZZ) at the LHC is of great interest since it provides an excellent opportunity to test the predictions on the structure of the gauge couplings of the electroweak sector of the Standard Model at the TeV energy scale. In addition, WW and ZZ pairs constitute the irreducible background in important Higgs boson search channels like $H \rightarrow WW$ and $H \rightarrow ZZ$.

The dominant Standard Model W^+W^- production mechanisms are s -channel and t -channel quark-antiquark annihilation. The s -channel production occurs only through the triple gauge coupling vertex and accounts for $\sim 10\%$ of the full W^+W^- production cross section. The leading-order Feynman diagrams for the dominant $q\bar{q}' \rightarrow W^+W^-$ production mechanisms at the LHC are shown in the left and middle diagrams of Fig. 18. The total cross section $\sigma(q\bar{q}, q\bar{q}') \rightarrow W^+W^-$ are known at next-to-leading order. The gluon fusion through quark loops, shown in the right diagram of Fig. 18, contributes an additional 2.9%.

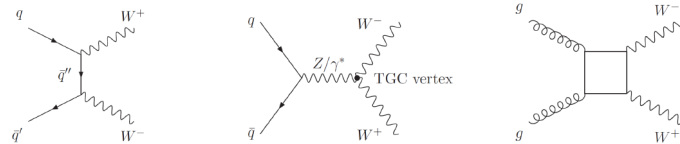


Fig. 18: (Left): The Standard Model tree-level Feynman diagram for W^+W^- production through the $q\bar{q}$ initial state in the t -channel. (Middle): The corresponding Standard Model tree-level diagram in the s -channel, which contains the WWZ and $WW\gamma$ triple gauge boson coupling (TGC) vertices. (Right): The gluon fusion process, mediated by quark loops.

The ZZ production proceeds at leading order via t -channel quark-antiquark interactions. The ZZZ and $ZZ\gamma$ triple gauge boson couplings (nTGCs) are absent. Hence there is no contribution from s -channel $q\bar{q}$ annihilation at tree level. Many models of physics beyond the Standard Model predict values of nTGCs at the level of 10^{-4} to 10^{-3} [86]. The signature of nonzero nTGCs is an increase of the ZZ cross section at high ZZ invariant mass and high transverse momentum of the Z bosons [87].

The ATLAS and CMS collaborations have measured the cross sections for all diboson production processes, $W\gamma$ [88, 89], WW [90–92], WZ [91, 93], ZZ [91, 94]. Several analyses are already based on the full data set from 2011. The results are found to be in good agreement with the predictions from the Standard Model and first constraints on anomalous triple gauge boson couplings have been set. The agreement between the measurements and the Standard Model predictions is shown for the WW and ZZ production in Fig. 19. The constraints on the triple gauge boson couplings are still limited by the number of observed diboson events.

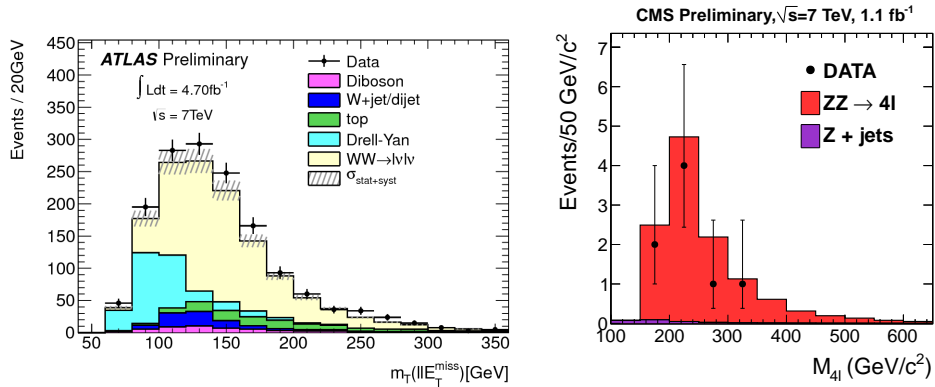


Fig. 19: (Left): The distributions of m_T of the dilepton+ E_T^{miss} system for the W^+W^- candidates in the ATLAS experiment (from Ref. [92]). (Right): The distribution of the four-lepton invariant mass for the ZZ candidate events in the CMS experiment (from Ref. [91]).

4.5 Summary

As discussed in the previous subchapters, the first two years have seen a very successful operation of the LHC collider and of the experiments. The data collected have been used to extract precise measurements of many Standard Model processes. They range from the measurement of W and Z production with cross sections in the order of picobarns via the measurement of $t\bar{t}$ production to the measurement of important diboson processes. The summary of all measured cross sections by the ATLAS collaboration is shown in Fig. 20 together with the theoretical predictions. Within the uncertainties, excellent agreement is found for all the processes considered. This is a remarkable achievement of the Standard Model and the underlying theoretical concepts, including QCD and factorization. The smallest cross sections measured, the diboson production cross sections, are extremely relevant for the Higgs boson search, as discussed in the next section.

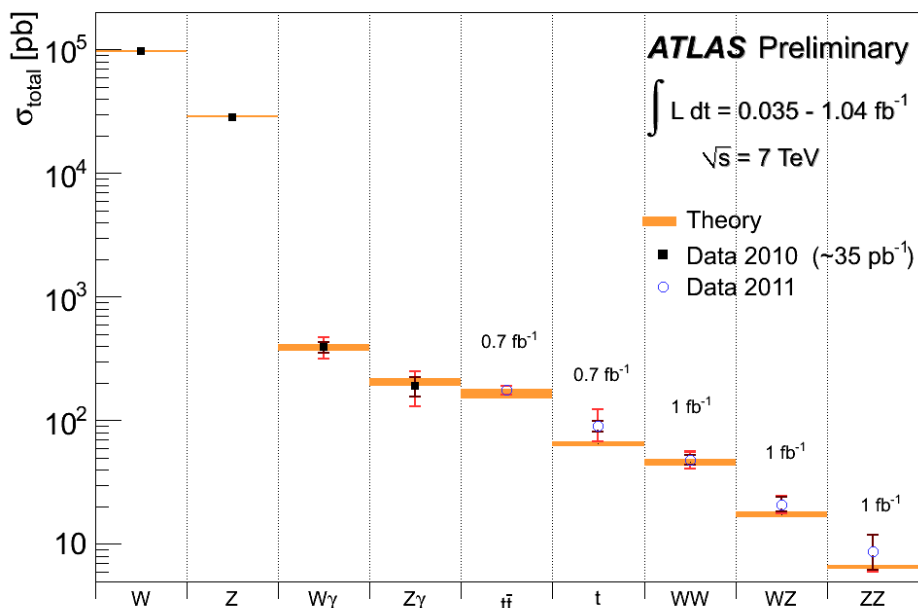


Fig. 20: Summary of several Standard Model total production cross-section measurements from the ATLAS collaboration compared to the corresponding theoretical expectations. The integrated luminosities used for the measurements are indicated on the figure. The dark error bars represent the statistical uncertainties. The red error bars represent the full uncertainties, including systematics and luminosity uncertainties. All theoretical expectations were calculated at NLO or higher.

5 Search for the Higgs boson

The Higgs boson is the only Standard Model particle that has not been discovered so far. Indirectly, high precision electroweak data constrain its mass via their sensitivity to radiative corrections. Assuming the overall validity of the Standard Model, a global fit [95] to all electroweak data leads to $m_H = 94^{+29}_{-24}$ GeV. On the basis of the present theoretical knowledge, the Higgs sector in the Standard Model remains largely unconstrained. While there is no direct prediction for the mass of the Higgs boson, an upper limit of ~ 1 TeV can be inferred from unitarity arguments [96].

Direct searches at the e^+e^- collider LEP has led to a lower bound on its mass of 114.4 GeV [99]. Before the LHC started its operation, the Fermilab Tevatron $p\bar{p}$ collider with a centre-of-mass energy of 1.96 TeV was the leading accelerator exploring the energy frontier. Until the end of data taking in September 2011, the two experiments CDF and $D\bar{O}$ have collected data corresponding to an integrated luminosity of 11.9 fb^{-1} . During the past years, they were able to exclude Higgs boson masses around 160 GeV, mainly based on the search for the $H \rightarrow WW^{(*)} \rightarrow \ell\nu\ell\nu$ decay mode. In Summer 2011, the combination of the results from the two experiments, based on data corresponding to an integrated luminosity of 8.6 fb^{-1} , excluded a mass range from 156 - 177 GeV [100]. At the same time, the first exclusions from the ATLAS and CMS experiments, based on a data corresponding to an integrated luminosity of up to 2.3 fb^{-1} , were presented. The ATLAS experiment excluded mass ranges from 146 - 230 GeV, 256-282 GeV and 296 - 459 GeV [101]. The CMS analysis was based on data corresponding to an integrated luminosity of up to 1.7 fb^{-1} and the Higgs boson was excluded in the mass ranges from 145 - 216 GeV, 226 - 288 GeV and 310 - 400 GeV [102].

Since then the full data set of the LHC taken until the end of 2011 has been analyzed. Preliminary results were presented in a special seminar at CERN in December 2011 and updates were presented at the

Moriond conference 2012. They created a lot of attention and excitement in the community since the data show tantalizing hints of a possible Higgs boson signal in the low mass region around 125 GeV. However, it must be stressed that the background-only probability still shows acceptable values, in particular if the look-elsewhere effect [103] is taken into account.

In the following, these results are summarized since they supersede those presented at the CERN school in September 2011. Before entering the discussion, the Higgs boson production at hadron colliders and the Higgs boson decay properties as well as a few statistical issues are briefly summarized.

5.1 Higgs boson production at the LHC

At hadron colliders, Higgs bosons can be produced via four different production mechanisms:

- gluon fusion, $gg \rightarrow H$, which is mediated at lowest order by a heavy quark loop;
- vector boson fusion (VBF), $qq \rightarrow qqH$;
- associated production of a Higgs boson with weak gauge bosons, $qq \rightarrow W/Z H$ (Higgs strahlung, Drell-Yan like production);
- associated Higgs boson production with heavy quarks, $gg, qq \rightarrow t\bar{t}H, gg, qq \rightarrow b\bar{b}H$ (and $gb \rightarrow bH$).

The dominant production mode is the gluon-fusion process, followed by the vector boson fusion. In the low mass region it amounts at leading order to about 20% of the gluon-fusion cross section, whereas it reaches the same level for masses around 800 GeV. The associated WH , ZH and $t\bar{t}H$ production processes are relevant only for the search of a light Standard Model Higgs boson with a mass close to the LEP limit.

The Higgs boson production cross sections are computed up to next-to-next-to-leading order (NNLO) [104] in QCD for the gluon-fusion process. In addition, QCD soft-gluon resummations up to next-to-next-to-leading log (NNLL) improve the NNLO calculation [105]. The next-to-leading order (NLO) electroweak corrections [106] are also applied, assuming factorization between QCD and electroweak corrections. The cross sections for the VBF process are calculated with full NLO QCD and electroweak corrections [108], and approximate NNLO QCD corrections are available [109]. The $W/Z H$ processes are calculated at NLO [110] and at NNLO [111], and NLO electroweak radiative corrections [112] are applied. Also for the associated $t\bar{t}H$ production the full NLO QCD corrections are available [113]. For a more detailed review of the theoretical aspects of Higgs boson production the reader is referred to Ref. [114]. The results of the calculations and the estimated theoretical uncertainties are shown for the different production processes in Fig. 21 (left) as a function of the Higgs boson mass [114].

5.2 Higgs boson decays

The branching ratios and the total decay width of the Standard Model Higgs boson are shown in Fig. 21 (right) as a function of the Higgs boson mass. They have been calculated taking into account both electroweak and QCD corrections [115, 116]. When kinematically accessible, decays of the Standard Model Higgs boson into vector boson pairs WW or ZZ dominate over all other decay modes. Above the kinematic threshold, the branching fraction into $t\bar{t}$ can reach up to 20%. All other fermionic decays are only relevant for Higgs boson masses below ~ 140 GeV, with $H \rightarrow b\bar{b}$ dominating. The branching ratios for both $H \rightarrow \tau\tau$ and $H \rightarrow gg$ reach up to about 8% at Higgs boson masses between 100 and 120 GeV. Decays into two photons, which are of interest due to their relatively clean experimental signature, can proceed via charged fermion and W loops with a branching ratio of up to $2 \cdot 10^{-3}$ at low Higgs boson masses.

Compared to the mass resolution of hadron collider experiments, the total decay width of the Standard Model Higgs boson is small at low masses and becomes significant only above the threshold

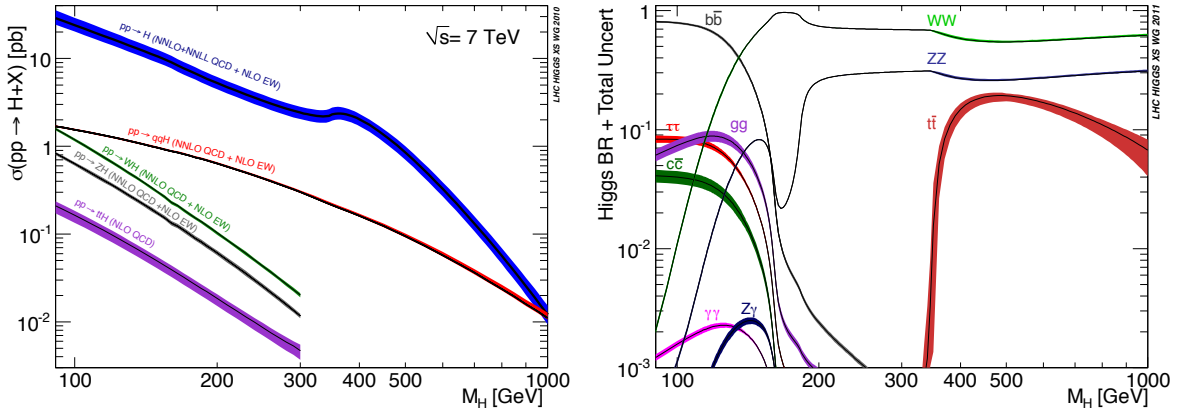


Fig. 21: (Left): Production cross sections for the different production processes for a Standard Model Higgs boson as a function of the Higgs boson mass at the LHC. (Right): Branching ratios of the Standard Model Higgs boson as a function of Higgs boson mass (from Ref. [114]).

for decays into ZZ . For a Higgs boson with a mass of ~ 1 TeV the resonance is broad with a width of about 600 GeV. In this mass regime, the Higgs field is coupling strongly, resulting in large corrections [114, 117].

5.3 Search for the Standard Model Higgs boson at the LHC

The Standard Model Higgs boson is searched for at the LHC in various decay channels, the choice of which is given by the signal rates and the signal-to-background ratios in the different mass regions. The search strategies and background rejection methods have been established in many studies over the past years [118]. Among the most important channels are the inclusive $H \rightarrow \gamma\gamma$ and $H \rightarrow ZZ^{(*)} \rightarrow llll$ decay channels. These channels are characterized by a very good mass resolution. In the low mass region, the Higgs boson appears as a sharp resonance, the width of which is dominated by the detector resolution, on top of flat backgrounds which are dominated by $\gamma\gamma$ and ZZ continuum production, respectively. In addition, the $H \rightarrow WW$ decay mode contributes in particular in the mass region around 160 GeV, however, due to the neutrinos in the final state, no mass peak can be reconstructed. Evidence for Higgs boson production is given by a broad peak in the transverse mass distribution (see below). From the fermionic decays, only the modes $H \rightarrow \tau\tau$ and $H \rightarrow b\bar{b}$ have a chance to be detected. For the $H \rightarrow \tau\tau$ decays the selection of the vector boson fusion production mode is important to improve the signal-to-background ratio by exploiting forward jet tagging [121]. The $b\bar{b}$ decay mode is searched for in the associated production of the Higgs boson with a vector boson or with a $t\bar{t}$ pair [122, 123].

In the following the present status (March 2012) of the Higgs boson search in the various final states at the LHC is described. Before the individual channels are discussed some common issues on the statistical treatment are given. At the end of this section the combination of the results is presented for both the ATLAS and CMS collaborations.

5.3.1 Limit setting, statistical issues

In the following the distributions of reconstructed masses or other distributions as measured in data are compared to the expectations from Standard Model background processes. In order to test the compatibility of the data with the background-only hypothesis a so-called p_0 probability value is calculated. It quantifies the probability that a background-only experiment is more signal-like than that observed. The *local* p_0 probability is assessed for a fixed m_H hypothesis and the equivalent formulation in terms of number of standard deviations is referred to as the *local* significance. Since fluctuations of the back-

ground could occur at any point in the mass range the results have to be corrected for the look-elsewhere effect [103]. The probability for a background-only experiment to produce a local significance of this size or larger anywhere in a given mass region is referred to as the *global* p_0 . The corresponding reduction in the significance is estimated using the prescription described in Ref. [124].

The data can also be used to set 95% confidence level (C.L.) upper limits (σ_{95}) on the cross section for Higgs boson production. These cross sections are usually normalized to the expected Standard Model value (σ_{95}/σ_{SM}). All exclusion limits quoted in the following have been calculated using the CL_s method [125]. In addition to the *observed* limits based on the observed data, also the *expected* limits are calculated. They are calculated as a function of m_H and are based on the central values of the expected background in case no Higgs signal is present. The 1σ and 2σ fluctuations around the expected exclusion limits are calculated as well.

Excluded mass regions are determined from a comparison of the observed cross-section limit to the Standard Model cross-section value. If the observed value of σ_{95}/σ_{SM} is smaller than 1 (Standard Model cross-section expectation) for a particular hypothetical Higgs boson mass, this mass value can be excluded with a confidence level of 95%. Systematic uncertainties are incorporated by introducing nuisance parameters with constraints. Asymptotic formulae [126] are used to derive the limits and p_0 values. This procedure has been validated using ensemble tests and a Bayesian calculation of the exclusion limits with a uniform prior on the signal cross section. These approaches to the limits typically agree with the asymptotic median results to within a few percent [127].

5.3.2 Search for $H \rightarrow \gamma\gamma$ decays

The decay $H \rightarrow \gamma\gamma$ is a rare decay mode, which is only detectable in a limited Higgs boson mass region between 100 and 150 GeV, where both the production cross section and the decay branching ratio are relatively large. Excellent energy and angular resolution are required to observe the narrow mass peak above the irreducible prompt $\gamma\gamma$ continuum. In addition, there is a reducible background resulting from direct photon production or from two-jet production via QCD processes. These processes contribute if one or both jets are misidentified as a photon. The background can be determined from a fit to the data (sidebands) such that uncertainties from Monte Carlo predictions or uncertainties due to normalizations in control regions are avoided. Due to the rather large amount of material in the tracking detectors of the LHC experiments there is a high probability for a photon to undergo conversion and therefore both unconverted and converted photons need to be reconstructed.

Both collaborations have presented results on the $H \rightarrow \gamma\gamma$ search in a mass range between 110 and 150 GeV based on the full data set collected until the end of 2011 [128, 129]. The ATLAS analysis [128] separates events into nine independent categories. The categorisation is based on the direction of each photon and whether it was reconstructed as a converted or unconverted photon, together with the momentum component of the diphoton system transverse to the thrust axis. The distribution of the invariant mass of the diphoton events, $m_{\gamma\gamma}$, summed over all categories, is shown in Fig. 22 (left). The fit to the background is performed separately in each category in the mass range 100 - 160 GeV by using an exponential function with free slope and normalization parameters. The result for the total sample is superimposed in Fig. 22. The signal expectation for a Higgs boson with $m_H = 120$ GeV is also shown. The mass resolution depends on the classification of the photon (calorimeter η region, conversion status) and is found to be 1.4 GeV in the best category and 1.7 GeV on average. The residuals of the data with respect to the total background as a function of $m_{\gamma\gamma}$ is also shown in Fig. 22. Around a mass of 126 GeV an excess of events above the background is seen (see discussion below). The 95% C.L. upper limits on the cross section for Higgs boson production normalized to the Standard Model value, σ_{95}/σ_{SM} , are shown in Fig. 22 (right). The observed exclusion limits follow well the expectations over a large mass range, except in the region around 126 GeV. The ATLAS data allow for a 95% C.L. exclusion of a Standard Model Higgs boson in the mass ranges between 113–115 GeV and 134.5–136 GeV.

The analysis of the CMS collaboration [129] is done in a similar way. Diphoton events are split

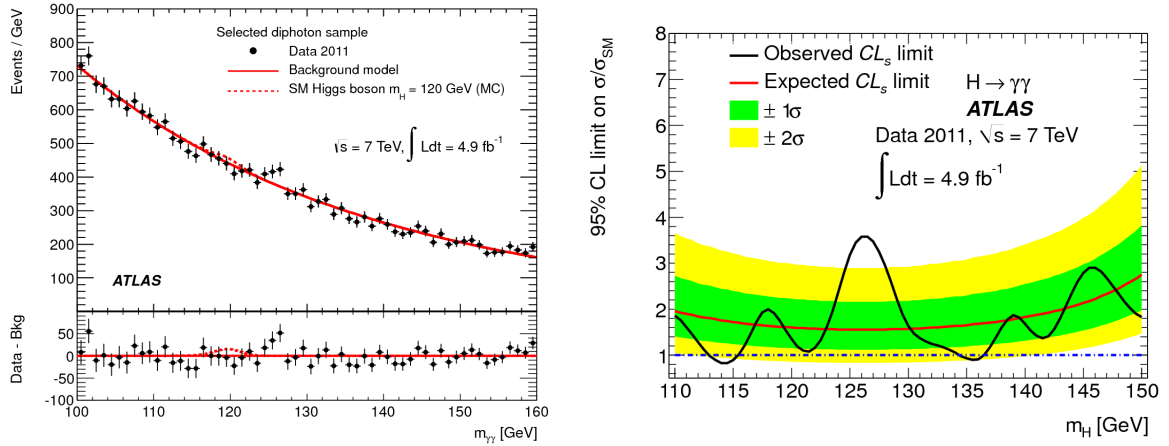


Fig. 22: (Left): Invariant mass distribution for the selected data sample in the ATLAS experiment, overlaid with the total background (see text). The bottom inset displays the residual of the data with respect to the total background. The Higgs boson expectation for a mass hypothesis of 120 GeV corresponding to the Standard Model cross section is also shown. (Right): Observed and expected 95% C.L. limits on the Standard Model Higgs boson production cross section normalized to the predicted one as a function of m_H (from Ref. [128]).

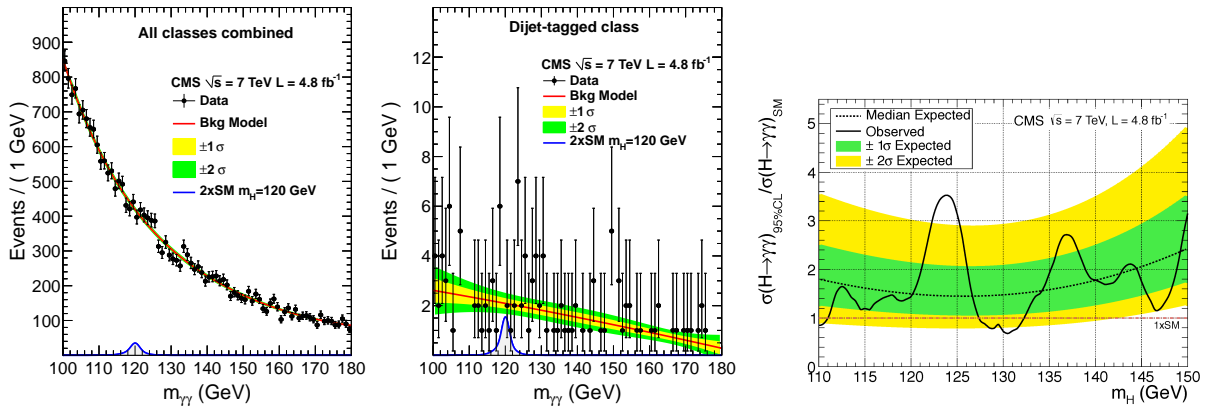


Fig. 23: (Left): Invariant mass distribution for the selected data sample in the CMS experiment, overlaid with the total background. (Middle): The invariant mass distribution for diphotons fulfilling the VBF selection (see text). The Higgs boson expectation for a mass hypothesis of 120 GeV corresponding to the Standard Model cross section multiplied by a factor of two is also shown. (Right): Observed and expected 95% C.L. limits on the Standard Model Higgs boson production cross section normalized to the predicted one as a function of m_H (from Ref. [129]).

into four categories depending on their η value and shower shape characteristics (to distinguish converted from unconverted photons). The diphoton mass resolution is best for the class of two central unconverted photons and reaches a value of 1.2 GeV (full width at half maximum divided by 2.35) for a Higgs boson mass of 120 GeV. Including the other classes a weighted average resolution of ~ 1.8 GeV is found. A further class of events is introduced to select the vector boson fusion topology (VBF topology). By requiring two jets with a large separation in pseudorapidity, a class of events is defined for which the expected signal-to-background ratio is about an order of magnitude larger than for the events in the four classes defined by photon properties. The $m_{\gamma\gamma}$ distributions observed in the data for the sum of the five event classes and for the VBF topology separately are shown in Fig. 23 (left, middle) together with the background fits based on polynomial functions. The uncertainty bands shown are computed from the

fit uncertainty on the background yields. The limit set on the cross section of a Higgs boson decaying to two photons normalized to the Standard Model value is shown in Fig. 23 (right). The CMS analysis excludes at the 95% C.L. the Standard Model Higgs boson decaying into two photons in the mass range 128 to 132 GeV. However, it should be noted that this exclusion, as well as the ATLAS exclusions in this channel, are *lucky* since the expected sensitivities are larger than one and the observed values of $\sigma_{95}/\sigma_{\text{SM}}$ are at the edges of the 2σ bands. The fluctuations of the observed limit about the expected limit are consistent with statistical fluctuations to be expected in scanning the mass range. The largest deviation in the CMS experiment is seen at $m_{\gamma\gamma} = 124$ GeV.

In order to quantify the fluctuations seen in both experiments, the probabilities for the background-only hypothesis have been calculated. The observed and expected local p_0 values obtained are displayed in Fig. 24 for the ATLAS (left) and CMS (right) data. Before considering the uncertainty on the signal mass position, the largest excess with respect to the background-only hypothesis in the mass range 110–150 GeV is observed at 126.5 GeV in the ATLAS data with a local significance of 2.9σ . The uncertainty on the mass position (± 0.7 GeV) due to the imperfect knowledge of the photon energy scale has a small effect on the significance. When this uncertainty is taken into account, the significance is slightly reduced to 2.8σ . The local p_0 value corresponding to the largest upwards fluctuation in the CMS data at 124 GeV has a significance of 3.1σ . The observed significances reduce to 1.5σ for ATLAS and 1.8σ for CMS, when the look-elsewhere effect is taken into account over the mass range 110–150 GeV.

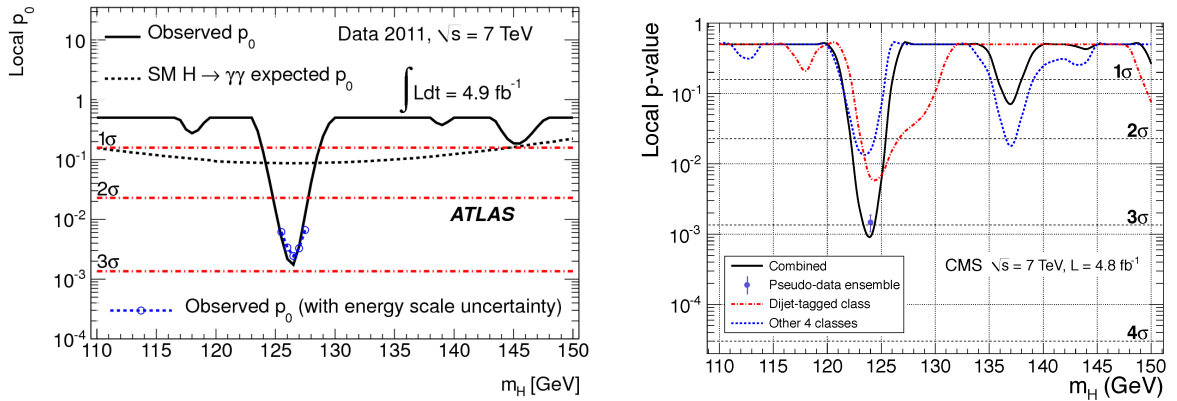


Fig. 24: The observed local p_0 , the probability that the background fluctuates to the observed number of events or higher, for the ATLAS (left) and CMS (right) data. In the ATLAS case, the open points indicate the observed local p_0 value when energy scale uncertainties are taken into account. The dotted line shows the expected median local p_0 for the signal hypothesis when tested at m_H . In the CMS case, the p_0 values are shown for the VBF-tagged class separately (from Refs. [128, 129]).

5.3.3 Search for $H \rightarrow ZZ^{(*)} \rightarrow \ell\ell\ell\ell$ decays

The decay channel $H \rightarrow ZZ^{(*)} \rightarrow \ell\ell\ell\ell$ provides a rather clean signature in the mass range $115 \text{ GeV} < m_H < 2 m_Z$. In addition to the irreducible backgrounds from ZZ^* and $Z\gamma^*$ production, there are large reducible backgrounds from $t\bar{t}$ and $Zb\bar{b}$ production. Due to the large production cross section, the $t\bar{t}$ background dominates at production level, whereas the $Zb\bar{b}$ events contain a genuine Z boson in the final state and are therefore more difficult to reject. In addition, there is background from ZZ continuum production, where one of the Z bosons decays into a τ pair, with subsequent leptonic decays of the τ leptons, and the other Z decays into an electron or muon pair.

Both collaborations have performed the $H \rightarrow ZZ^{(*)} \rightarrow \ell\ell\ell\ell$ search for m_H hypotheses in the full 110 to 600 GeV mass range using data corresponding to an integrated luminosity of $\sim 4.8 \text{ fb}^{-1}$ [130,

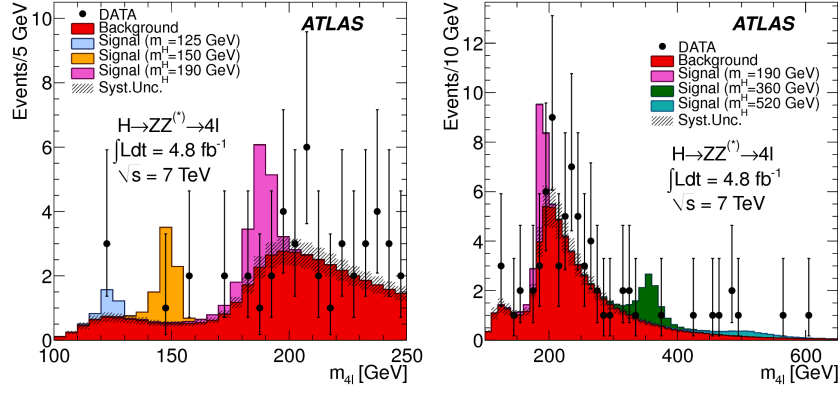


Fig. 25: Distributions of the four-lepton invariant mass, $m_{4\ell}$ of the selected candidates, compared to the background expectation for the 100 - 250 GeV mass range (left) and the full mass range (right) in the ATLAS experiment. The signal expectations for several m_H hypotheses are also shown (from Ref. [130]).

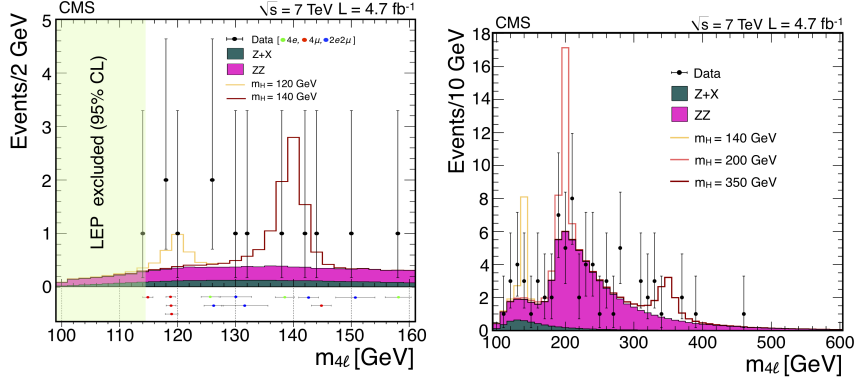


Fig. 26: Distributions of the four-lepton invariant mass, $m_{4\ell}$ of the selected candidates, compared to the background expectation for the 100 - 160 GeV mass range (left) and the full mass range (right) in the CMS experiment. The signal expectations for several m_H hypotheses are also shown (from Ref. [131]).

[131]. It has been shown that in both experiments calorimeter and track isolation requirements together with impact parameter requirements can be used to suppress the irreducible background well below the irreducible ZZ^* continuum background. The residual irreducible Z +jets and $t\bar{t}$ backgrounds, which have an impact mostly for low invariant four-lepton masses, are estimated from control regions in the data. The irreducible ZZ^* background is estimated using Monte Carlo simulation. The events are categorised according to the lepton flavour combinations. Mass resolutions of approximately 1.5% in the four-muon channel and 2% in the four-electron channel are achieved at $m_H \sim 120$ GeV [130]. The four-lepton invariant mass is used as a discriminant variable. The observed and expected mass distributions for events selected after all cuts are displayed in Figs. 25 and 26 for the ATLAS and CMS experiments, respectively.

The measured mass distributions are again confronted to the background-only hypotheses. The corresponding p_0 values are shown in Fig. 27 for the two experiments. In the ATLAS experiment large upward deviations from the background-only hypothesis are observed for $m_H = 125$ GeV, 244 GeV and 500 GeV with local significances of 2.1σ , 2.2σ and 2.1σ , respectively. After accounting for the look-elsewhere effect none of these excesses is significant. The CMS collaboration observes excesses of events around 119 GeV, 126 GeV and 320 GeV. The most significant excess for a mass value near

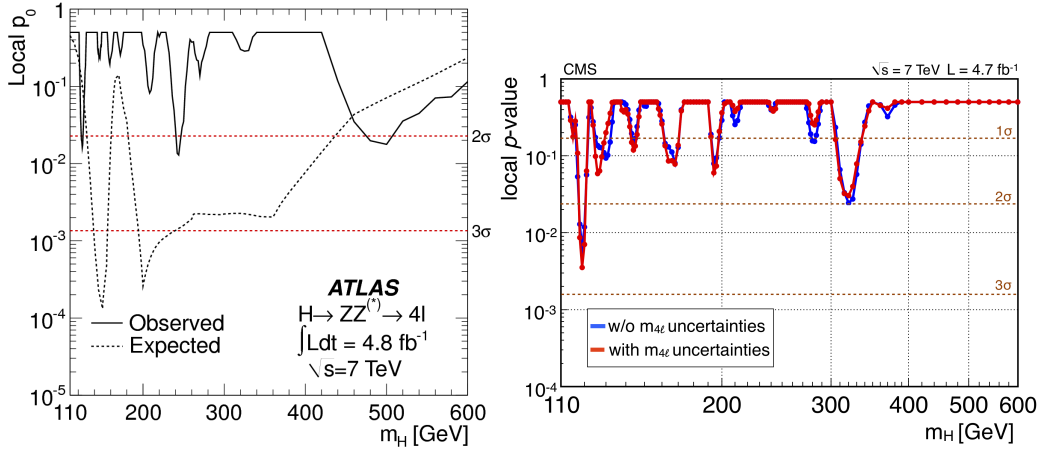


Fig. 27: The observed local p_0 values as a function of the Higgs boson mass in the $H \rightarrow ZZ^{(*)} \rightarrow \ell\ell\ell\ell$ channel in the ATLAS (left) and CMS (right) experiments. The dashed curve shows the expected median local p_0 . The horizontal lines indicate values of constant significance of 1σ , 2σ and 3σ (from Refs. [130, 131]).

119 GeV corresponds to a local (global) significance of about 2.5σ (1.0σ).

5.3.4 Search for $H \rightarrow WW^{(*)} \rightarrow \ell\nu\ell\nu$ decays

The decay mode $H \rightarrow WW^{(*)} \rightarrow \ell\nu\ell\nu$ has the highest sensitivity for Higgs boson masses around 170 GeV. Based on searches in this channel, mass regions could be excluded by both the Tevatron and the LHC experiments already in Summer 2011 [100–102]. However, this channel is more challenging in the low mass region around 125 GeV since due to the reduced $H \rightarrow WW$ branching ratio the expected signal rates are small. Due to the presence of neutrinos it is not possible to reconstruct a Higgs boson mass peak and evidence for a signal must be extracted from an excess of events above the expected backgrounds. Usually, the WW transverse mass (m_T), computed from the leptons and the missing transverse momentum,

$$m_T = \sqrt{(E_T^{\ell\ell} + E_T^{\text{miss}})^2 - |\mathbf{p}_T^{\ell\ell} + \mathbf{p}_T^{\text{miss}}|^2},$$

where $E_T^{\ell\ell} = \sqrt{|\mathbf{p}_T^{\ell\ell}|^2 + m_{\ell\ell}^2}$, $|\mathbf{p}_T^{\text{miss}}| = E_T^{\text{miss}}$ and $|\mathbf{p}_T^{\ell\ell}| = p_T^{\ell\ell}$, is used to discriminate between signal and background. The WW , $t\bar{t}$ and single-top production processes constitute severe backgrounds and the signal significance depends critically on their absolute knowledge.

The analyses of the ATLAS and CMS collaborations are based on the full data set ($\sim 4.7 \text{ fb}^{-1}$) [132, 133]. In order to optimize the sensitivity, the analyses are split into different lepton final states (ee , $e\mu$ and $\mu\mu$) and different jet multiplicities. In addition, they have been optimized for different mass regions (low and high mass). Typical selection cuts require the presence of two isolated high p_T leptons with a significant missing transverse energy and a small azimuthal angular separation. The latter requirement is motivated by the decay characteristics of a spin-0 Higgs boson decaying into two W bosons with their subsequent $W \rightarrow \ell\nu$ decay [134]. The various jet categories are sensitive to different Higgs boson production mechanisms and have very different background compositions. The 0-jet category is mainly sensitive to the gluon-fusion process and has the non-resonant WW production as major background. The 2-jet category is more sensitive to the vector-boson fusion process, with $t\bar{t}$ as dominant background. As a final discriminant the WW transverse mass distribution is used. This distribution is shown in Fig. 28 (left) for events passing the 0-jet selection in ATLAS. The observed data are well described by the expected background contributions which are dominated by the WW production. As another example, Fig. 29 (left) shows the distribution of the azimuthal angle difference

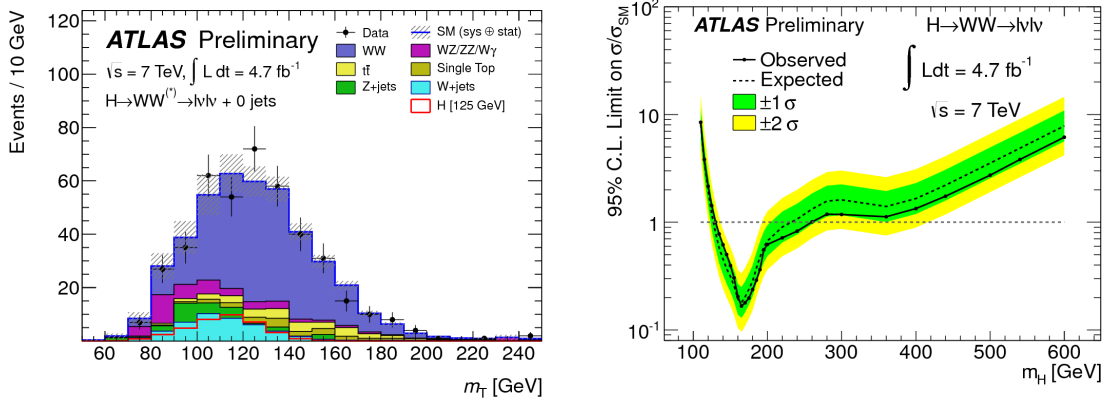


Fig. 28: (Left): The distribution of the transverse mass m_T in the $H+0$ jet channel of the ATLAS analysis. The expected signal for a Standard Model Higgs boson with $m_H = 125$ GeV is superimposed. (Right): Expected (dashed) and observed (solid) 95% C.L. upper limits on the cross section, normalized to the Standard Model cross section, as a function of m_H . The results at neighbouring mass points are highly correlated due to the limited mass resolution in this final state (from Ref. [132]).

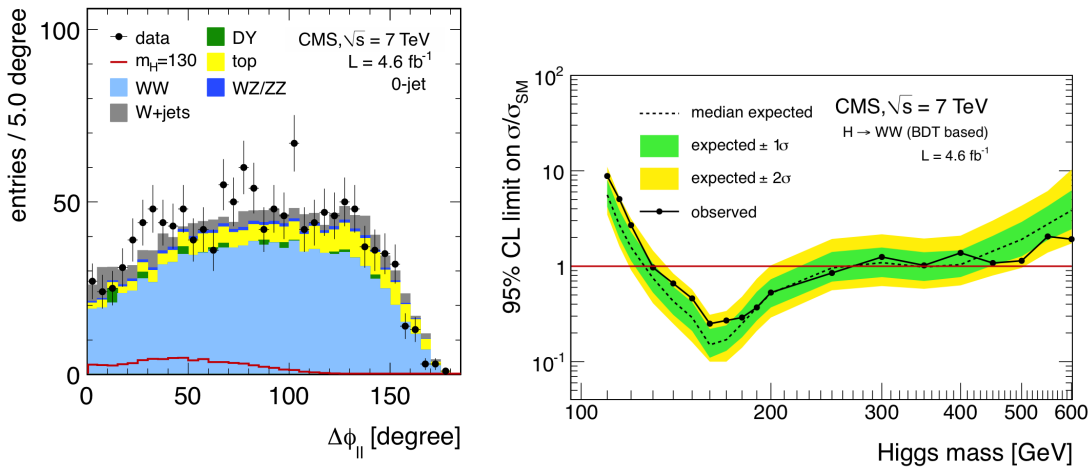


Fig. 29: (Left): The distribution of the azimuthal angle separation $\Delta\phi_{\ell\ell}$ in the $H+0$ jet channel of the CMS analysis. The expected signal for a Standard Model Higgs boson with $m_H = 130$ GeV is superimposed. (Right): Expected (dashed) and observed (solid) 95% C.L. upper limits on the cross section, normalized to the Standard Model cross section, as a function of m_H . The results at neighbouring mass points are highly correlated due to the limited mass resolution in this final state (from Ref. [133]).

($\Delta\phi_{\ell\ell}$) between the two selected leptons for events in the 0-jet category in the CMS experiment. Also this distribution is well described by the expected background processes. To enhance the sensitivity, the CMS experiment exploits two different analysis strategies for the 0-jet and 1-jet categories, the first one using a cut-based approach and the second one using a multivariate technique [133].

Since no significant excesses of events are found in any of the event categories in both the ATLAS and CMS experiments, upper limits on the production cross section are set, as shown in Figs. 28 and 29. The ATLAS experiment excludes the existence of a Standard Model Higgs boson over a mass range from 130 - 260 GeV, while the expected exclusion, in case no Higgs boson is present, is $127 \leq m_H \leq$

234 GeV. The CMS experiments excludes a mass range from 129 - 270 GeV, with an expected range from 127 - 270 GeV.

5.3.5 Search for $H \rightarrow \tau\tau$ and $H \rightarrow b\bar{b}$ decays

In addition to the searches described above, the search for the Higgs boson has also been performed in the $H \rightarrow \tau\tau$ [135,136] and $H \rightarrow b\bar{b}$ final states [137,138]. These searches do not yet reach the sensitivity of the others described above. They are, however, included in the overall combination of the results of the two collaborations [139,140]. The observed and expected cross section limits are included in Fig. 31.

5.3.6 Search for the Higgs boson in the high mass region

For higher Higgs boson masses ($m_H > 2m_Z$) the decays $H \rightarrow WW$ and $H \rightarrow ZZ$ dominate. Due to the higher mass and improved signal-to-background conditions, also the decays $H \rightarrow ZZ \rightarrow \ell\ell\nu\nu$ [141,142], $H \rightarrow ZZ \rightarrow \ell\ell qq$ [143,144], $H \rightarrow ZZ \rightarrow \ell\ell\tau\tau$ [145] and $H \rightarrow WW \rightarrow \ell\nu qq$ [146] provide additional sensitivity.

The $H \rightarrow ZZ \rightarrow \ell\ell\nu\nu$ is the most sensitive channel. The selection of two leptons and large missing transverse energy gives rather good signal-to-background conditions. The dominant backgrounds are from diboson and $t\bar{t}$ production. Also in this case the transverse mass m_T of the $\ell\ell - E_T^{\text{miss}}$ system is used as discriminating variable. The distributions are shown in Fig. 30 for the ATLAS (left) and CMS (right) experiments together with expected signals at 400 GeV. No indications for excesses are seen and upper limits on the Higgs boson production cross sections are set. They are included as well in Fig. 31.

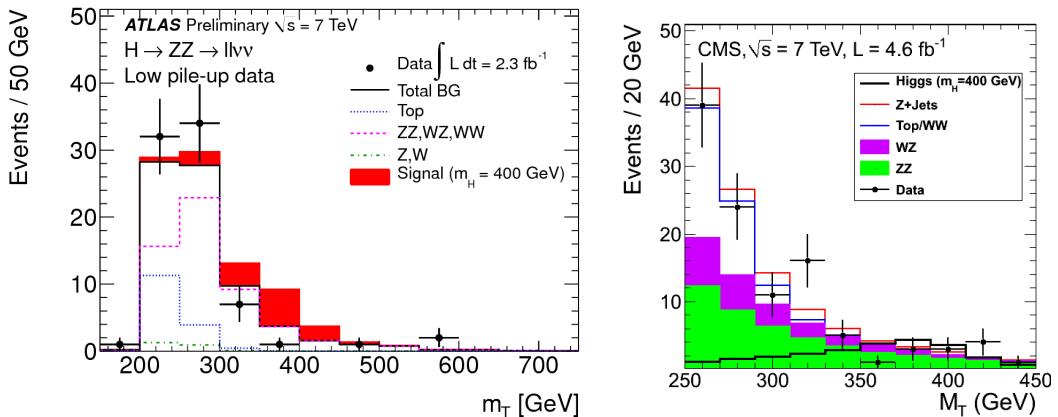


Fig. 30: The distributions of the transverse mass of $H \rightarrow ZZ \rightarrow \ell\ell\nu\nu$ candidates in the ATLAS (left) and CMS (right) experiments. Expected signals for a Higgs boson with a mass of 400 GeV are superimposed (from Refs. [141,142]).

5.4 Combination results of searches for the Standard Model Higgs boson

5.4.1 Excluded mass ranges

The ATLAS and CMS experiments have combined their respective search results on the Standard Model Higgs boson [139,140]. The combination procedure is based on the profile likelihood ratio test statistic $\lambda(\mu)$ [126], which extracts the information on the signal strength $\mu = \sigma/\sigma_{\text{SM}}$ from a full likelihood including all the parameters describing the systematic uncertainties and their correlations. More details on the statistical procedure used are described in Ref. [124].

In Figure 31 the expected and observed 95% C.L. limits are shown from the individual channels entering this combination, separately for the ATLAS and CMS experiments. The combined 95% C.L.

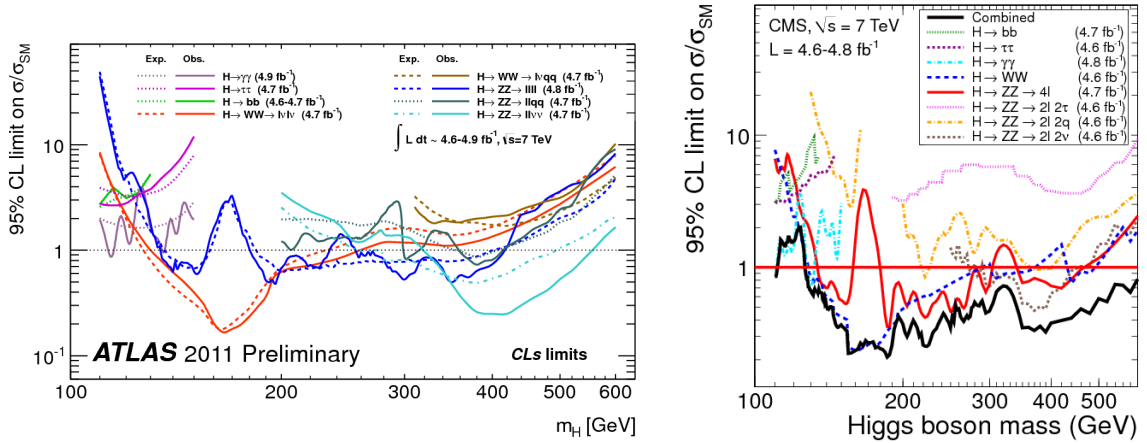


Fig. 31: The observed (solid) and expected (dashed) 95% C.L. cross section upper limits for the individual search channels in the ATLAS (left) and CMS (right) experiments, normalized to the Standard Model Higgs boson production cross section, as a function of the Higgs boson mass. The expected limits are those for the background-only hypothesis, i.e. in the absence of a Higgs boson signal (from Refs. [139, 140]).

exclusion limits are shown in Fig. 32 as a function of m_H for the full mass range and for the low mass range. The combined expected 95% C.L. exclusion regions for the two experiments are very similar and cover the m_H range from 120 to 555 GeV for the ATLAS and from 118 to 543 GeV for the CMS experiment. Based on the observed limit, the ATLAS experiment excludes at the 95% C.L. the Standard Model Higgs boson in three mass ranges: from 110.0 - 117.5 GeV, from 118.5 to 122.5 GeV and from 129 to 539 GeV. The 95% C.L. CMS exclusion covers the range 127 - 600 GeV. The observed exclusion covers a large part of the expected exclusion range, with the exception of the low mass region where an excess of events above the expected background is observed. It is striking that both experiments are not able to cover the mass window from about 118 to 129 GeV, despite their sensitivity in this range.

5.4.2 Compatibility with the background-only hypothesis

Excesses of events are observed in the ATLAS experiment near 126 GeV in the $H \rightarrow \gamma\gamma$ and $H \rightarrow ZZ^{(*)} \rightarrow llll$ channels, both of which provide fully reconstructed candidates with high-resolution in invariant mass. The CMS experiment observes two localized excesses, one at 119.5 GeV associated with three $Z \rightarrow 4l$ events and the other one at 124 GeV, arising mainly from the $\gamma\gamma$ channel. In addition, a broad offset of about one standard deviation is seen for the low resolution channels $H \rightarrow WW$, $H \rightarrow \tau\tau$ and $H \rightarrow b\bar{b}$. The observed local p_0 values, calculated using the asymptotic approximation, as a function of m_H and the expected value in the presence of a Standard Model Higgs boson signal are shown in Fig. 33 in the low mass region for the two experiments.

In the ATLAS data the local significance for the combined result reaches 2.6σ for $m_H=126$ GeV with an expected value in the presence of a signal at that mass of 2.9σ . The local significance for the combination of the CMS channels at $m_H = 124$ GeV amounts to 3.1σ

The significance of the excesses is mildly sensitive to energy scale systematic (ESS) uncertainties and the resolution for photons and electrons. The observed effect of the ESS uncertainty is small and reduces the maximum local significance in the ATLAS experiment from 2.6σ to 2.5σ .

The global p_0 for local excesses depends on the range of m_H and the channels considered. The global probability for an excess as large as the one observed in the ATLAS combination at 126 GeV to occur anywhere in the mass range 110–600 GeV is estimated to be approximately 30%, decreasing to 10% in the range 110–146 GeV, which is not excluded at the 99% confidence level by the LHC combined Standard Model Higgs boson search [147]. The global significance for the CMS excess is estimated to

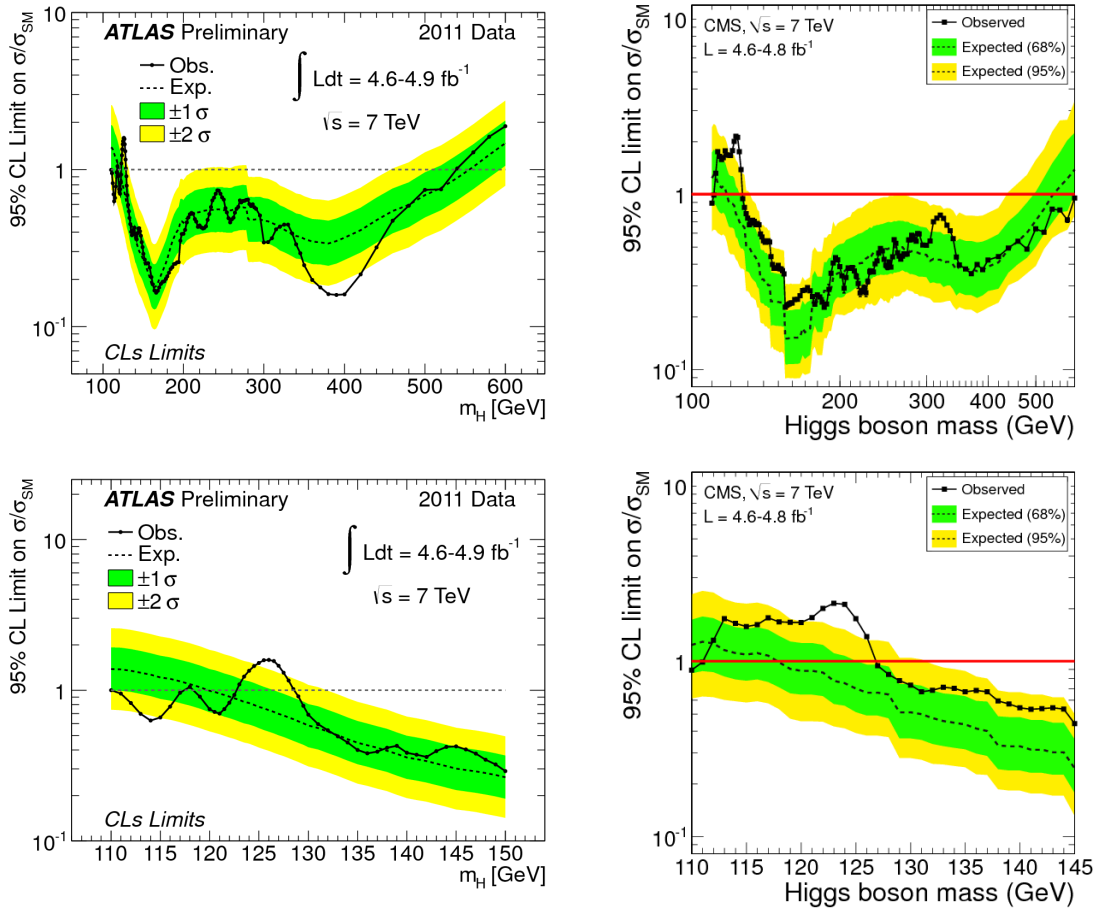


Fig. 32: The observed (full line) and expected (dashed line) 95% C.L. combined upper limits on the Standard Model Higgs boson production cross section divided by the Standard Model expectation as a function of m_H in the full mass range considered in the analyses (top) and in the low mass range (bottom) for the ATLAS (left) and CMS (right) experiments. The dotted curves show the median expected limit in the absence of a signal and the green and yellow bands indicate the corresponding 68% and 95% intervals (from Refs. [139, 140]).

be 1.5σ for the full search range from 110–600 GeV and 2.1σ for the restricted search range from 110–145 GeV.

The best-fit value of μ , denoted $\hat{\mu}$, is displayed for the combination of all channels for the two experiments in Fig. 34. The bands around $\hat{\mu}$ illustrate the μ interval corresponding to $-2 \ln \lambda(\mu) < 1$ and represent an approximate $\pm 1\sigma$ variation. The excess observed for $m_H = 126$ GeV in the ATLAS experiment corresponds to $\hat{\mu}$ of approximately $0.9^{+0.4}_{-0.3}$, which is compatible with the signal strength expected from a Standard Model Higgs boson at that mass ($\mu = 1$). Also for the CMS experiment the $\hat{\mu}$ values are within one sigma of unity in the mass range from 117–126 GeV.

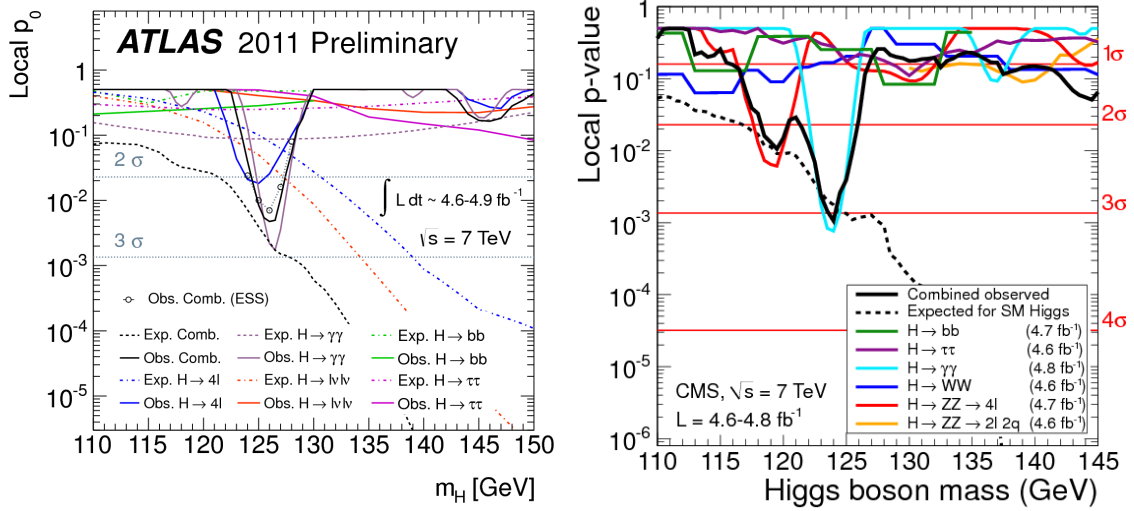


Fig. 33: The local probability p_0 for a background-only experiment to be more signal-like than the observation in the low mass range as a function of m_H for the ATLAS (left) and CMS (right) experiments. The p_0 values are shown for individual channels as well as for the combination. The dashed curves show the median expected local p_0 under the hypothesis of a Standard Model Higgs boson production signal at that mass. The horizontal dashed lines indicate the p values corresponding to significances of 1σ to 5σ (from Refs. [139, 140]).

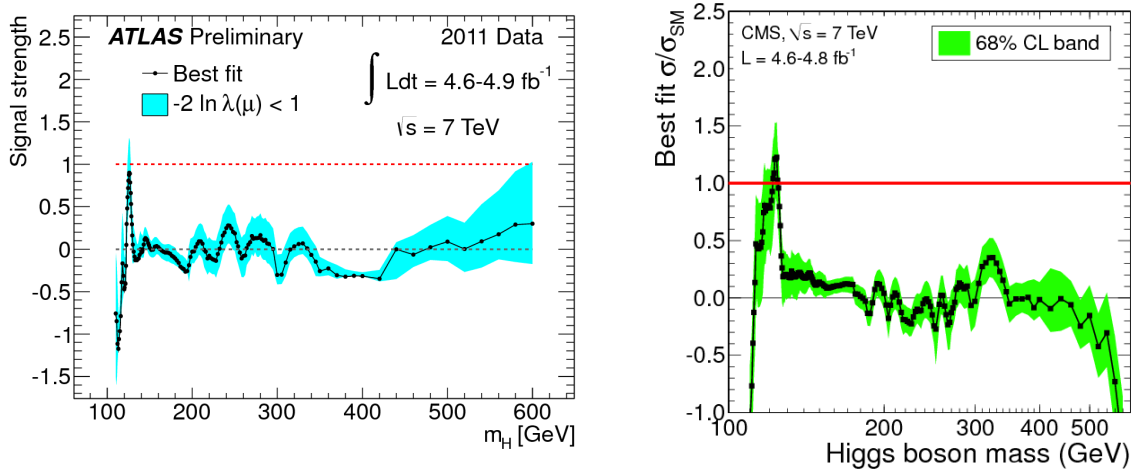


Fig. 34: The best-fit signal strength $\hat{\mu}$ as a function of the Higgs boson mass hypothesis in the full mass range for the combination of the ATLAS (left) and CMS (right) analyses. The μ value indicates by what factor the Standard Model Higgs boson cross section would have to be scaled to best match the observed data. The band shows the interval around $\hat{\mu}$ corresponding to a variation of $-2 \ln \lambda(\mu) < 1$ (from Refs. [139, 140]).

6 Search for Supersymmetric Particles

Due to the high centre-of-mass energy of 7 TeV, the LHC has a large discovery potential for new heavy particles beyond the Tevatron limits. This holds in particular for particles with colour charge, such as squarks and gluinos in supersymmetry (SUSY) [148]. However, due to the excellent luminosity performance of the LHC in 2011, sensitivity also exists for electroweak production of charginos and neutralinos, the supersymmetric partners of the electroweak gauge bosons and the Higgs boson. In the following a few results of the searches by the ATLAS and CMS collaborations for supersymmetry with up to 2 fb^{-1} of LHC pp data at $\sqrt{s} = 7 \text{ TeV}$ are summarized. Since none of the analyses have observed any excess above the Standard Model expectations, limits on SUSY parameters or masses of SUSY particles are set. The discussion presented here follows largely the review of Ref. [150] on the results from the ATLAS collaboration.

6.1 Searches with jets and missing momentum

Assuming conservation of R-parity, the lightest supersymmetric particle (LSP) is stable and weakly interacting, and will typically escape detection. If the primary produced particles are squarks or gluinos (and assuming a negligible lifetime of these particles), they will decay to final states with energetic jets and significant missing transverse momentum. This final state can be produced in a large number of R-parity conserving models [151], in which squarks, \tilde{q} , and gluinos, \tilde{g} , can be produced in pairs as $\tilde{g}\tilde{g}$, $\tilde{g}\tilde{q}$, or $\tilde{q}\tilde{q}$. They can decay via $\tilde{q} \rightarrow q\tilde{\chi}_1^0$ and $\tilde{g} \rightarrow q\tilde{q}\tilde{\chi}_1^0$ to weakly interacting neutralinos, $\tilde{\chi}_1^0$. However, also charginos or heavier neutralinos might appear in the decay cascade and these particles may produce high transverse momentum leptons in their decays into the LSP.

The ATLAS and CMS collaborations have carried out analyses with a lepton veto [153, 154], requiring one isolated lepton [155, 156], or requiring two or more leptons [157, 158]. In addition, a dedicated search was performed for events with high jet multiplicity with six or more jets [159]. Data samples corresponding to integrated luminosities between 1.0 and 1.3 fb^{-1} were used. Events are triggered either on the presence of a jet plus large missing momentum, or on the presence of at least one high- p_T lepton. Backgrounds to the searches arise from Standard Model processes such as vector boson production plus jets ($W + \text{jets}$, $Z + \text{jets}$), top quark pair production and single top production, QCD multijet production, and diboson production. They are estimated in a semi-data-driven way, using control regions in combination with a transfer factor obtained from simulation. The results are interpreted in the MSUGRA/CMSSM model [160], and in particular as limits in the plane spanned by the common scalar mass parameter at the GUT scale m_0 and the common gaugino mass parameter at the GUT scale $m_{1/2}$, for values of the common trilinear coupling parameter $A_0 = 0$, Higgs mixing parameter $\mu > 0$, and ratio of the vacuum expectation values of the two Higgs doublets $\tan \beta = 10$. Figure 35 (left) shows the results for the analyses of the ATLAS collaboration with ≥ 2 , ≥ 3 or ≥ 4 jets plus missing transverse momentum, and the multijets plus missing momentum analysis. For a choice of parameters leading to equal squark and gluino masses, squark and gluino masses below approximately 1 TeV are excluded. The 1-lepton and 2-lepton results are less constraining in MSUGRA/CMSSM for this choice of parameters, but these analyses are complementary, and therefore no less important. The exclusion contours obtained by the CMS collaboration in different final states, including the lepton channels, are shown in Fig. 36.

6.2 Simplified model interpretation

The various analyses have also been interpreted in simplified models assuming specific production and decay modes. The constraints implied by the MSUGRA/CMSSM models [160] are relaxed, leaving more freedom for the variation of particle masses and decay modes. Interpretations in simplified models thus show better the limitations of the analyses as a function of the relevant kinematic variables.

Inclusive search results with jets and missing momentum are interpreted using simplified models with either pair production of squarks or of gluinos, or production of squark-gluino pairs. Direct squark

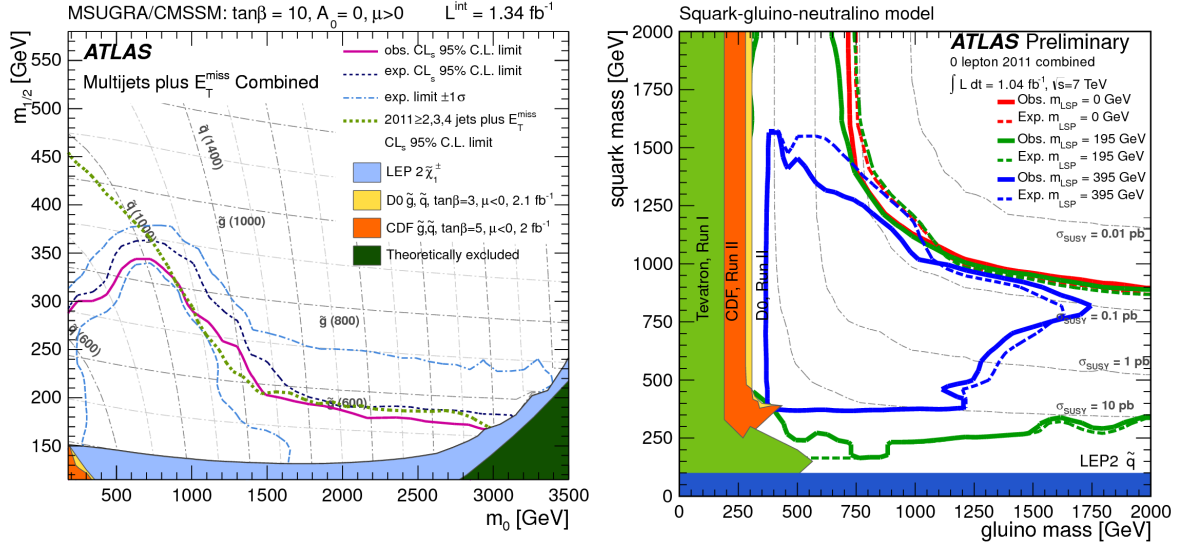


Fig. 35: (Left): Exclusion contours in the MSUGRA/CMSSM ($m_0 - m_{1/2}$)-plane for $A_0 = 0$, $\tan\beta = 10$ and $\mu > 0$, arising from the analysis of the ATLAS collaboration with ≥ 2 , ≥ 3 or ≥ 4 jets plus missing transverse momentum, and the multijets plus missing momentum analysis (from Ref. [159]). (Right): Exclusion contours from the ATLAS analyses in the squark-gluino mass plane for three values of the LSP mass using the simplified model description (see text) (from Ref. [161]).

decays ($\tilde{q} \rightarrow q\tilde{\chi}_1^0$) or direct gluino decays ($\tilde{g} \rightarrow q\tilde{q}\tilde{\chi}_1^0$) are dominant if all other particle masses have multi-TeV values, so that those do not play a role. Using these assumptions, the excluded mass regions are sensitive to the mass of the LSP ($\tilde{\chi}_1^0$). Figure 35 (right) shows the ATLAS results interpreted in terms of limits on (first and second generation) squark and gluino masses, for three values of the LSP ($\tilde{\chi}_1^0$) mass, and assuming that all other SUSY particles are very massive [161]. Further interpretations are also done in terms of limits on gluino mass versus LSP mass assuming high squark masses, or in terms of limits on squark mass vs LSP mass assuming large gluino masses [155, 161].

The results of the inclusive jets plus missing momentum searches, interpreted in these simplified models, indicate that masses of first and second generation squarks and of gluinos must be above approximately 750 GeV. An important caveat in this interpretation is the fact that this is only true for neutralino LSP masses below approximately 250 GeV (as in MSUGRA/CMSSM [160] for values of $m_{1/2}$ below ~ 600 GeV). For higher LSP masses, the squark and gluino mass limits are significantly less restricting. It will be a challenge for further analyses to extend the sensitivity of inclusive squark and gluino searches to the case of heavy neutralinos. If the LSP is heavy, events are characterized by less energetic jets and less missing transverse momentum. This will be more difficult to trigger on, and lead to higher Standard Model backgrounds in the analysis.

6.3 Search for stop and sbottom production

Important motivations for electroweak-scale supersymmetry are the facts that SUSY might provide a natural solution to the hierarchy problem by preventing ‘unnatural’ fine-tuning of the Higgs sector, and that the lightest stable SUSY particle is an excellent dark matter candidate. It is instructive to consider what such a motivation really requires from SUSY: a relatively light top quark partner (the stop, \tilde{t} and an associated sbottom-left, \tilde{b}_L), a gluino not much heavier than about 1.5 TeV to keep the stop light, given that it receives radiative corrections from loops like $\tilde{t} \rightarrow \tilde{g}t \rightarrow \tilde{t}$, and electroweak gauginos below the TeV scale [162]. There are no strong constraints on first and second generation squarks and sleptons; in fact heavy squarks and sleptons make it easier for SUSY to satisfy the strong constraints from flavour

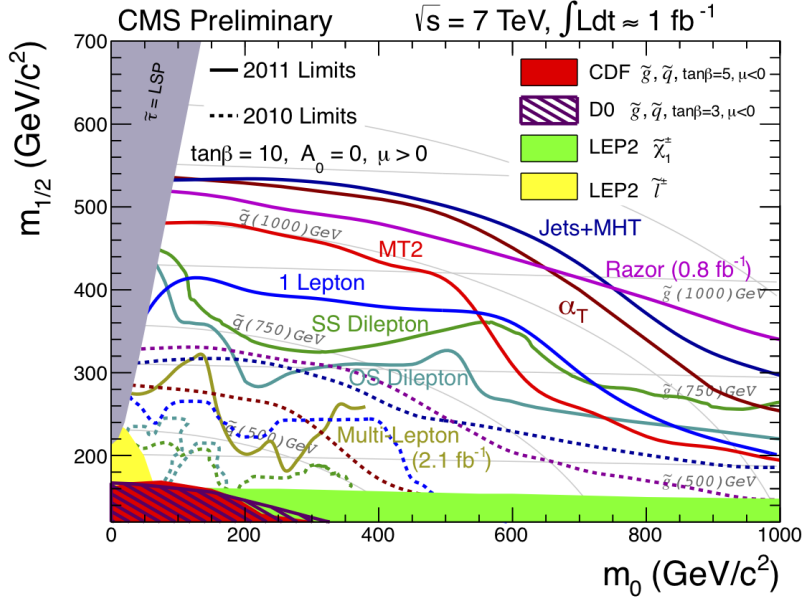


Fig. 36: Summary of exclusion contours in the MSUGRA/CMSSM ($m_0 - m_{1/2}$)-plane for the parameters $A_0 = 0$, $\tan \beta = 10$ and $\mu > 0$ for various analyses and different final states from the CMS collaboration (from Ref. [156]).

physics.

Motivated by these considerations, the ATLAS and CMS collaborations have also carried out a number of searches for supersymmetry with b -tagged jets, which are sensitive to sbottom and stop production, either in direct production or in production via gluino decays. Jets are tagged as originating from b -quarks by an algorithm that exploits both track impact parameter and secondary vertex information.

Direct sbottom pair production is searched for in a data sample corresponding to an integrated luminosity of 2 fb^{-1} by requiring two b -tagged jets with $p_T > 130, 50 \text{ GeV}$ and significant missing transverse momentum of more than 130 GeV [163]. The final discriminant in the ATLAS analysis is the boost-corrected contranverse mass m_{CT} [164], and signal regions with $m_{CT} > 100, 150, 200 \text{ GeV}$ are considered. No excesses are observed above the expected backgrounds from top, W +heavy flavour and Z +heavy flavour production. Figure 37 (left) shows the resulting limits in the sbottom-neutralino mass plane, assuming sbottom pair production and sbottom decays into a b -quark plus a neutralino (LSP) with a 100% branching fraction. Under these assumptions, sbottom masses up to 390 GeV are excluded for neutralino masses below 60 GeV .

The ATLAS collaboration has searched for stop quark production in gluino decays [165] using an analysis requiring at least four high- p_T jets of which at least one should be b -tagged, one isolated lepton, and significant missing transverse momentum. Since the number of observed events agrees with the expectations from Standard Model processes, limits are set in the gluino-stop mass plane, assuming the gluino to decay as $\tilde{g} \rightarrow \tilde{t}t$, and the stop quark to decay as $\tilde{t} \rightarrow b\tilde{\chi}_1^\pm$. The obtained mass limits are shown in Fig. 37 (right).

Further searches for direct stop pair production are in progress. These searches are challenging due to the similarity with the top-quark pair-production final state for stop masses similar to the top mass, and due to the low cross section for the production of stops with high mass. The ATLAS collaboration has searched for signs of new phenomena in events passing a top-quark pair selection with large missing transverse momentum [166]. Such an analysis is sensitive to pair production of massive partners of the top quark, decaying to a top quark and a long-lived undetected neutral particle. No excess above background was observed, and limits on the cross section for pair production of top quark partners are

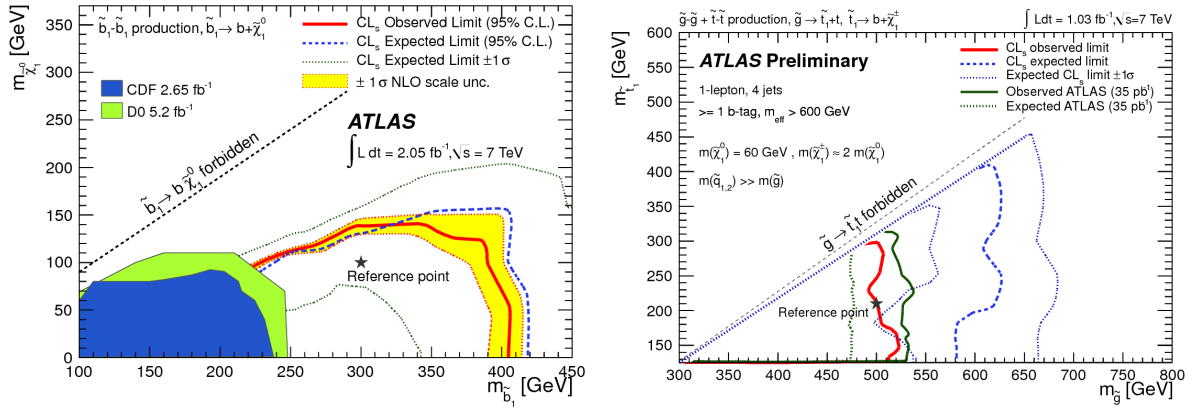


Fig. 37: (Left): Exclusion contours from the ATLAS analyses in the sbottom-neutralino mass plane resulting from the analysis searching for sbottom pair production assuming $\tilde{b}_1 \rightarrow b\tilde{\chi}_1^0$ decays (from Ref. [163]). (Right): Exclusion contours from the ATLAS analyses in the gluino-stop mass plane resulting from the analysis searching for stop production via gluino decays. The assumptions made to derive the limits are given in the figure (from Ref. [165]).

set. These limits constrain fermionic exotic fourth generation quarks, but not yet scalar partners of the top quark, such as the stop quark [166].

6.4 Search for supersymmetry in multilepton final states

The search for final states with several leptons and missing transverse momentum are sensitive to the production of charginos and/or heavier neutralinos (other than the LSP), decaying leptonically into the LSP. These analyses comprise the golden search modes at the Tevatron, but are also rapidly gaining relevance at the LHC and both the ATLAS and CMS collaborations have performed corresponding analyses [157, 158]. The ATLAS collaboration has published results of various analyses searching for dilepton events plus missing momentum in data corresponding to an integrated luminosity of 1.0 fb^{-1} [157]. Three searches are performed for new phenomena in final states with opposite-sign and same-sign dileptons and missing transverse momentum. These searches also include signal regions that place requirements on the number and p_T of energetic jets in the events. For all signal regions good agreement is found between the numbers of observed events and the predictions of expected events from Standard Model processes. Additionally, in opposite-sign events, a search is made for an excess of same-flavour over different-flavour lepton pairs. Effective production cross sections in excess of 9.9 fb for opposite-sign events with missing transverse momentum greater than 250 GeV are excluded at 95% C.L. For same-sign events with missing transverse momentum greater than 100 GeV , effective production cross sections in excess of 14.8 fb are excluded at 95% C.L. The latter limit is interpreted in a simplified electroweak gaugino production model excluding chargino masses up to 200 GeV , under the assumption that slepton decays are dominant [157].

The CMS collaboration has presented preliminary results, based on data corresponding to an integrated luminosity of 2.1 fb^{-1} , on the search for supersymmetric particles in three- and four-lepton final states, including hadronic decays of τ leptons [158]. The backgrounds from Standard Model processes are suppressed by requiring missing transverse energy, Z-mass vetos of the invariant dilepton mass or high jet activity. Control samples in data are used to obtain reliable background estimates. Within the statistical and systematic uncertainties the numbers of observed events are consistent with the expectations from Standard Model processes. These results are used to exclude previously unexplored regions of the supersymmetric parameter space assuming R-parity conservation with the lightest supersymmet-

ric particle being a neutralino. The corresponding exclusion contours in the MSUGRA/CMSSM [160] interpretation are shown in Fig. 38 in the $(m_0 - m_{1/2})$ plane for $A_0 = 0$, $\mu > 0$, and for $\tan \beta$ values of 3 and 10. They extend significantly the regions excluded by the CDF [167] and DØ [168] experiments and those excluded with previous searches at the LHC [169].

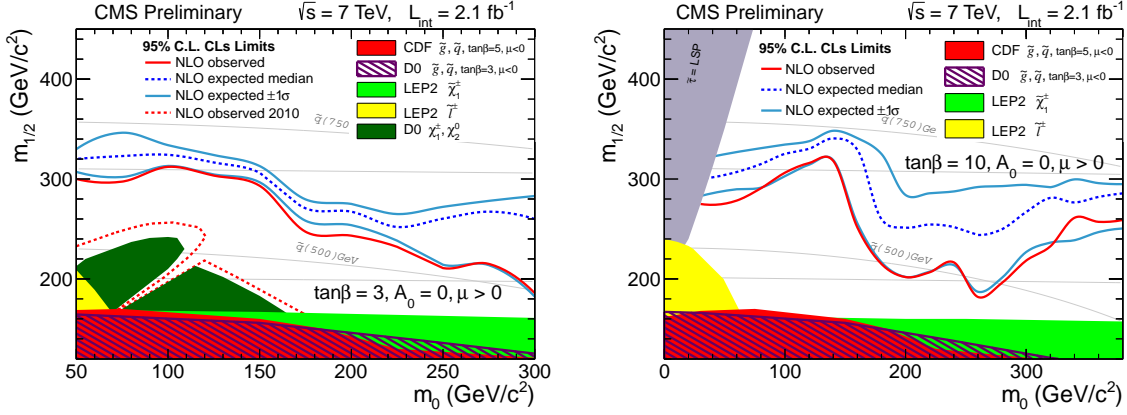


Fig. 38: Exclusion contours in the MSUGRA/CMSSM $(m_0 - m_{1/2})$ -plane for the parameters $A_0 = 0$, $\mu > 0$ and $\tan \beta = 3$ (left) and $\tan \beta = 10$ (right) obtained from searches for SUSY production in final states with multileptons by the CMS collaboration (from Ref. [158]).

6.5 Summary and outlook on SUSY searches

Many different searches for the production of supersymmetric particles have been performed in a large variety of final states by the ATLAS and CMS collaborations at the LHC. Data corresponding to integrated luminosities in the range between 1.0 and 4.7 fb^{-1} taken during the year 2011 have been analyzed. In all channels, the number of observed events is in agreement with the expectations from Standard Model processes and no evidence for the production of supersymmetric particles has been found so far. The data have been used to set already rather strong limits on the masses of possible supersymmetric particles. A summary of the most important mass limits is given in Fig. 39.

In addition to the analyses summarized here, many other analyses have been performed and many different final states have been explored. There are investigations of SUSY searches in gauge mediated supersymmetry breaking models, by using final states with photons or multileptons. In addition, in many models (split SUSY, R-hadrons, anomaly-mediated SUSY breaking and in certain parts of the phase space of gauge-mediated SUSY breaking scenarios) SUSY particles may be long-lived either because their decay is kinematically suppressed or due to very small couplings, e.g. in R-parity violating models. Many of these scenarios have already been explored and the reader is referred to the corresponding publications of the ATLAS and CMS collaborations. Also in all these searches for more exotic SUSY scenarios the number of observed events is in agreement with the expectations from background from Standard Model processes.

Although no signs of supersymmetry have been found so far, it is important to realize that actual tests of ‘natural’ supersymmetry are only just beginning. In this respect, the LHC run of 2012, with an expected luminosity of more than 10 fb^{-1} , possibly at $\sqrt{s} = 8$ TeV, will be very important. However, experimentally there will be considerable challenges in triggering and in dealing with high pile-up conditions. In the longer term, increasing the LHC beam energy to > 6 TeV will again enable the crossing of kinematical barriers and open the way for multi-TeV SUSY searches.

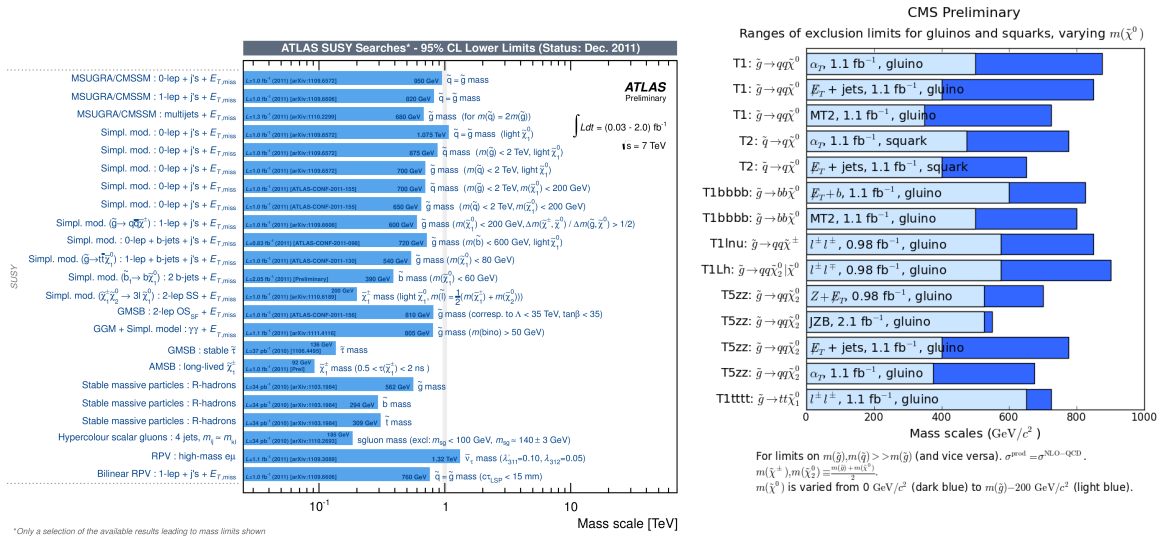


Fig. 39: Summary of excluded mass ranges from a variety of searches for the production of supersymmetric particles from the ATLAS (left) and CMS (right) collaborations. Only a representative selection of available results is shown. The CMS results indicate the change of the limits under variation of the neutralino mass from 0 to 200 GeV.

7 Search for other Physics Scenarios Beyond the Standard Model

As already mentioned in Section 2, the Standard Model is an extremely successful effective theory which has been extensively tested over the past forty years. However, a number of fundamental questions are left unanswered. Many models for physics Beyond the Standard Model (BSM) have been proposed and the ATLAS and CMS experiments have used the data collected in 2010 and 2011 to search for indications of new physics. An impressive list of analyses has been performed. So far, no indications for deviations from the Standard Model have been found. The event numbers and kinematical distributions in all final states considered agree with the expectations from Standard Model processes. Therefore, these analyses have been used to constrain the parameter space of many BSM models.

Since it is impossible to present and discuss all analyses in such a summary paper, a few benchmark processes are selected and the search results are presented in the following. This concerns the search for new vector bosons, or more general the search for heavy dilepton resonances, the search for compositeness and the search for dijet resonances. Finally the results from other searches are briefly summarized.

7.1 Search for heavy dilepton resonances

The ATLAS and CMS collaborations have performed searches for narrow high-mass neutral and charged resonances decaying into e^+e^- or $\mu^+\mu^-$ pairs or $e\nu$ or $\mu\nu$, respectively. In several extensions of the Standard Model new heavy spin-1 neutral gauge bosons such as Z' [170–172], technimesons [173–175], as well as spin-2 Randall-Sundrum gravitons, G^{**} , [176] are predicted. Additional heavy charged gauge bosons appear e.g. in left-right-symmetric models [177].

The benchmark models considered in the analyses for the Z' are the Sequential Standard Model [170], with the same couplings to fermions as the Z boson, and the E_6 grand unified symmetry group [172], broken into $SU(5)$ and two additional $U(1)$ groups, leading to new neutral gauge fields ψ and χ . The particles associated with the additional fields can mix in a linear combination to form the Z' candidate: $Z'(\theta_{E_6}) = Z'_\psi \cos \theta_{E_6} + Z'_\chi \sin \theta_{E_6}$, where θ_{E_6} is the mixing angle between the two gauge bosons. The

pattern of spontaneous symmetry breaking and the value of θ_{E_6} determine the Z' couplings to fermions.

Other models predict additional spatial dimensions as a possible explanation for the gap between the electroweak symmetry breaking scale and the gravitational energy scale. The Randall-Sundrum (RS) model [176] predicts excited Kaluza-Klein modes of the graviton, which appear as spin-2 resonances. These modes have a narrow intrinsic width when $k/\bar{M}_{\text{Pl}} < 0.1$, where k is the spacetime curvature in the extra dimension, and $\bar{M}_{\text{Pl}} = M_{\text{Pl}}/\sqrt{8\pi}$ is the reduced Planck scale.

The search performed by the ATLAS experiment [178] is based on a dataset corresponding to an integrated luminosity of up to 1.2 fb^{-1} . The observed invariant mass spectrum is shown in Fig. 40 (left) for the e^+e^- final state after final selections. The backgrounds from Drell-Yan, $t\bar{t}$, diboson and W +jets production are determined from Monte Carlo simulation after normalization to the respective (N)NLO cross sections. The background from QCD multijet production is estimated using data-driven methods with the inversion of lepton identification criteria. The simulated backgrounds are rescaled so that the total sum of the backgrounds matches the observed number of events observed in data in the 70-110 GeV mass interval. The scaling factor is within 1% of unity. The advantage of this approach is that the uncertainty on the luminosity and any mass independent uncertainties on efficiencies, cancel between the Z' (G^*) and the Z boson. The dilepton invariant mass distributions are well described by the prediction from Standard Model processes. Figure 40 (left) also displays the expected Z' signals in the Sequential Standard Model for three mass hypotheses.

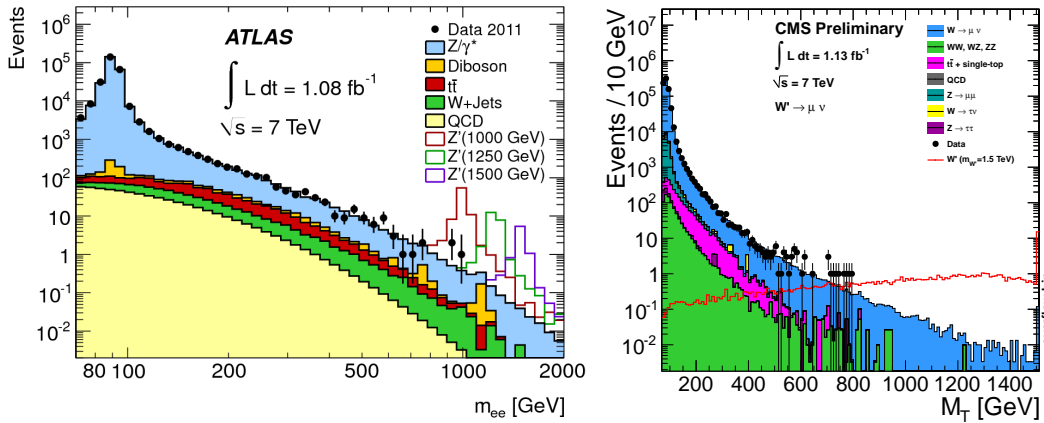


Fig. 40: (Left): Distribution of the dielectron invariant mass after final selections in the ATLAS experiment, compared to the stacked sum of all expected backgrounds, with three example Z'_{SSM} signals overlaid. The bin width is constant in $\log m_{\ell\ell}$ (from Ref. [178]). (Right): Distribution of the $\mu - E_{\text{T}}^{\text{miss}}$ transverse mass after final selections in the CMS experiment. The expected signal from a hypothetical W' boson with a mass of 1.5 TeV is superimposed (from Ref. [179]).

Given the good agreement between the data and the Standard Model expectations, limits are set on the cross section times branching ratio for the different Z' models. The resulting mass limits are 1.83 TeV for the Sequential Standard Model Z' boson, 1.49-1.64 TeV for various E_6 -motivated Z' bosons, and 0.71-1.63 TeV for a Randall-Sundrum graviton with couplings (k/\bar{M}_{Pl}) in the range 0.01-0.1. Similar analyses have been performed by the CMS collaboration [180] and comparable limits have been extracted. They are included in the summary of results from different experiments for various physics models in Table 1.

The benchmark model considered in the search for the W' is the Sequential Standard Model [170], with the same couplings to fermions as the W boson. In this case the transverse mass of the lepton and $E_{\text{T}}^{\text{miss}}$ system is used as discriminating variable. As an example, the measured transverse mass distribution in the muon final state in the CMS experiment [179] is shown in Fig. 40 (right). The expectation

Table 1: Observed 95% C.L. mass lower limits on Z' , G^* gravitons and W' resonances obtained for various models in the ATLAS and CMS experiments. The results from searches at the Tevatron are included for comparison.

Model	Experiment	L_{int} (fb^{-1})	95% C.L. limits			Ref.
			e^+e^- (TeV)	$\mu^+\mu^-$ (TeV)	$\ell^+\ell^-$ (TeV)	
Z'_{SSM}	CDF/DØ	5.5			1.07	[182]
	ATLAS/CMS	0.036	0.96	0.83	1.05/1.14	[184]
	ATLAS	1.1 / 1.2	1.70	1.61	1.83	[178]
	CMS	1.1			1.94	[180]
$Z' E_6$ models	ATLAS	1.1 / 1.2			1.49 - 1.64	[178]
	CMS	1.1			1.62	[186]
$G^* k/M_{P1} = 0.01$	ATLAS	1.1 / 1.2			0.71	[178]
$G^* k/M_{P1} = 0.03$		1.1 / 1.2			1.03	
$G^* k/M_{P1} = 0.05$		1.1 / 1.2			1.33	
$G^* k/M_{P1} = 0.10$		1.1 / 1.2			1.63	
$G^* k/M_{P1} = 0.05$		CMS	1.1			
$G^* k/M_{P1} = 0.10$		1.1			1.78	
W'_{SSM}	ATLAS	1.04	2.08	1.98	2.15	[181]
	CMS	1.1			2.27	[179]

for a W' signal with a mass of 1.5 TeV is superimposed. Also the transverse mass distributions measured by the LHC experiments are well described by the prediction from Standard Model processes and the data allow to exclude heavy W' bosons with masses below 2.15 TeV (ATLAS) [181] and 2.25 TeV (CMS) [179] at the 95% C.L.

The mass limits obtained at the LHC are the most stringent to date, including indirect limits set by LEP2. It is striking to see how fast the LHC experiments have superseded the limits obtained with much higher luminosity at the Tevatron. The analyses based on the data from 2010 ($L_{\text{int}} = 36 \text{ pb}^{-1}$) resulted in comparable limits to those obtained at the Tevatron based on an integrated luminosity of 5.5 fb^{-1} (see Table 1).

7.2 Limits on new physics from jet production

The measurements on inclusive and dijet production, as discussed in Section 4.1, can also be used to constrain contributions from new physics that would modify the expected QCD behaviour in the jet production cross sections. Two examples are discussed in the following.

7.2.1 Substructure of quarks

Both collaborations have searched for quark compositeness by investigating the angular distribution of jet events [187, 188]. At small scattering angles in the centre-of-mass system of the two partons, the angular distribution is expected to be proportional to the Rutherford cross section, $d\hat{\sigma}/d\cos\theta^* \sim 1/(1-\cos\theta^*)^2$. For the scattering of massless partons, which are assumed to be collinear with the beam protons, the longitudinal boost of the parton-parton centre-of-mass frame with respect to the proton-proton centre-of-mass frame, y_{boost} , and θ^* are obtained from the rapidities y_1 and y_2 of the jets from the two scattered partons by $y_{\text{boost}} = \frac{1}{2}(y_1 + y_2)$ and $|\cos\theta^*| = \tanh y^*$, where $y^* = \frac{1}{2}|y_1 - y_2|$ and where $\pm y^*$ are the rapidities of the two jets in the parton-parton centre-of-mass frame. The variable $\chi_{\text{dijet}} = e^{2y^*}$ is used to measure the dijet angular distribution, which for collinear massless-parton scattering takes the form $\chi_{\text{dijet}} = (1 + |\cos\theta^*|)/(1 - |\cos\theta^*|)$. This choice of χ_{dijet} , rather than θ^* , is motivated by the fact that $d\sigma_{\text{dijet}}/d\chi_{\text{dijet}}$ is flat for Rutherford scattering.

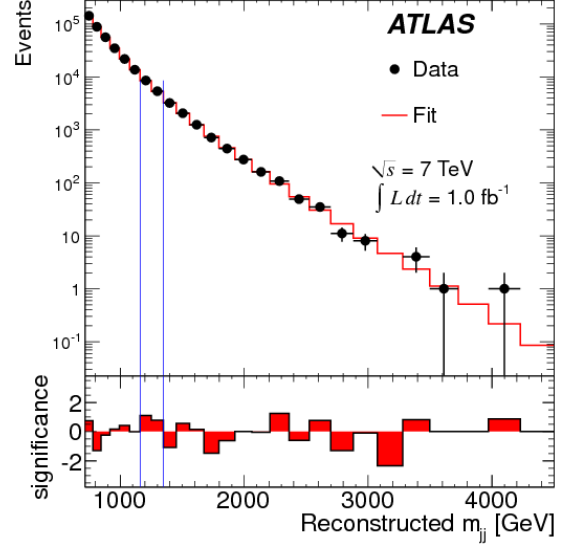
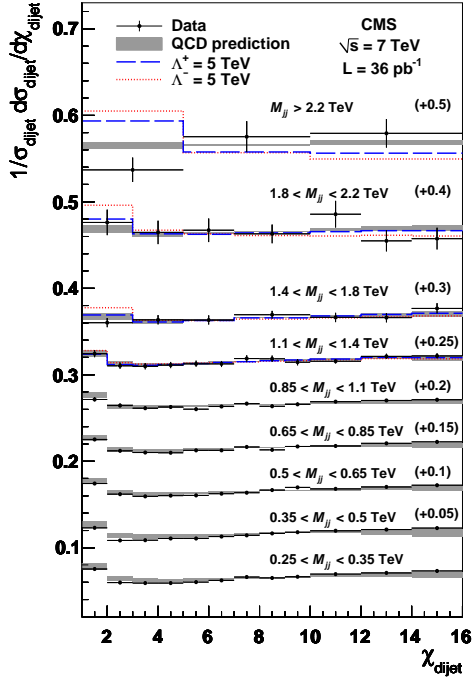


Fig. 41: (Left): Normalized dijet angular distributions in several ranges of the dijet mass as measured by the CMS collaboration. The data points include statistical and systematic uncertainties. The results are compared with the predictions of pQCD at NLO (shaded bands) and with the predictions including a contact interaction term of compositeness scale $\Lambda^+ = 5$ TeV (dashed histogram) and $\Lambda^- = 5$ TeV (dotted histogram). The shaded bands show the effect on the NLO pQCD predictions due to μ_R and μ_F scale variations and PDF uncertainties, as well as the uncertainties from the non-perturbative corrections added in quadrature (from Ref. [188]). (Right): The reconstructed dijet mass distribution (filled points) measured by the ATLAS collaboration fitted with a smooth functional form describing the QCD background. The bin-by-bin significance of the data-background difference is shown in the lower panel. Vertical lines show the most significant excess found (from Ref. [189]).

The differential dijet angular distributions for different m_{jj} ranges, and corrected for detector effects as measured by the CMS experiment using the 2010 data ($L_{\text{int}} = 36 \text{ pb}^{-1}$) are shown in Fig. 41 (left). The data are found to be in good agreement with pQCD predictions at NLO calculated with NLOJET++ [32, 33], which are superimposed on the figure. The measured dijet angular distributions can be used to set limits on quark compositeness parametrized by a four-fermion contact interaction term in addition to the QCD Lagrangian. The value of the mass scale Λ characterizes the strengths of the quark substructure binding interactions and the physical size of the composite states. A color- and isospin-singlet contact interaction (CI) of left-handed quarks gives rise to an effective Lagrangian term [190, 191]

$$L_{qq} = \eta_0 \frac{2\pi}{\Lambda^2} (\bar{q}_L \gamma^\mu q_L) (\bar{q}_L \gamma_\mu q_L), \quad (4)$$

where $\eta_0 = +1$ corresponds to destructive interference between the QCD and the new physics term, and $\eta_0 = -1$ to constructive interference. From the measured χ_{dijet} distribution, lower limits on the contact interaction scale of $\Lambda^+ = 5.6$ TeV and $\Lambda^- = 6.7$ TeV for destructive and constructive interference, respectively, have been set by the CMS collaboration at the 95% C.L. [188]. The expected limits in case of no substructure are 5.0 TeV and 5.8 TeV, respectively. The ATLAS collaboration has performed a similar analysis and excludes at the 95% C.L. quark contact interactions with a scale $\Lambda < 9.5$ TeV [187]. How-

Table 2: *The 95% C.L. mass lower limits on dijet resonance models.*

Model	Experiment	L_{int} (fb^{-1})	95% C.L. limits		Ref.
			Expected (TeV)	Observed (TeV)	
Excited quark q^*	ATLAS	1.0	2.81	2.99	[189]
	CMS	1.0	2.68	2.49	[193]
Axigluon	ATLAS	1.0	3.07	3.32	[189]
	CMS	1.0	2.66	2.47	[193]
Colour Octet Scalar	ATLAS	1.0	1.77	1.92	[189]
E_6 diquarks	CMS	1.0	3.28	3.52	[193]

ever, it should be noted that this observed limit is significantly above the expected limit of 5.7 TeV for the data sample corresponding to an integrated luminosity of 36 pb^{-1} . Very recently, the CMS collaboration has published the results of an updated analysis based on data corresponding to an integrated luminosity of 2.2 fb^{-1} [192] and taking NLO calculations for the QCD predictions into account. Also this larger data set has been found to be in good agreement with the QCD expectations. For the contact interaction model described above, 95% C.L. limits of $\Lambda^+ = 7.5 \text{ TeV}$ and $\Lambda^- = 10.5 \text{ TeV}$ have been set. The expected limits are 7.0 TeV and 9.7 TeV, respectively.

7.2.2 Dijet resonances

The ATLAS and CMS collaborations have also examined the dijet mass spectrum for resonances due to new phenomena localised near a given mass, employing data-driven background estimates that do not rely on detailed QCD calculations [189, 193]. The searches are based on data corresponding to an integrated luminosity of 1.0 fb^{-1} . As an example, the observed dijet mass distribution measured in the ATLAS experiment, which extend up to masses of $\sim 4 \text{ TeV}$ is displayed in Fig. 41 (right). It is found to be in good agreement with a smooth function representing the Standard Model expectation. Since no evidence for the production of new resonances is found, 95% C.L. mass limits have been set in the context of several models of new physics: excited quarks (q^*) [194, 195], axigluons [196–198], scalar colour octet states [199] and scalar diquarks predicted in Grand Unified Theories based on the E_6 gauge group [200]. The results are summarized in Table 2. Also these limits are the most stringent ones to date.

7.3 Summary of results on other searches

Many different searches for the Beyond the Standard Model processes have been performed by the ATLAS and CMS collaborations at the LHC. Data corresponding to integrated luminosities in the range between 1.0 and 4.7 fb^{-1} taken during the year 2011 have been analyzed and many different final states have been investigated. So far, no indications for deviations from the Standard Model have been found. The event numbers and kinematical distributions in all final states considered agree with the expectations from Standard Model processes. Therefore, these analyses have been used to constrain the parameter space of many BSM models. A summary of the most important limits from the ATLAS collaboration is given in Fig. 42. Comparable limits have been set by the CMS collaboration.

8 Conclusions

With the start-up of the operation of the LHC at high energies particle physics has entered a new era. Both the accelerator and the detectors have worked magnificently. Until the end of 2011 data corresponding to an integrated luminosity of 5.5 fb^{-1} have been recorded with high efficiency by the LHC experiments. Based on these data, many tests of the predictions of the Standard Model and searches for physics Beyond the Standard Model have been performed in the new energy regime. So far, all measurements have been found to be in good agreement with the predictions from the Standard Model. Towards the end of 2011,

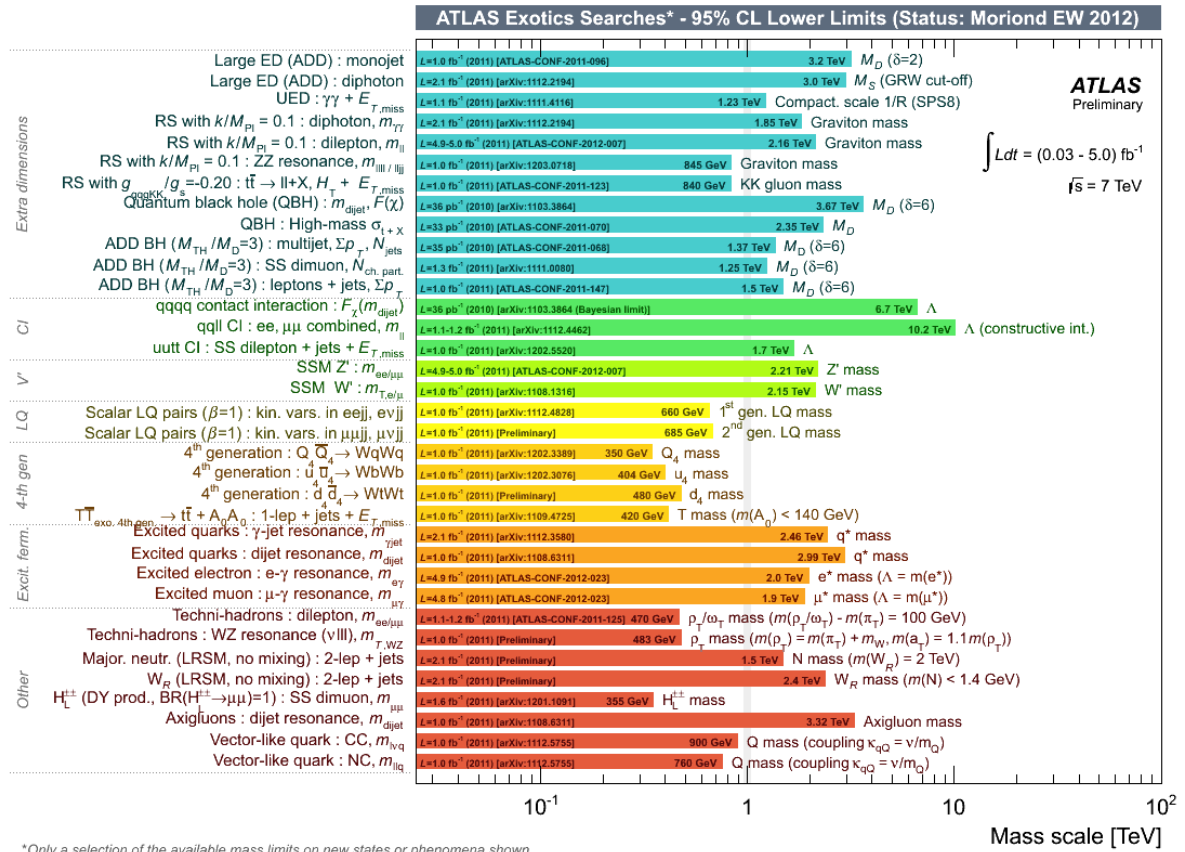


Fig. 42: Summary of excluded mass ranges from a variety of searches from the ATLAS experiment for Beyond the Standard Model physics processes. Only a representative selection of available results is shown.

the experiments have reached sensitivity for the Standard Model Higgs boson. A large fraction of the possible Higgs boson mass range has already been excluded by the ATLAS and CMS experiments with a confidence level of 95%. However, it is striking that both experiments are not able to exclude the existence of the Higgs boson in the mass range from 118 - 129 GeV, despite their sensitivity in this range. In addition, tantalizing hints for a Higgs boson signal have been seen by both experiments in the two high resolution channels $H \rightarrow \gamma\gamma$ and $H \rightarrow ZZ^{(*)} \rightarrow llll$. However, the statistical significance is not sufficient to claim evidence. More data are needed to clarify the situation. With a successful run of the LHC in 2012 a final conclusion on the existence of the Standard Model Higgs boson might be reached and the year 2012 might enter as the “Year of the Higgs Boson” into the history of Physics.

References

- [1] S. Glashow, *Partial Symmetries of Weak Interactions*, Nucl. Phys. **22** (1961) 579.
- [2] S. Weinberg, *A Model of Leptons*, Phys. Rev. Lett. **19** (1967) 1264.
- [3] A. Salam, in: *Elementary Particle Theory*, W. Svartholm, ed., Almquist and Wiksell, Stockholm (1968).
- [4] H. D. Politzer, *Reliable Perturbative Results for Strong Interactions?*, Phys. Rev. Lett. **30** (1973) 1346.
- [5] D. J. Gross and F. Wilczek, *Ultraviolet Behavior of Non-Abelian Gauge Theories*, Phys. Rev. Lett. **30** (1973) 1343.

- [6] H. Fritzsch and M. Gell-Mann, *Proc. XVI Int. Conf. on High Energy Physics*. Fermilab, 1972.
- [7] P. Higgs, *Broken symmetries, massless particles and gauge fields*, Phys. Lett. **12** (1964) 132.
- [8] F. Englert and R. Brout, *Broken Symmetry and the Mass of Gauge Vector Mesons*, Phys. Rev. Lett. **13** (1964) 321.
- [9] G. S. Guralnik, C. R. Hagen, and T. W. B. Kibble, *Global Conservation Laws and Massless Particles*, Phys. Rev. Lett. **13** (1964) 585.
- [10] P. W. Higgs, *Broken Symmetries and the Masses of Gauge Bosons*, Phys. Rev. Lett. **13** (1964) 508.
- [11] P. W. Higgs, *Spontaneous Symmetry Breakdown without Massless Bosons*, Phys. Rev. **145** (1966) 1156.
- [12] T. W. B. Kibble, *Symmetry breaking in non-Abelian gauge theories*, Phys. Rev. **155** (1967) 1554.
- [13] W. Alberico and S. Bilenky, *Neutrino oscillations, masses and mixing*, Phys. Part. Nucl. **35** (2004) 297, and references therein.
- [14] For a review, see: M. Drees and G. Garbier, *Dark matter*, in 2011 Review of Particle Physics, K. Nakamura *et al.* (Particle Data Group), J. Phys. G**37**, 075021 (2010) and 2011 partial update for the 2012 edition.
- [15] For a review, see: R. Gaitskell, *Direct detection of dark matter*, Annual Review of Nuclear and Particle Science **54** (2004) 315, and references therein.
- [16] J. M. Campbell, J. W. Huston, and W. J. Stirling, *Hard interactions of quarks and gluons: a primer for LHC physics*, Reports on Progress in Physics **70** (2007) 89.
- [17] L.N. Lipatov, Sov. J. Nucl. Phys. **20** (1975) 95;
V.N. Gribov, L.N. Lipatov, Sov. J. Nucl. Phys. **15** (1972) 438;
G. Altarelli, G. Parisi, Nucl. Phys. B **126** (1977) 298;
L. Yu Dokshitzer, Sov. Phys. - JETP **46** (1977) 641.
- [18] R. Devenish and A. Cooper-Sarkar, *Deep inelastic scattering*. Oxford University Press, 2004.
- [19] S. Alekhin, J. Blümlein, S. Klein, and S. Moch, *The 3-, 4-, and 5-flavor NNLO Parton from Deep-Inelastic-Scattering Data and at Hadron Colliders*, Phys. Rev. **D81** (2010) 014032, arXiv:0908.2766 [hep-ph].
- [20] P. M. Nadolsky *et al.*, *Implications of CTEQ global analysis for collider observables*, Phys. Rev. **D78** (2008) 013004, arXiv:0802.0007 [hep-ph].
- [21] H.-L. Lai *et al.*, *New parton distributions for collider physics*, Phys. Rev. **D82** (2010) 074024, arXiv:1007.2241 [hep-ph].
- [22] The H1 and ZEUS Collaboration, F. D. Aaron *et al.*, *Combined Measurement and QCD Analysis of the Inclusive ep Scattering Cross Sections at HERA*, JHEP **01** (2010) 109, arXiv:0911.0884 [hep-ex].
- [23] The H1 and ZEUS Collaboration, V. Radescu, *HERA Precision Measurements and Impact for LHC Predictions*, arXiv:1107.4193 [hep-ex].
- [24] P. Jimenez-Delgado and E. Reya, *Dynamical NNLO parton distributions*, Phys. Rev. **D79** (2009) 074023, arXiv:0810.4274 [hep-ph].
- [25] A. D. Martin, W. J. Stirling, R. S. Thorne, and G. Watt, *Parton distributions for the LHC*, Eur. Phys. J. **C63** (2009) 189, arXiv:0901.0002 [hep-ph].
- [26] R. D. Ball *et al.*, *A first unbiased global NLO determination of parton distributions and their uncertainties*, Nucl. Phys. **B838** (2010) 136, arXiv:1002.4407 [hep-ph].
- [27] R. D. Ball *et al.*, *Impact of Heavy Quark Masses on Parton Distributions and LHC Phenomenology*, Nucl. Phys. **B849** (2011) 296, arXiv:1101.1300 [hep-ph].
- [28] The ATLAS Collaboration, *Measurement of the Muon Charge Asymmetry from W Bosons Produced in pp Collisions at $\sqrt{s} = 7$ TeV with the ATLAS detector*, Phys. Lett. **B701** (2011) 31,

- arXiv:1103.2929 [hep-ex].
- [29] The CMS Collaboration, S. Chatrchyan et al., *Measurement of the lepton charge asymmetry in inclusive W production in pp collisions at $\sqrt{s} = 7$ TeV*, JHEP **04** (2011) 050, arXiv:1103.3470 [hep-ex].
- [30] R. D. Ball et al., *Reweighting and Unweighting of Parton Distributions and the LHC W lepton asymmetry data*, arXiv:1108.1758 [hep-ph].
- [31] B.L. Combridge, J. Kripfganz, and J. Ranft, *Hadron Production at Large Transverse Momentum and QCD*, Phys. Lett. **B70** (1977) 234.
- [32] Z. Nagy, *Three jet cross-sections in hadron hadron collisions at next-to-leading order*, Phys. Rev. Lett. **88** (2002) 122003, arXiv:hep-ph/0110315 [hep-ph].
- [33] Z. Nagy, *Next-to-leading order calculation of three-jet observables in hadron-hadron collisions*, Phys. Rev. D **68** (2003) 094002.
- [34] R. Hamberg, W. L. van Neerven, and T. Matsuura, *A Complete calculation of the order α_s^2 correction to the Drell-Yan K factor*, Nucl. Phys. **B359** (1991) 343.
- [35] W. L. van Neerven and E. B. Zijlstra, *The $O(\alpha_s^2)$ corrected Drell-Yan K factor in the DIS and $\overline{\text{MS}}$ scheme*, Nucl. Phys. **B382** (1992) 11.
- [36] P. J. Rijken and W. L. van Neerven, *Order α_s^2 contributions to the Drell-Yan cross-section at fixed target energies*, Phys. Rev. **D51** (1995) 44, arXiv:hep-ph/9408366.
- [37] C. Anastasiou, L. J. Dixon, K. Melnikov, and F. Petriello, *High precision QCD at hadron colliders: Electroweak gauge boson rapidity distributions at NNLO*, Phys. Rev. **D69** (2004) 094008, arXiv:hep-ph/0312266.
- [38] S. Dittmaier and M. Krämer, *Electroweak radiative corrections to W boson production at hadron colliders*, Phys. Rev. **D65** (2002) 073007, arXiv:hep-ph/0109062 [hep-ph].
- [39] S. Dittmaier and M. Huber, *Radiative corrections to the neutral-current Drell-Yan process in the Standard Model and its minimal supersymmetric extension*, JHEP **01** (2010) 060, arXiv:0911.2329 [hep-ph].
- [40] M. Cacciari, G. Salam, and G. Soyez, *The anti- k_t jet clustering algorithm*, JHEP **04** (2008) 063, arXiv:0802.1189.
- [41] The ATLAS Collaboration, *Calorimeter Clustering Algorithms: Description and Performance*, ATLAS-LARG-PUB-2008-002.
- [42] The ATLAS Collaboration, *Expected Performance of the ATLAS Experiment - Detector, Trigger and Physics*, arXiv:0901.0512.
- [43] The CMS Collaboration, *Particle-Flow Event Reconstruction in CMS and Performance for Jets, Taus and MET*, CMS-PAS-PFT-09-001.
- [44] The CMS Collaboration, *Commissioning of the Particle-flow Event Reconstruction with the first LHC collisions recorded in the CMS detector*, CMS-PAS-PFT-10-001.
- [45] The ATLAS Collaboration, *Measurement of inclusive jet and dijet production in pp collisions at $\sqrt{s} = 7$ TeV using the ATLAS detector*, submitted to Physical Review D. arXiv:1112.6297v1.
- [46] The CMS Collaboration, *Measurement of the inclusive jet cross section in pp collisions at 7 TeV*, Phys. Rev. Lett. **107** (2011) 132001, arXiv:1106.0208.
- [47] The CMS Collaboration, *Measurement of the differential dijet mass cross section in proton-proton collisions at $\sqrt{s} = 7$ TeV*, Phys. Rev. Lett. **B700** (2011) 187, arXiv:1104.1693.
- [48] The CMS Collaboration, *Measurement of Dijet Angular Distributions and Search for Quark Compositeness in pp Collisions at 7 TeV*, Phys. Rev. Lett. **106** (2011) 201804, arXiv:1102.2020.
- [49] The CMS Collaboration, *Dijet azimuthal decorrelations in pp collisions at $\sqrt{s} = 7$ TeV*, Phys. Rev. Lett. **106** (2011) 122003, arXiv:1101.5029.

- [50] The ATLAS Collaboration, *Measurement of multi-jet cross sections in proton-proton collisions at a 7 TeV center-of-mass energy*, Eur. Phys. J. **C71** (2011) 1763, arXiv:1107.2092 [hep-ex].
- [51] The CMS Collaboration, *Measurement of the Ratio of the 3-jet to 2-jet Cross Sections in pp Collisions at $\sqrt{s} = 7$ TeV*, Phys. Lett. **B702** (2011) 336, arXiv:1106.0647 [hep-ex].
- [52] The CDF Collaboration, A. Abulencia et al., *Measurements of Inclusive W and Z Cross-sections in $p\bar{p}$ Collisions at $\sqrt{s} = 1.96$ TeV*, J. Phys. **G34** (2007) 2457.
- [53] The ATLAS Collaboration, *Measurement of the $W \rightarrow l\nu$ and $Z/\gamma^* \rightarrow \ell\ell$ production cross sections in proton-proton collisions at $\sqrt{s} = 7$ TeV with the ATLAS detector*, JHEP **1012** (2010) 060, arXiv:1010.2130 [hep-ex].
- [54] The CMS Collaboration, *Measurements of Inclusive W and Z Cross Sections in pp Collisions at $\sqrt{s}=7$ TeV*, JHEP **1101** (2011) 080, arXiv:1012.2466 [hep-ex].
- [55] The CMS Collaboration, *Measurement of the Inclusive W and Z Production Cross Sections in pp Collisions at $\sqrt{s} = 7$ TeV*, JHEP **1110** (2011) 132, arXiv:1107.4789 [hep-ex].
- [56] The ATLAS Collaboration, *Measurement of the inclusive W^\pm and Z/γ^* cross sections in the electron and muon decay channels in pp collisions at $\sqrt{s} = 7$ TeV with the ATLAS detector*, arXiv:1109.5141 [hep-ex].
- [57] The UA1 Collaboration, C. Albajar et al., *Intermediate Vector Boson Cross-sections at the CERN Super Proton Synchrotron Collider and the Number of Neutrino Types*, Phys. Lett. **B198** (1987) 271.
- [58] The UA2 Collaboration, J. Alitti et al., *A Measurement of the W and Z Production Cross-sections and a Determination of $\Gamma(W)$ at the CERN $p\bar{p}$ collider*, Phys. Lett. **B276** (1992) 365.
- [59] The DØ Collaboration, conference notes: *Measurement of the Cross Section for W and Z Production to Electron Final States with the DØ Detector at $\sqrt{s} = 1.96$ TeV*, 4403-CONF; *Measurement of the Cross-section for Inclusive W Production in the Muon Channel at $\sqrt{s} = 1.96$ TeV using the DØ Detector*, 4750-CONF.
- [60] PHENIX Collaboration, A. Adare et al., *Cross Section and Parity Violating Spin Asymmetries of W^\pm Boson Production in Polarized p+p Collisions at $\sqrt{s} = 500$ GeV*, arXiv:1009.0505 [hep-ex].
- [61] The ATLAS Collaboration, *Measurement of the $Z \rightarrow \tau\tau$ Cross Section with the ATLAS Detector*, Phys. Rev. **D84** (2011) 112006, arXiv:1108.2016 [hep-ex].
- [62] The ATLAS Collaboration, *Measurement of the $W \rightarrow \tau\nu$ Cross Section in pp collisions at $\sqrt{s} = 7$ TeV with the ATLAS experiment*, Phys. Lett. **B706** (2012) 276–294, arXiv:1108.4101 [hep-ex].
- [63] The CMS Collaboration, *Measurement of the Inclusive Z Cross Section via Decays to Tau Pairs in pp Collisions at $\sqrt{s}=7$ TeV*, JHEP **1108** (2011) 117, arXiv:1104.1617 [hep-ex].
- [64] The ATLAS Collaboration, *Determination of the strange quark density of the proton from ATLAS measurements of the $W \rightarrow \ell\nu$ and $Z \rightarrow \ell\ell$ cross sections*, arXiv:1203.4051 [hep-ex].
- [65] The CMS Collaboration, *Jet Production Rates in Association with W and Z Bosons in pp Collisions at $\sqrt{s} = 7$ TeV*, JHEP **01** (2012) 010, arXiv:1110.3226 [hep-ex].
- [66] The CMS Collaboration, *Measurement of the Rapidity and Transverse Momentum Distributions of Z Bosons in pp Collisions at $\sqrt{s}=7$ TeV*, Phys. Rev. **D 85** (2012) 032002, arXiv:1110.4973 [hep-ex].
- [67] The ATLAS Collaboration, *Measurement of the production cross section for Z/γ^* in association with jets in pp collisions at $\sqrt{s} = 7$ TeV with the ATLAS detector*, Phys. Rev. **D85** (2012) 032009, arXiv:1111.2690 [hep-ex].
- [68] The ATLAS Collaboration, *Study of jets produced in association with a W boson in pp collisions*

- at $\sqrt{s} = 7 \text{ TeV}$ with the ATLAS detector, arXiv:1201.1276 [hep-ex].
- [69] M. L. Mangano, M. Moretti, F. Piccinini, R. Pittau, and A. D. Polosa, *ALPGEN, a generator for hard multiparton processes in hadronic collisions*, JHEP **0307** (2003) 001, arXiv:hep-ph/0206293 [hep-ph].
- [70] T. Gleisberg, S. Hoeche, F. Krauss, M. Schönherr, S. Schumann, et al., *Event generation with SHERPA 1.1*, JHEP **0902** (2009) 007, arXiv:0811.4622 [hep-ph].
- [71] J. M. Campbell and R. K. Ellis, *An update on vector boson pair production at hadron colliders*, Phys. Rev. **D60** (1999) 113006, arXiv:hep-ph/9905386.
- [72] C. F. Berger, Z. Bern, L. J. Dixon, F. Febres Cordero, D. Forde, T. Gleisberg, H. Ita, D. A. Kosower, and D. Maître, *Precise Predictions for $W + 4\text{-Jet}$ Production at the Large Hadron Collider*, Phys. Rev. Lett. **106** (2011) 092001.
- [73] The CMS Collaboration, *Measurement of the $t\bar{t}$ production cross section and the top quark mass in the dilepton channel in pp collisions at $\sqrt{s} = 7 \text{ TeV}$* , JHEP **1107** (2011) 049, arXiv:1105.5661 [hep-ex].
- [74] The CMS Collaboration, *Measurement of the $t\bar{t}$ Production Cross Section in pp Collisions at 7 TeV in Lepton + Jets Events Using b -quark Jet Identification*, Phys. Rev. **D84** (2011) 092004, arXiv:1108.3773 [hep-ex].
- [75] The ATLAS Collaboration, *Measurement of the top quark pair production cross section in pp collisions at $\sqrt{s} = 7 \text{ TeV}$ in dilepton final states with ATLAS*, Phys. Lett. **B707** (2012) 459–477, arXiv:1108.3699 [hep-ex].
- [76] The ATLAS Collaboration, *Measurement of the top quark pair production cross-section with ATLAS in the single lepton channel*, arXiv:1201.1889 [hep-ex].
- [77] The ATLAS Collaboration, *Measurement of the $t\bar{t}$ production cross section in the final state with a hadronically decaying tau lepton and jets using the ATLAS detector*, ATLAS-CONF-2012-032.
- [78] S. Moch and P. Uwer, *Theoretical status and prospects for top-quark pair production at hadron colliders*, Phys. Rev. **D78** (2008) 034003, arXiv:0804.1476 [hep-ph].
- [79] U. Langenfeld, S. Moch, and P. Uwer, *New results for $t\bar{t}$ production at hadron colliders*, arXiv:0907.2527 [hep-ph].
- [80] The ATLAS Collaboration, *Measurement of the t -channel single top-quark production cross section in 0.70fb of pp collisions at $\sqrt{s} = 7 \text{ TeV}$* , ATLAS-CONF-2011-101.
- [81] The CMS Collaboration, *Measurement of the t -channel single top quark production cross section in pp collisions at $\sqrt{s} = 7 \text{ TeV}$* , Phys. Rev. Lett. **107** (2011) 091802, arXiv:1106.3052 [hep-ex].
- [82] The ATLAS Collaboration, *Measurement of the top quark mass from 2011 ATLAS data using the template method*, ATLAS-CONF-2011-120.
- [83] The ATLAS Collaboration, *Determination of the Top Quark Mass with a Template Method in the All Hadronic Decay Channel using 2.04 fb^{-1} of ATLAS data*, ATLAS-CONF-2012-030.
- [84] The CMS Collaboration, *Measurement of the top mass by using the muon+jets channel*, CMS-PAS-TOP-11-015.
- [85] The CMS Collaboration, *Measurement of the top quark mass in the dilepton channel in pp collisions at $\sqrt{s} = 7 \text{ TeV}$* , CMS-PAS-TOP-11-016.
- [86] J. Ellison and J. Wudka, *Study of trilinear gauge boson couplings at the Tevatron collider*, Ann. Rev. Nucl. Part. Sci. **48** (1998) 33, arXiv:hep-ph/9804322 [hep-ph].
- [87] U. Baur and D. Rainwater, *Probing neutral gauge boson self-interactions in ZZ production at hadron colliders*, Phys. Rev. **D62** (2000) 113011.
- [88] The CMS Collaboration, *Measurement of $W\gamma$ and $Z\gamma$ production in pp collisions at $\sqrt{s} = 7 \text{ TeV}$* ,

- Phys. Lett. **B701** (2011) 535–555, arXiv:1105.2758 [hep-ex].
- [89] The ATLAS Collaboration, *Measurement of W/γ and Z/γ^* production in proton-proton collisions at $\sqrt{s} = 7$ TeV with the ATLAS detector*, JHEP **1109** (2011) 072, arXiv:1106.1592 [hep-ex].
- [90] The ATLAS Collaboration, *Measurement of the WW cross section in $\sqrt{s} = 7$ TeV pp collisions with ATLAS*, Phys. Rev. Lett. **107** (2011) 041802, arXiv:1104.5225 [hep-ex].
- [91] The CMS Collaboration, *Measurement of the WW , WZ and ZZ cross sections at CMS*, CMS-PAS-EWK-11-010.
- [92] The ATLAS Collaboration, *Measurement of the W^+W^- production cross section in proton-proton collisions with the ATLAS Detector*, ATLAS-CONF-2012-025.
- [93] The ATLAS Collaboration, *Measurement of the WZ production cross section and limits on anomalous triple gauge couplings in proton-proton collisions at $\sqrt{s} = 7$ TeV with the ATLAS detector*, Phys. Lett. **B709** (2012) 341, arXiv:1111.5570 [hep-ex].
- [94] The ATLAS Collaboration, *Measurement of the ZZ production cross section and limits on anomalous neutral triple gauge couplings in proton-proton collisions at $\sqrt{s} = 7$ TeV with the ATLAS detector*, Phys. Rev. Lett. **108** (2012) 041804, arXiv:1110.5016 [hep-ex].
- [95] LEP Electroweak Group, SLD Electroweak Group, Updated numbers March 2012, <http://lepwwg.web.cern.ch/LEPEWWG>.
- [96] B. W. Lee, C. Quigg, and H. B. Thacker, *Strength of Weak Interactions at Very High Energies and the Higgs Boson Mass*, Phys. Rev. Lett. **38** (1977) 883.
- [97] M. Quiros, *Constraints on the Higgs boson properties from the effective potential*, arXiv:hep-ph/9703412 [hep-ph], *Perspectives on Higgs Physics II*, G. L. Kane, ed., World Scientific, Singapore.
- [98] A. Ghinculov and T. Binoth, *Perturbative and nonperturbative Higgs signals*, Acta Phys. Polon. **B30** (1999) 99, arXiv:hep-ph/9807227 [hep-ph].
- [99] LEP Working Group for Higgs boson searches, ALEPH Collaboration, DELPHI Collaboration, L3 Collaboration, OPAL Collaboration, *Search for the Standard Model Higgs boson at LEP*, Phys. Lett. **B565** (2003) 61, arXiv:hep-ex/0306033 [hep-ex].
- [100] The Tevatron New Phenomena and Higgs Working Group, the CDF and the DØ Collaboration, *Combined CDF and DØ Upper Limits on Standard Model Higgs Boson Production with up to 8.6 fb^{-1} of Data*, arXiv:1107.5518 [hep-ex]. Submitted to the EPS 2011 Conference.
- [101] The ATLAS Collaboration, *Update of the Combination of Higgs Boson Searches in pp Collisions at $\sqrt{s} = 7$ TeV with the ATLAS Experiment at the LHC*, ATLAS-CONF-2011-135.
- [102] The CMS Collaboration, *Combination of Higgs Searches*, CMS-PAS-HIG-11-022.
- [103] E. Gross, O. Vitells, *Trial factors for the look elsewhere effect in high energy physics*, Eur. Phys. J. **C70** (2010) 525.
- [104] A. Djouadi, M. Spira, P. Zerwas, *Production of Higgs bosons in proton colliders, QCD corrections*, Phys. Lett. **B264**, 440 (1991);
 S. Dawson, *Radiative corrections to Higgs boson production*, Nucl. Phys. **B359**, 283 (1991);
 M. Spira, A. Djouadi, D. Graudenz, P. Zerwas, *Higgs boson production at the LHC*, Nucl. Phys. **B453**, 17 (1995);
 R. Harlander, W. Kilgore, *Next-to-Next-to-Leading Order Higgs Production at Hadron Colliders*, Phys. Rev. Lett. **88**, 201801 (2002);
 C. Anastasiou, K. Melnikov, *Higgs boson production at hadron colliders in NNLO QCD*, Nucl. Phys. **B646**, 220 (2002);
 V. Ravindran, J. Smith, W. van Neerven, *NNLO corrections to the total cross section for Higgs boson production in hadron-hadron collisions*, Nucl. Phys. **B665**, 325 (2003).

- [105] S. Catani, D. de Florian, M. Grazzini, P. Nason, *Soft-gluon resummation for Higgs boson production at hadron colliders*, JHEP **07** (2003) 028.
- [106] U. Aglietti, R. Bonciani, G. Degrossi, A. Vicini, *Two-loop light fermion contribution to Higgs production and decays*, Phys. Lett. B **595** (2004) 432;
- [107] S. Actis, G. Passarino, C. Sturm, S. Uccirati, *NLO electroweak corrections to Higgs boson production at hadron colliders*, Phys. Lett. B **670** (2008) 12.
- [108] M. Ciccolini, A. Denner, S. Dittmaier, *Strong and Electroweak Corrections to the Production of a Higgs Boson+2 Jets via Weak Interactions at the Large Hadron Collider*, Phys. Rev. Lett. **99**, 161803 (2007);
M. Ciccolini, A. Denner, S. Dittmaier, *Electroweak and QCD corrections to Higgs production via vector-boson fusion at the CERN LHC*, Phys. Rev. **D77**, 013002 (2008);
K. Arnold et al, *VBFNLO: A parton level Monte Carlo for processes with electroweak bosons*, Comput. Phys. Commun. **180**, 1661 (2009).
- [109] P. Bolzoni, F. Maltoni, S. Moch, M. Zaro, *Higgs production via vector-boson fusion at NNLO in QCD*, Phys. Rev. Lett. **105** (2010) 011801.
- [110] T. Han, S. Willenbrock, *QCD correction to the $pp \rightarrow WH$ and ZH total cross-sections*, Phys. Lett. **B273** (1991) 167.
- [111] O. Brein, A. Djouadi, R. Harlander, *NNLO QCD corrections to the Higgs-strahlung processes at hadron colliders*, Phys. Lett. **B579** (2004) 149.
- [112] M. L. Ciccolini, S. Dittmaier, M. Kramer, *Electroweak radiative corrections to associated WH and ZH production at hadron colliders*, Phys. Rev. **D68** (2003) 073003.
- [113] W. Beenakker et al., *Higgs Radiation off Top Quarks at the Tevatron and the LHC*, Phys. Rev. Lett. **87**, 201805 (2001);
W. Beenakker et al., *NLO QCD corrections to $t\bar{t}H$ production in hadron collisions*, Nucl. Phys. **B653**, 151 (2003);
S. Dawson, L. H. Orr, L. Reina, D. Wackerroth, *Associated Top Quark-Higgs Boson Production at the LHC*, Phys. Rev. **D67**, 071503 (2003);
S. Dawson, C. Jackson, L. Orr, L. Reina, D. Wackerroth, *Associated Higgs boson production with top quarks at the CERN Large Hadron Collider: NLO QCD corrections*, Phys. Rev. **D68**, 034022 (2003).
- [114] LHC Higgs Cross Section Working Group, S. Dittmaier, C. Mariotti, G. Passarino, R. Tanaka (Eds.), CERN-2011-002 arXiv:1101.0593 (2011) and arXiv:1201.3084 (2012).
- [115] A. Djouadi, J. Kalinowski, and M. Spira, *HDECAY: A Program for Higgs boson decays in the Standard Model and its supersymmetric extension*, Comput. Phys. Commun. **108** (1998) 56, arXiv:hep-ph/9704448 [hep-ph].
- [116] A. Djouadi, M. Spira, and P. Zerwas, *QCD corrections to hadronic Higgs decays*, Z. Phys. **C70** (1996) 427, arXiv:hep-ph/9511344 [hep-ph].
- [117] A. Ghinculov, T. Binoth, and J. van der Bij, *Higgs mass saturation effect and the LHC discovery potential*, Phys. Lett. **B427** (1998) 343, arXiv:hep-ph/9802367 [hep-ph].
- [118] The ATLAS Collaboration, *Detector and physics performance technical design report*, CERN/LHCC/99-15, 1999;
- [119] The CMS Collaboration, *CMS Physics Technical Design Report, Volume II: Physics Performance*, Journal of Physics G: Nuclear and Particle Physics **34** (2007) no. 6, 995;
- [120] The ATLAS Collaboration, *Expected Performance of the ATLAS Experiment - Detector, Trigger and Physics, Volume I: Performance*, CERN-OPEN-2008-20.
- [121] D.L. Rainwater, D. Zeppenfeld, *Searching for $H \rightarrow \gamma\gamma$ in weak boson fusion at the LHC*, J. High Energy Phys. **12**, (1997) 5;
D.L. Rainwater, D. Zeppenfeld, K. Hagiwara, *Searching for $H \rightarrow \tau\tau$ in weak boson fusion at the*

- LHC, Phys. Rev. **D59** (1999) 014037;
T. Plehn, D.L. Rainwater, D. Zeppenfeld, *Method for identifying $H \rightarrow \tau\tau e^\pm \mu^\mp p_T$ at the CERN LHC*, Phys. Rev. **D61** (2000) 093005;
D.L. Rainwater, D. Zeppenfeld, *Observing $H \rightarrow W^*W^* \rightarrow e^\pm \mu^\mp$ missing- p_T in weak boson fusion with dual forward jet tagging at the CERN LHC*, Phys. Rev. **D60** (1999) 113004 [Erratum Phys. Rev. **D61** (2000) 099901];
N. Kauer, T. Plehn, D.L. Rainwater, D. Zeppenfeld, *$H \rightarrow WW$ as the discovery mode for a light Higgs boson*, Phys. Lett. **B503** (2001) 113.
- [122] J. M. Butterworth, A. R. Davison, M. Rubin, and G. P. Salam, *Jet substructure as a new Higgs search channel at the LHC*, Phys. Rev. Lett. **100** (2008) 242001, arXiv:0802.2470 [hep-ph].
- [123] The ATLAS Collaboration, *ATLAS Sensitivity to the Standard Model Higgs in the HW and HZ Channels at High Transverse Momenta*, ATL-PHYS-PUB-2009-088.
- [124] The ATLAS and CMS Collaborations, LHC Higgs Combination Group, *Procedure for the LHC Higgs boson search combination in summer 2011*, ATL-PHYS-PUB-2011-011, online at <https://cdsweb.cern.ch/record/1375842> (2011) .
- [125] A. L. Read, *Presentation of search results: The CL_s technique*, J. Phys. **G28** (2002) 2693.
- [126] G. Cowan, K. Cranmer, E. Gross, O. Vitells, *Asymptotic formulae for likelihood-based tests of new physics*, Eur. Phys. J. **C71** (2011) 1554.
- [127] The ATLAS Collaboration, *Combined search for the Standard Model Higgs boson using up to 4.9 fb^{-1} of pp collisions at $\sqrt{s} = 7 \text{ TeV}$ with the ATLAS detector at the LHC*, [hep-ex], submitted to Phys. Lett. B (2012) .
- [128] The ATLAS Collaboration, *Search for the Standard Model Higgs boson in the diphoton decay channel with 4.9 fb^{-1} of pp collisions at $\sqrt{s}=7 \text{ TeV}$ with ATLAS*, arXiv:1202.1414 [hep-ex].
- [129] The CMS Collaboration, *Search for the Standard Model Higgs boson decaying into two photons in pp collisions at $\sqrt{s}=7 \text{ TeV}$* , oai:cds.cern.ch:1422613, . Submitted to Physics Letters B.
- [130] The ATLAS Collaboration, *Search for the Standard Model Higgs boson in the decay channel $H \rightarrow ZZ^{(*)} \rightarrow 4l$ with 4.8 fb^{-1} of pp collision data at $\sqrt{s} = 7 \text{ TeV}$ with ATLAS*, arXiv:1202.1415 [hep-ex].
- [131] The CMS Collaboration, *Search for the Standard Model Higgs boson in the decay channel $H \rightarrow ZZ \rightarrow 4l$ in pp collisions at $\sqrt{s} = 7 \text{ TeV}$* , oai:cds.cern.ch:1423188, submitted to Physical Review Letters.
- [132] The ATLAS Collaboration, *Search for the Standard Model Higgs boson in the $H \rightarrow WW^{(*)} \rightarrow \ell\nu\ell\nu$ decay mode with 4.7 fb^{-1} of ATLAS data at $\sqrt{s} = 7 \text{ TeV}$* , ATLAS-CONF-2012-012.
- [133] The CMS Collaboration, *Search for the Standard Model Higgs boson decaying to a W pair in the fully leptonic final state in pp collisions at $\sqrt{s} = 7 \text{ TeV}$* , CERN-PH-EP-2012-018.
- [134] M. Dittmar and H. Dreiner, *How to find a Higgs boson with a mass between 155 and 180 GeV at the CERN LHC*, Phys. Rev. **D55** (1997) 167.
- [135] The ATLAS Collaboration, *Search for the Standard Model Higgs boson in the $H \rightarrow \tau^+\tau^-$ decay mode with 4.7 fb^{-1} of ATLAS data at 7 TeV*, ATLAS-CONF-2012-014.
- [136] The CMS Collaboration, *Search for neutral Higgs bosons decaying to tau pairs in pp collisions at $\sqrt{s}=7 \text{ TeV}$* , oai:cds.cern.ch:1425572, submitted to Physics Letters B.
- [137] The ATLAS Collaboration, *Search for the Standard Model Higgs boson produced in association with a vector boson and decaying to a b -quark pair using up to 4.7 fb^{-1} of pp collision data at $\sqrt{s} = 7 \text{ TeV}$ with the ATLAS detector at the LHC*, ATLAS-CONF-2012-015.
- [138] The CMS Collaboration, *Search for the Standard Model Higgs boson decaying to bottom quarks in pp collisions at $\sqrt{s} = 7 \text{ TeV}$* , Phys. Lett. **B710** (2012) 284.

- [139] The ATLAS Collaboration, *An update to the combined search for the Standard Model Higgs boson with the ATLAS detector at the LHC using up to 4.9 fb^{-1} of pp collision data at $\sqrt{s} = 7 \text{ TeV}$* , ATLAS-CONF-2012-019.
- [140] The CMS Collaboration, *Combined results of searches for the Standard Model Higgs boson in pp collisions at $\sqrt{s} = 7 \text{ TeV}$* , oai:cds.cern.ch:1422614, submitted to Physics Letters B.
- [141] The CMS Collaboration, *Search for the Standard Model Higgs boson in the $H \rightarrow ZZ \rightarrow 2l2\nu$ channel in pp collisions at $\sqrt{s} = 7 \text{ TeV}$* , oai:cds.cern.ch:1424785, submitted to JHEP.
- [142] The ATLAS Collaboration, *Search for a Standard Model Higgs in the $H \rightarrow ZZ \rightarrow \ell^+ \ell^- \nu \bar{\nu}$ decay channel with 4.7 fb^{-1} with the ATLAS detector*, ATLAS-CONF-2012-016.
- [143] The ATLAS Collaboration, *Search for a Standard Model Higgs in the mass range 200-600 GeV in the channel $H \rightarrow ZZ \rightarrow \ell\ell q\bar{q}$ with the ATLAS detector*, ATLAS-CONF-2012-017.
- [144] The CMS Collaboration, *Search for a Higgs boson in the decay channel $H \rightarrow ZZ^{(*)} \rightarrow q\bar{q}\ell^-\ell^+$ in pp collisions at $\sqrt{s} = 7 \text{ TeV}$* , submitted to the Journal of High Energy Physics.
- [145] The CMS Collaboration, *Search for the Standard Model Higgs boson in the $H \rightarrow ZZ \rightarrow l^+ l^- \tau^+ \tau^-$ decay channel in pp collisions at $\sqrt{s}=7 \text{ TeV}$* , oai:cds.cern.ch:1424911, submitted to JHEP.
- [146] The ATLAS Collaboration, *Search for the Higgs boson in the $H \rightarrow WW \rightarrow \ell\nu jj$ decay channel using 4.7 fb^{-1} of pp collisions at $\sqrt{s} = 7 \text{ TeV}$ with the ATLAS detector*, ATLAS-CONF-2012-018.
- [147] The ATLAS and the CMS Collaboration, *Combined Standard Model Higgs boson searches with up to 2.3 fb^{-1} of pp collisions at $\sqrt{s}=7 \text{ TeV}$ at the LHC*, ATLAS-CONF-2011-157.
- [148] For a review, see: S. P. Martin, *A Supersymmetry primer*, arXiv:hep-ph/9709356 [hep-ph].
- [149] H. Nilles, *Supersymmetry, supergravity and particle physics*, Phys. Rep. **110** (1984) 1, and references therein.
- [150] P. de Jong, *SUSY Searches at ATLAS*, arXiv:1201.4548 [hep-ex].
- [151] P. Fayet, *Spontaneously broken supersymmetric theories of weak, electromagnetic and strong interactions*, Phys. Lett. **B69** (1977) 489;
- [152] G. R. Farrar and P. Fayet, *Phenomenology of the production, decay, and detection of new hadronic states associated with supersymmetry*, Phys. Lett. **B76** (1978) 575.
- [153] The ATLAS Collaboration, *Search for squarks and gluinos using final states with jets and missing transverse momentum with the ATLAS detector in $\sqrt{s} = 7 \text{ TeV}$ proton-proton collisions*, arXiv:1109.6572 [hep-ex].
- [154] The CMS Collaboration, *Search for Supersymmetry at the LHC in Events with Jets and Missing Transverse Energy*, Phys. Rev. Lett. **107** (2011) 221804, arXiv:1109.2352 [hep-ex].
- [155] The ATLAS Collaboration, *Search for supersymmetry in final states with jets, missing transverse momentum and one isolated lepton in $\sqrt{s} = 7 \text{ TeV}$ pp collisions using 1 fb^{-1} of ATLAS data*, Phys. Rev. **D85** (2012) 012006, arXiv:1109.6606 [hep-ex], to appear in Physical Review D.
- [156] The CMS Collaboration, *Search for new physics with single-leptons at the LHC*, CMS-PAS-SUS-11-015.
- [157] The ATLAS Collaboration, *Searches for supersymmetry with the ATLAS detector using final states with two leptons and missing transverse momentum in $\sqrt{s} = 7 \text{ TeV}$ proton-proton collisions*, Phys. Lett. **B709** (2012) 137, arXiv:1110.6189 [hep-ex].
- [158] The CMS Collaboration, *Multileptonic SUSY searches*, CMS-PAS-SUS-11-013.
- [159] The Atlas Collaboration, *Search for new phenomena in final states with large jet multiplicities and missing transverse momentum using $\sqrt{s}=7 \text{ TeV}$ pp collisions with the ATLAS detector*, JHEP **1111** (2011) 099, arXiv:1110.2299 [hep-ex].
- [160] A. H. Chamseddine et al., *Locally Supersymmetric Grand Unification*, Phys. Rev. Lett. **49** (1982)

- 970;
- R. Barbieri et al., *Gauge models with spontaneously broken local supersymmetry*, Phys. Lett. **B119** (1982) 343;
- L. E. Ibanez, *Locally supersymmetric SU(5) grand unification*, Phys. Lett. **B118** (1982) 73;
- L. J. Hall et al., *Supergravity as the messenger of supersymmetry breaking*, Phys. Rev. **D27** (1983) 2359;
- N. Ohta, *Grand Unified Theories Based on Local Supersymmetry*, Prog. Theor. Phys. **70** (1983) 542;
- G. L. Kane et al., *Study of constrained minimal supersymmetry*, Phys. Rev. **D49** (1994) 6173.
- [161] The ATLAS Collaboration, *Search for supersymmetry with jets and missing transverse momentum: Additional model interpretations*, ATLAS conference note: ATLAS-CONF-2011-155.
- [162] R. Barbieri, *SUSY phenomenology*, talk at the Hadron Collider Symposium 2011 (Paris).
- [163] The ATLAS Collaboration, *Search for scalar bottom pair production with the ATLAS detector in pp Collisions at $\sqrt{s} = 7$ TeV*, arXiv:1112.3832 [hep-ex].
- [164] G. Polesello and D. R. Tovey, *Supersymmetric particle mass measurement with the boost-corrected contranverse mass*, JHEP **1003** (2010) 030, arXiv:0910.0174 [hep-ph].
- [165] The ATLAS Collaboration, *Search for supersymmetry in pp collisions at $\sqrt{s} = 7$ TeV in final states with missing transverse momentum, b-jets and one lepton with the ATLAS detector*, ATLAS-CONF-2011-130.
- [166] The ATLAS Collaboration, *Search for New Phenomena in $t\bar{t}$ Events With Large Missing Transverse Momentum in Proton-Proton Collisions at $\sqrt{s} = 7$ TeV with the ATLAS Detector*, Phys. Rev. Lett. **108** (2012) 041805, arXiv:1109.4725 [hep-ex].
- [167] The CDF Collaboration, *Search for Anomalous Production of Multilepton Events in $p\bar{p}$ Collisions at $\sqrt{s}=1.96$ TeV*, Phys. Rev. Lett. **98** (2007) 131804.
- [168] The DØ Collaboration, V. Abazov et al., *Search for associated production of charginos and neutralinos in the trilepton final state using 2.3 fb^{-1} of data*, Phys. Lett. **B680** (2009) 34.
- [169] The CMS Collaboration, S. Chatrchyan et al., *Search for Physics Beyond the Standard Model Using Multilepton Signatures in pp Collisions at $\sqrt{s}=7$ TeV*, Phys. Lett. **B704** (2011) 411, arXiv:1106.0933 [hep-ex].
- [170] P. Langacker, *The physics of heavy Z' gauge bosons*, Rev. Mod. Phys. **81** (2009) 1199.
- [171] J. Erler, P. Langacker, S. Munir, and E. Rojas, *Improved Constraints on Z-prime Bosons from Electroweak Precision Data*, JHEP **0908** (2009) 017, arXiv:0906.2435 [hep-ph].
- [172] D. London and J. L. Rosner, *Extra gauge bosons in E_6* , Phys. Rev. **D34** (1986) 1530.
- [173] K. Lane and E. Eichten, *Two-scale technicolor*, Phys. Lett. **B222** (1989) 274.
- [174] K. Lane and S. Mrenna, *Collider phenomenology of technihadrons in the technicolor straw man model*, Phys. Rev. **D67** (2003) 115011.
- [175] A. Belyaev, R. Foadi, M. T. Frandsen, M. Järvinen, F. Sannino, and A. Pukhov, *Technicolor walks at the LHC*, Phys. Rev. **D79** (2009) 035006.
- [176] L. Randall and R. Sundrum, *Large Mass Hierarchy from a Small Extra Dimension*, Phys. Rev. Lett. **83** (1999) 3370.
- [177] J.C. Pati and A. Salam, *Lepton number as the fourth "color"*, Phys. Rev. **D10** (1974) 275;
- R. Mohapatra and J.C. Pati, *"Natural" left-right symmetry*, Phys. Rev. **D11** (1975) 2558;
- G. Senjanovic and R.N. Mohapatra, *Exact left-right symmetry and spontaneous violation of parity*, Phys. Rev. **D12** (1975) 1502.
- [178] The ATLAS Collaboration, *Search for dilepton resonances in pp collisions at $\sqrt{s} = 7$ TeV with the ATLAS detector*, Phys. Rev. Lett. **107** (2011) 272002, arXiv:1108.1582 [hep-ex].

- [179] The CMS Collaboration, *Search for W' in the leptonic channels in pp Collisions at $\sqrt{s} = 7$ TeV*, CMS-PAS-EXO-11-024.
- [180] The CMS Collaboration, *Search for Resonances in the Dilepton Mass Distribution in pp Collisions at $\sqrt{s} = 7$ TeV*, CMS-PAS-EXO-11-019.
- [181] The ATLAS Collaboration, *Search for a heavy gauge boson decaying to a charged lepton and a neutrino in 1 fb^{-1} of pp collisions at $\sqrt{s} = 7$ TeV using the ATLAS detector*, Phys. Lett. **B705** (2011) 28, arXiv:1108.1316 [hep-ex].
- [182] The DØ Collaboration, *Search for a heavy neutral gauge boson in the dielectron channel with 5.4 fb^{-1} of $p\bar{p}$ collisions at $\sqrt{s} = 1.96$ TeV*, Phys. Lett. **B695** (2011) 88.
- [183] The CDF Collaboration, *Search for High Mass Resonances Decaying to Muon Pairs in $\sqrt{s} = 1.96$ TeV $p\bar{p}$ Collisions*, Phys. Rev. Lett. **106** (2011) 121801.
- [184] The ATLAS Collaboration, *Search for high mass dilepton resonances in pp collisions at $\sqrt{s} = 7$ TeV with the ATLAS experiment*, Phys. Lett. **B700** (2011) 163, arXiv:1103.6218 [hep-ex].
- [185] The CMS Collaboration, *Search for Resonances in the Dilepton Mass Distribution in pp Collisions at $\sqrt{s} = 7$ TeV*, JHEP **1105** (2011) 093, arXiv:1103.0981 [hep-ex].
- [186] The CMS Collaboration, *Search for W' (or techni- ρ) to WZ* , CMS-PAS-EXO-11-041.
- [187] The ATLAS Collaboration, *Search for New Physics in Dijet Mass and Angular Distributions in pp Collisions at $\sqrt{s} = 7$ TeV Measured with the ATLAS Detector*, New J. Phys. **13** (2011) 053044, arXiv:1103.3864 [hep-ex].
- [188] The CMS Collaboration, *Measurement of Dijet Angular Distributions and Search for Quark Compositeness in pp Collisions at $\sqrt{s} = 7$ TeV*, Phys. Rev. Lett. **106** (2011) 201804, arXiv:1102.2020 [hep-ex].
- [189] The ATLAS Collaboration, *Search for New Physics in the Dijet Mass Distribution using 1 fb^{-1} of pp Collision Data at $\sqrt{s} = 7$ TeV collected by the ATLAS Detector*, Phys. Lett. **B708** (2012) 37–54, arXiv:1108.6311 [hep-ex].
- [190] E. J. Eichten, K. D. Lane, and M. E. Peskin, *New Tests for Quark and Lepton Substructure*, Phys. Rev. Lett. **50** (1983) 811.
- [191] E. Eichten, I. Hinchliffe, K. Lane, and C. Quigg, *Supercollider physics*, Rev. Mod. Phys. **56** (1984) 579.
- [192] The CMS Collaboration, *Search for quark compositeness in dijet angular distributions from pp collisions at $\sqrt{s} = 7$ TeV*, arXiv:1202.5535 [hep-ex].
- [193] The CMS Collaboration, *Search for Resonances in the Dijet Mass Spectrum from 7 TeV pp Collisions at CMS*, Phys. Lett. **B704** (2011) 123, arXiv:1107.4771 [hep-ex].
- [194] U. Baur, I. Hinchliffe, and D. Zeppenfeld, *Excited quark production at hadron colliders*, Int. J. Mod. Phys. **A2** (1987) 1285.
- [195] U. Baur, M. Spira, and P. M. Zerwas, *Excited-quark and -lepton production at hadron colliders*, Phys. Rev. **D42** (1990) 815.
- [196] P. H. Frampton and S. L. Glashow, *Chiral color: An alternative to the Standard Model*, Phys. Lett. **B190** (1987) 157.
- [197] P. H. Frampton and S. L. Glashow, *Unifiable Chiral Color with Natural Glashow-Iliopoulos-Maiani Mechanism*, Phys. Rev. Lett. **58** (1987) 2168.
- [198] J. Bagger, C. Schmidt, and S. King, *Axigluon production in hadronic collisions*, Phys. Rev. **D37** (1988) 1188.
- [199] T. Han, I. Lewis, and Z. Liu, *Colored Resonant Signals at the LHC: Largest Rate and Simplest Topology*, JHEP **1012** (2010) 085, arXiv:1010.4309 [hep-ph].
- [200] J. L. Hewett and T. G. Rizzo, *Low-Energy Phenomenology of Superstring Inspired $E(6)$ Models*,

Phys. Rept. **183** (1989) 193.